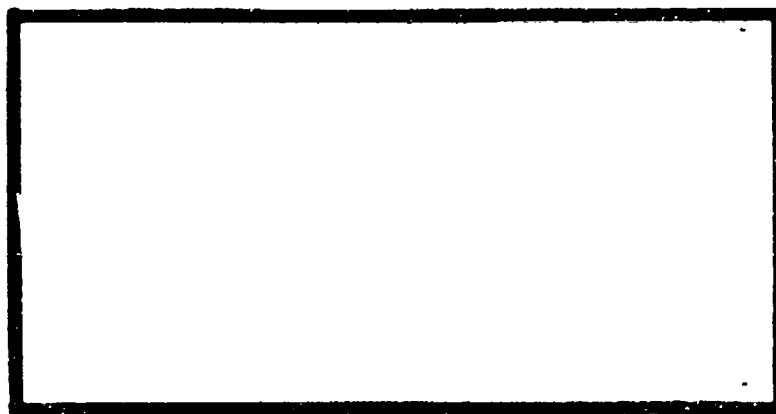


ADA034283



UNITED STATES AIR FORCE  
AIR UNIVERSITY  
**AIR FORCE INSTITUTE OF TECHNOLOGY**  
Wright-Patterson Air Force Base, Ohio

DISTRIBUTION STATEMENT A  
Approved for public release;

DDC  
JAN 10 1977

GEF/PH/76-3

⑥ THE GEOMETRIC THEORY OF  
ROOF REFLECTOR RESONATORS \*

THESIS

④ GEF/PH/76-3

⑩ Howard E. Evans, II  
Captain USAF

Elms

⑪ D. 76

⑫ 127.

012 25

Approved for public release; distribution unlimited

D D C

RECEIVED  
JAN 10 1977  
LTCOL W. B. L.

A

GEP/PH/76-3

THE GEOMETRIC THEORY OF  
ROOF REFLECTOR RESONATORS

THESIS

Presented to the Faculty of the School of Engineering  
of the Air Force Institute of Technology

Air University  
in Partial Fulfillment of the  
Requirements for the Degree of  
Master of Science

by  
Howard E. Evans II, B.S.  
Captain USAF  
Graduate Engineering Physics  
December 1976

Approved for public release; distribution unlimited.

RECEIVED	
DATE	NOV 1976
CDC	NOV 1976
UNANNOUNCED	
JUSTIFICATION	
BY	
DISTRIBUTION/AVAILABILITY CODES	
DISC	APPROPRIATE
A	

## Preface

In the past, many more laser designers have probably used roof reflectors than have reported their experiments in the literature. They have undoubtedly tried using roof reflectors to gain relief from the chronic problem of alignment sensitivity that plagues laser resonators, but they obtained poor quality output beams and large divergences. So the roof reflectors were shelved in favor of the better understood plane or spherical mirror resonator. This thesis provides a geometric understanding of what is going on inside of a roof reflector resonator. After reading it, the laser designer should have a solid feeling about how to avoid the problems. As a result, roof reflectors can return to the laboratory as a real alternative to ordinary mirrors.

In developing this geometric theory, it has been assumed that the interested laser designer - and reader of this thesis - is already familiar with (1) first-order matrix optics and (2) the geometric analysis of stable resonators. (For the reader who is not familiar with these topics, Chapter 8 of A. E. Siegman's text, An Introduction to Lasers and Masers (Ref 37), and Kogelnik and Li's excellent review article, "Laser Beams and Resonators" (Ref 25), are recommended as preliminary reading.) It will be found that results drawn from these areas are taken to be generally known and are not specifically referenced. But otherwise, the analysis of roof reflector resonators presented in the body of this thesis is not exactly traditional, although every effort has been made to make the presentation logical

and easy to follow. Two appendices treat certain aspects of roof reflector resonators in the same manner as conventional resonators, to emphasize the contrast between roof reflectors and ordinary mirrors.

On the other side of the house, the reader of this theoretical thesis will be interested to know that experiments on the same subject have also been performed. Simultaneously with the author's research, fellow student R. Grotbeck has built and tested a CO<sub>2</sub> laser using roof reflectors. His work, entitled An Experimental Investigation of the Resonant Modes of a Roof-Top Laser (Ref 19), gives an account of his findings and, as an independent thesis, is complementary to the present work.

The author wishes to express gratitude to his thesis advisor, H. Weichel, for the helpful suggestions and many hours of time given during the course of this investigation.

Howard E. Evans II

## Contents

	Page
Preface . . . . .	11
List of Figures . . . . .	vi
Abstract . . . . .	1x
I. Introduction . . . . .	1
Roof Reflectors . . . . .	1
Desirability of Roof Reflectors . . . . .	3
Purpose and Scope of this Thesis . . . . .	4
Criteria and Assumptions . . . . .	5
How the Theory is Developed . . . . .	6
II. The Literature of Roof Reflectors . . . . .	8
Experimental Papers . . . . .	8
Theoretical Papers . . . . .	18
Discussion . . . . .	24
III. Characteristics of Roof Reflectors . . . . .	28
Rotational Invariance . . . . .	28
Roof Reflector Ray Matrix . . . . .	35
IV. Resonators With Roofs Parallel . . . . .	42
Stable Rays . . . . .	42
Stability Conditions . . . . .	53
Resonant Modes . . . . .	60
V. Resonators With Roofs Crossed . . . . .	70
Three-Dimensional Ray Tracing . . . . .	70
The General Case . . . . .	79
Resonant Modes of the First Pattern . . . . .	94
VI. Conclusion . . . . .	99
Summary of Stability Conditions . . . . .	99
Major Predictions of This Thesis . . . . .	101
Recommendations for Further Study . . . . .	104
Bibliography . . . . .	108

Contents

	Page
Appendix A: Similarities Between Roof Reflectors and Spherical Mirrors . . . . .	112
Appendix B: Roof Reflectors and the g-Parameter . . . . .	117

# List of Figures

<u>Figure</u>		<u>Page</u>
1	Typical Roof Reflector . . . . .	2
2	Crossed Roof Reflector Interferometer (After Ref 18:533) . . . . .	9
3	Total Internal Reflection Laser Resonator (After Ref 3:1833) . . . . .	9
4	DeLang and Bouwhuis' Experiment (After Ref 14:48, 49) . . . . .	12
5	Soncini and Svelto's Experiment (After Ref 39:262) . . . . .	12
6	Roof Reflector Misalignment Sensitivity (From Ref 42:28) . . . . .	16
7	Laser Output Using One 90° Roof Reflector (From Ref 42:162) . . . . .	17
8	Pasqualetti and Ronchi's Result for $\alpha > 0^\circ$ (From Ref 31:293) . . . . .	21
9	Four-mirror Ring Resonator and Its Limit (After Ref 36:1051) . . . . .	21
10	Numerical Solutions for Ring Resonator (From Ref 36:1051) . . . . .	23
11	Ray Crossing Angle . . . . .	29
12	Unfolded Roof Reflector . . . . .	29
13	Roof Reflector Rotated Around Its Roof Edge . . . . .	32
14	The Standard Ray . . . . .	34
15	Ray Coordinate Transformation . . . . .	37
16	Discrete Nonlinearity . . . . .	40
17	Resonator with Roofs Parallel . . . . .	43
18	Equivalent Waveguides . . . . .	43

19	Ray Propagating Through Equivalent Waveguide - First Pattern . . . . .	46
20	Second Pattern . . . . .	46
21	Relation of First and Third Patterns . . . . .	50
22	Equivalent Waveguides for Higher-Order Patterns . . . . .	51
23	Dependence of Odd Patterns on Axis Length and Aperture . . . . .	55
24	Dependence of Even Patterns on Axis Length and Aperture . . . . .	57
25	Dependence of $p_2 = 1$ Ray Packet on L . . . . .	59
26	Dependence of Pattern Area on Axis Length . . . . .	61
27	Roof Reflector Aperture-Equivalent Waveguide . . . . .	61
28	Estimate of Maximum Ray Length . . . . .	68
29	Three-Dimensional Roof Reflector Resonator as a Superposition of Two-Dimensional Resonators . . . . .	71
30	Three-Dimensional Ray Coordinates . . . . .	73
31	Image Inversion by a Roof Reflector . . . . .	73
32	Stable $p_3 = 1$ Ray in Crossed-Roof Resonator With One Non-zero Variant Angle . . . . .	77
33	First Crossed-Roof $p_3 = 1$ Pattern . . . . .	82
34	Second Crossed-Roof $p_3 = 1$ Pattern . . . . .	83
35	First Geometric Tube of Rays for $p_3 = 1$ Pattern . . . . .	85
36	Second Geometric Tube of Rays for $p_3 = 1$ Pattern . . . . .	86
37	Central Rays . . . . .	88
38	A Possible $p_3 = 2$ Pattern . . . . .	92
39	Aperture Effects on $p_3 = 1$ Ray Tube . . . . .	95

40	Ray Tube Cross-Section . . . . .	95
41	Similarities Between Roof Reflectors and Spherical Mirrors . . . . .	113
42	Dissimilarities Between Roof Reflectors and Spherical Mirrors . . . . .	116
43	Operating Curve for $p_2 = 1$ . . . . .	119
44	Operating Curve for Parallel-Roof Resonator in Pattern $p_2$ . . . . .	121

Abstract

Laser resonators using roof reflectors with  $90^\circ - \alpha$  roof angles ( $\alpha$  small and positive) are analyzed geometrically when the roof edges at opposite ends of the resonator are aligned either parallel or perpendicular (crossed). Stability conditions, involving reflector dimensions, are found which specify a maximum axis length for the existence of stable rays. In the parallel-roof case, stable rays are shown to be ring-type, making any given number of round-trips before spatially repeating. Stable rays in the crossed-roof case are superpositions of two parallel-roof ray patterns in orthogonal planes. For any pattern, the reflector roof edges are shown to be geometrically excluded when the axis length is greater than one-half the maximum length for that pattern. It is then predicted that when the roof edges are excluded, the resonant modes are pure Gaussian.

# THE GEOMETRIC THEORY OF ROOF REFLECTOR RESONATORS

## I. Introduction

The objects studied in this thesis are laser resonators using roof reflectors - instead of curved mirrors - for end reflectors. This chapter first describes typical roof reflectors and gives some reasons why they are thought to be practical and useful devices in laser resonators. The purpose of this thesis is then presented, and its scope is narrowed to the specific approach taken here. Criteria to be applied and simplifying assumptions are next listed; and finally, the plan for development of the theory is given.

### Roof Reflectors

Roof reflectors are simple optical devices for redirecting light. In general, they are two plane, front-surface mirrors attached along one edge called the "roof edge." A suitably shaped prism could also be used as a roof reflector, if properly oriented. (The terms "roof-top prism," "right-angle prism," and - incorrectly - "Porro prism" are encountered in the literature.) Figure 1 is a line drawing of a typical roof reflector: surfaces ABFE and CDEF are mirrors joined along roof edge EF, and Angle AED is called the "roof angle." In the

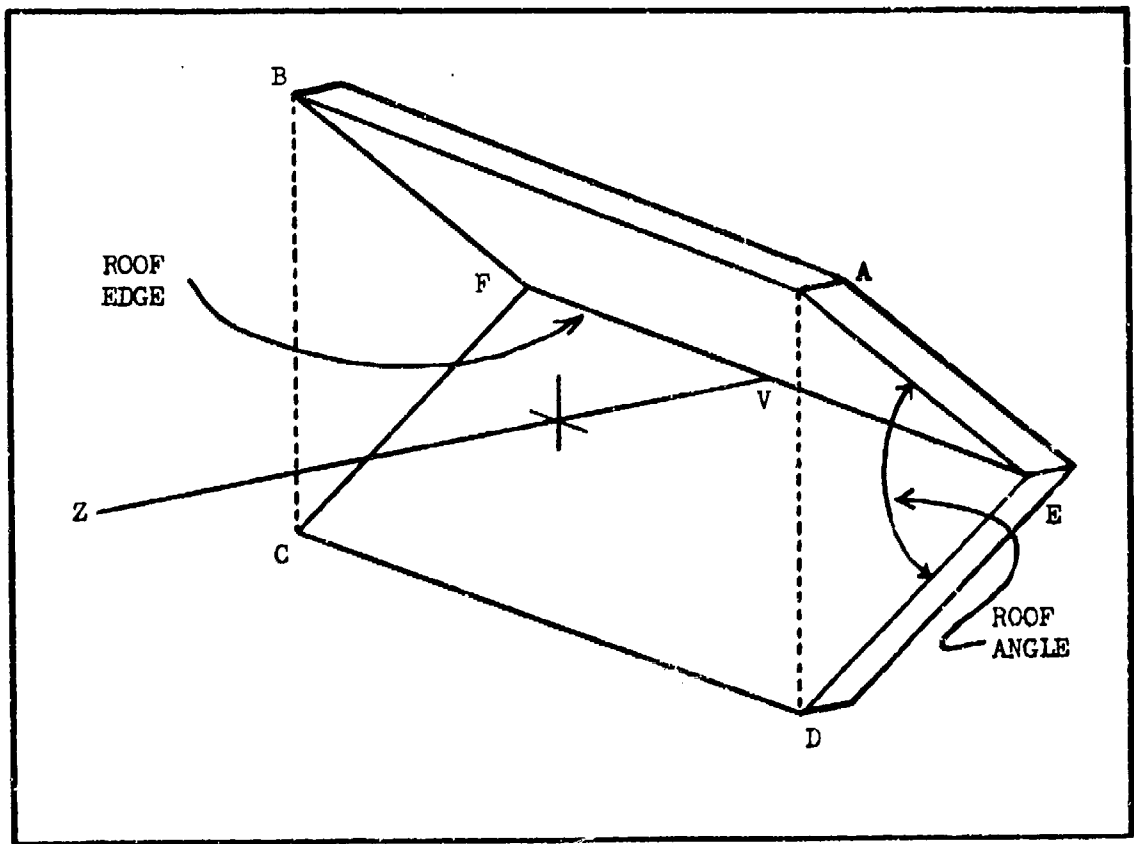


Fig. 1. Typical Roof Reflector

( figure, ABCD is the front face, or aperture, and line  $\overline{ZV}$  - here perpendicular to the front face - is called the "reflector axis."

The primary difference between ordinary mirrors and roof reflectors is that light beams, or rays, reflect once from a mirror but twice in a roof reflector. The two reflections - one at each of the two surfaces in succession - are specular and retro-reflect the light beams back toward their sources (if the roof angle is  $90^\circ$ ).

#### Desirability of Roof Reflectors

( Roof reflectors have occasionally been used as end mirrors in laser resonators. The primary reason that roof reflector resonators have been built recently is because they are reported to be particularly insensitive to misalignment, or tilt. Consequently, roof reflector resonators are attractive for use in high-vibration environments (laser range-finders on artillery pieces, for example) and under conditions which could mechanically deform the resonator (as a laser target designator on a tactical aircraft).

In addition to the optical (or alignment) stability that roof reflectors give to laser resonators, there are other reasons why they are desirable:

(1) Cost. In their simplicity, roof reflectors should be cheaper to make than spherical mirrors with large radii of curvature.

(2) No focusing. Since roof reflectors are made of plane mirrors, there is no focusing. Thus, in the absence of other focusing elements, electric field amplitudes will remain relatively small.

( 3) Large mode volume. Roof reflectors are made of plane mirrors, so the properties of a roof reflector resonator should be similar to those of a plane mirror resonator. One of these properties is a large mode volume - limited only by the smallest aperture.

These features point to the roof reflector resonator as being desirable for high energy lasers, where high field amplitudes in large volumes are prevented from focusing with negatively curved mirrors. Typically, high energy laser resonators are lossy, or unstable, but it is not known whether roof reflector resonators have unstable characteristics. Further (aside from mechanical stability having been observed) there is no known theory which specifies the resonator stability in terms of its physical dimensions, as for spherical mirror resonators.

#### Purpose and Scope of this Thesis

The purpose of this thesis is to provide a simple theory of the stability of the roof reflector resonator, in terms of its physical dimensions. Since this is the first known attempt to develop this theory, it is necessarily limited in scope. Only geometric optics is used to predict when the resonator is stable or unstable. In certain instances, however, it is possible to predict quantities which would otherwise require a physical optics analysis - such as resonant modes and cavity losses - and this has been done here.

The geometric theory presented here is limited in that only two resonator configurations are considered, but it is extended to include

a class of roof reflectors. The two special cases analyzed are (1) the parallel-roof resonator, where the roof edges of the reflectors at opposite ends of the resonator are coplanar, and (2) the crossed-roof resonator, where the roof edges are perpendicular, or crossed. The class of roof reflectors studied is that in which the roof angle is less than or equal to  $90^\circ$ . This is due, in part, to the reality that physical devices always have some manufacturing tolerance; so the roof angle is hereafter taken to be  $90^\circ - \alpha$ , where  $\alpha$  is called the "variant angle" and is either small and positive or zero.

#### Criteria and Assumptions

In geometric optics, the criterion for stability of laser resonators is that rays remain close to the axis and not diverge past the edges of the end reflectors. This is the criterion that will be used here to establish whether or not rays are stable in roof reflector resonators. Whatever dimensions are then required of the resonator in order for stable rays to exist - the distance between roof edges, the roof reflector apertures, and the variant angles - are called the "stability conditions."

The stability conditions for a laser resonator, in reality, depend on many physical variables. Since a geometric theory provides only the first approximation to the physical situation, two assumptions are listed below which simplify this analysis and eliminate many of the unknowns:

- (1) The roof reflectors are assumed to be as shown in Fig. 1 with rectangular apertures and perfectly reflecting, front-surface

( mirrors; but the roof edges are not necessarily assumed to be perfect, since they are not in reality.

(2) The space between the roof reflectors is assumed to be empty and contains no other optical elements or apertures.

### How the Theory is Developed

Before applying the above assumptions to develop a geometric theory, previously published literature on roof reflector resonators is reviewed in Chapter II. Articles that have been found directly involving the present topic are briefly summarized in two areas: experimental work and theoretical work. A short discussion emphasizes the important results of the other authors which have influenced the development of this theory.

( Chapter III considers roof reflectors individually. First, the class of reflectors considered here is shown, by geometrical demonstrations, to preserve the mechanical stability of roof reflectors with  $90^\circ$  roof angles. Second, the basic analytic tool used in geometric optics - the ray transformation matrix - is derived for a roof reflector. This is done in two dimensions, but is extended to three dimensions in later chapters.

Chapter IV combines two roof reflectors to form a laser resonator and treats the first of the two special configurations: roofs parallel. Rays are traced through this resonator and its equivalent waveguide with the matrix transformation derived in Chapter III. Stable rays are shown to be possible in an infinity of different geometric patterns, but these patterns are shown to be of only two

basic types which depend on resonator dimensions. The dimensions necessary for the stable rays to exist are given as the stability conditions. The resonant modes of the parallel-roof resonator are then predicted, based on the geometric theory.

Crossed-roof resonators are next treated in Chapter V. At first, both variant angles are taken to be zero; then one zero and one non-zero; finally both non-zero. An infinity of patterns is again shown to be possible, depending on the resonator dimensions, but they are related to those in Chapter IV. Again the resonator dimensions are given as the stability conditions, and the resonant modes of the crossed-roof resonator are predicted.

Finally, Chapter VI summarizes stability conditions from the previous two chapters. Based on the resonant modes predicted by the geometric theory, the major conclusion of this thesis is drawn: roof reflectors with roof angles less than  $90^\circ$  are more desirable in laser resonators than right-angled roof reflectors. Recommendations for areas of future study are then made with emphasis on problems relating to the design of laser systems using roof reflector resonators.

## II. The Literature of Roof Reflectors

The use of roof reflectors in laser resonators is not a new idea. Gould, et al., remark in a footnote that "a laser cavity of a crossed pair of  $90^\circ$  roof prisms was first described in an unpublished proposal to ARPA [Advanced Research Projects Agency], December 1958." (Ref 18:534) Since then, reports of the use of roof reflectors as static elements (not spinning Q-switch prisms) in laser resonators have been infrequent compared to the attention given spherical mirrors.

This chapter summarizes the relevant literature found during the course of thesis research. First, experimental papers are grouped together, and second, theoretical work is presented topically. The important results from both experimental and theoretical papers that influenced the development of this geometric theory are then discussed.

### Experimental Papers

There has been a variety of experiments using roof reflectors. Both parallel-roof and crossed-roof configurations have been studied.

Fabry-Perot Interferometer. The first experiments with roof reflector resonators appears to have been done by Gould, Jacobs, Rabinowitz, and Shultz in 1962. (Ref 18) Their work involved a Fabry-Perot interferometer in which  $90^\circ$  roof reflectors replaced the usual plane mirrors. Figure 2 shows the basic experimental arrangement these authors used to observe that the crossed-roof configuration indeed has relaxed alignment tolerances. Here, roof edges  $R_1$  and  $R_2$  are spaced an axial distance,  $L$ , apart, and the axis of the

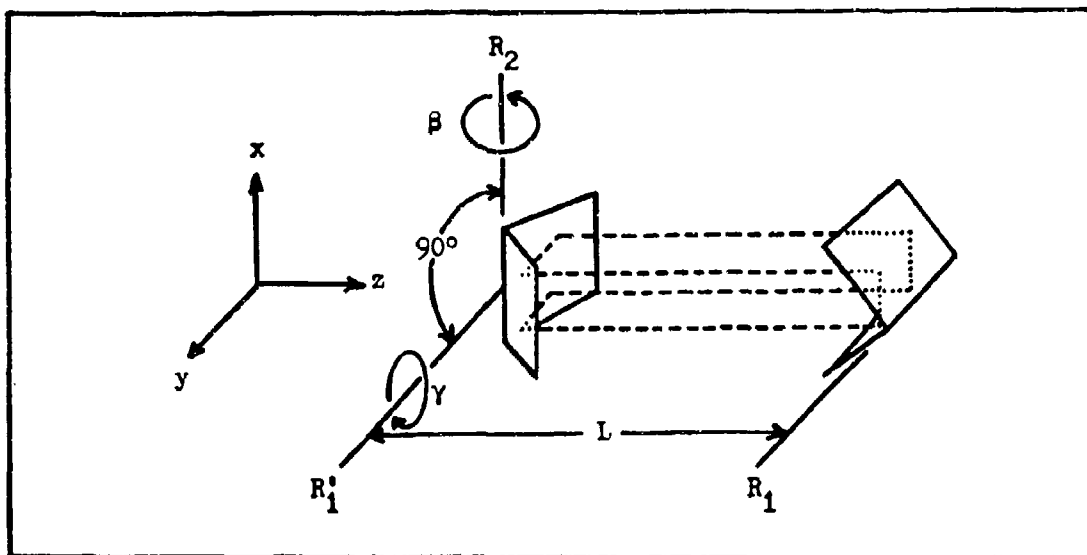


Fig. 2. Crossed-Roof Reflector Interferometer  
(After Ref 18:533)

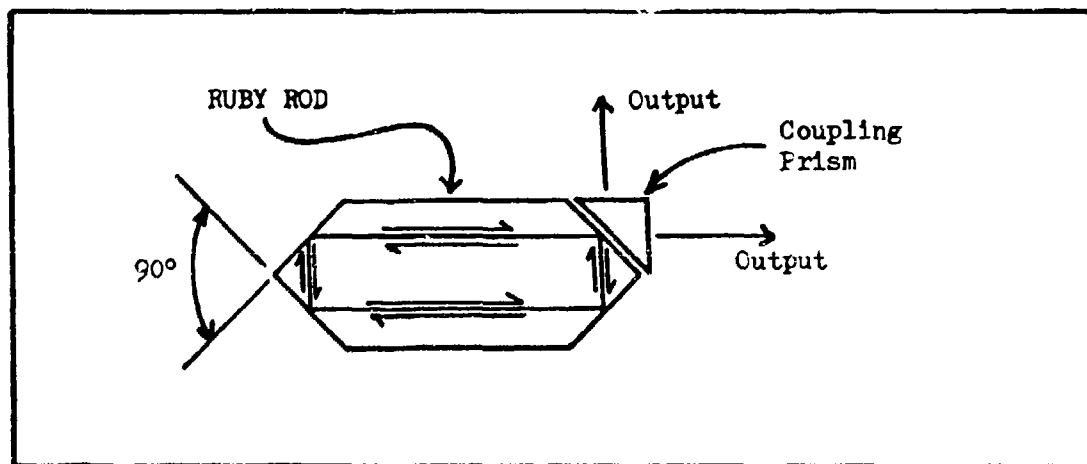


Fig. 3. Total Internal Reflection Laser Resonator  
(After Ref 3:1833)

interferometer is a line perpendicular to both roof edges. Line  $R_1'$  is parallel to  $R_1$ .

These experimenters observed Haidinger fringes with the same angular spacing and free spectral range as those in a plane Fabry-Perot with mirror spacing  $2L$ . They noted that rotating the left roof reflector around its roof edge - the  $\beta$ -direction in Fig. 2 - did not change the fringe pattern. Also, rotation around  $R_1'$  - the  $\gamma$ -direction - was seen to merely tilt the optic axis and consequently reduce the aperture. These greatly improved freedoms in the alignment of the crossed-roof interferometer thus led these authors to conclude that there is always a single direction in which rays (dashed lines in Fig. 2 ) remain undeviated - namely parallel to the optic axis.

Gould, et al., go on to predict that, if the crossed-roof interferometer were used for a laser resonator, there would always be at least one mode; and it would be the same as for a plane mirror resonator. They further suggest that, because of the mechanical alignment stability of rays parallel to the axis, the resonator would operate in just a single mode. It is also noted in the paper that the cavity of Fig. 2 has only two plane eigenpolarizations and that they become interchanged by the crossed roofs.

Roof-top Ruby Rods. The total internal reflection principle has been used with ruby lasers since 1962. In an experiment by Bergstein, Kahn, and Shulman (Ref 3), the ends of a ruby rod were shaped like roof reflectors, and outcoupling was accomplished by frustrated total internal reflection through one of the angled ruby faces (see Fig. 3 ). Similar experiments by Bertolotti, Muzii, and Sette (Ref 4) used roof

prisms in optical contact with the faces of a ruby rod, while outcoupling was through the slightly flattened roof edge of one of the prisms. These devices were observed to lase satisfactorily, with the output polarizations being dependent on the alignment of the roof edges with respect to the ruby crystal axes (investigated by Gibbs and Whitcher, Ref 17).

In general, the configurations studied by all of the above experimenters were parallel-roof, and more than one output was observed. This is shown in Fig. 3, which is the experimental arrangement used by Bergstein, et al., who noted the phenomenon and offered this explanation:

"...other optical-maser resonator cavities use either metallic or multi-layer dielectric coating of the end walls to normally reflect the light beam. As a result a definite phase relationship exists between the two contradirectionally traveling wave systems. No such relationship is established by the boundary conditions existing in the total reflection resonator. It would therefore appear that this configuration can support two mutually independent contradirectionally traveling resonant wave systems. The only process which might couple these two wave systems is the emission process." (Ref 3:1833)

Multiple Mode Operation. A roof prism was used as an end reflector in a He-Ne laser system at  $1.15\mu$  by DeLang and Bouwhuis in 1963 (Ref 14). Their experimental arrangement is shown in Fig. 4(a), where A and B are prism surfaces where total internal reflection takes place, and C is a flat multilayer interference mirror. The front face of the prism is at Brewster's angle to the axis of the gas tube, and its roof angle is slightly less than  $90^\circ$ . Drawings (b) - (d) of Fig. 4 are equivalent to the resonator, and the roof angle between surfaces A and B is  $90^\circ - \alpha$  where  $\alpha = 0.0020$  radians - the index of refraction

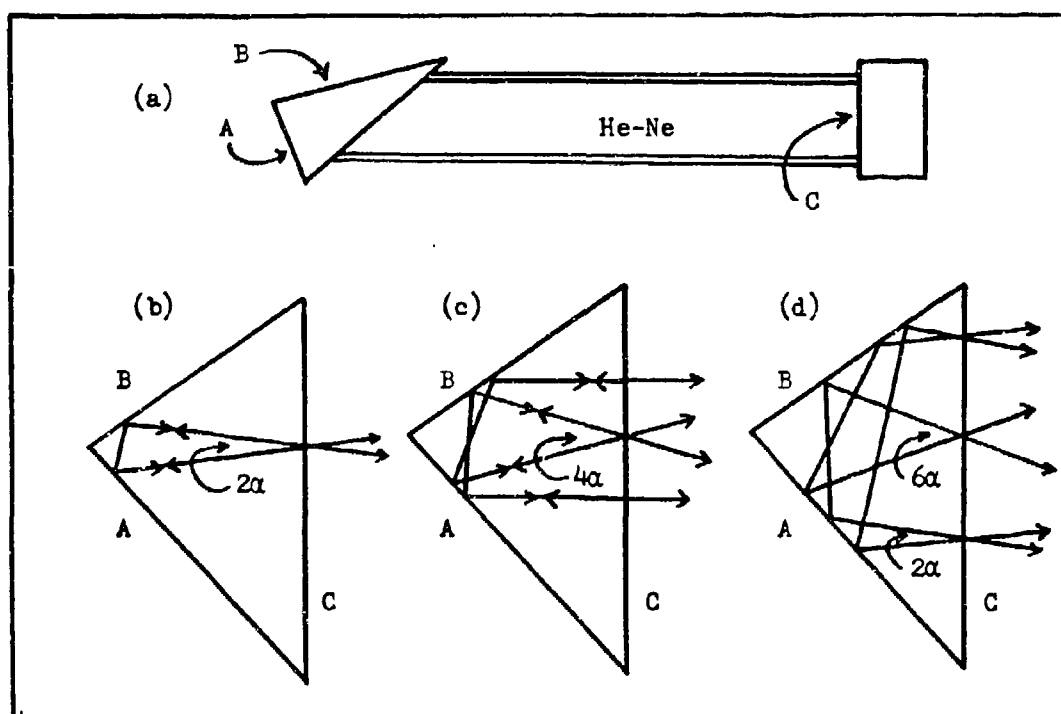


Fig. 4. DeLang and Bouwhuis' Experiment  
(After Ref 14:48, 49)

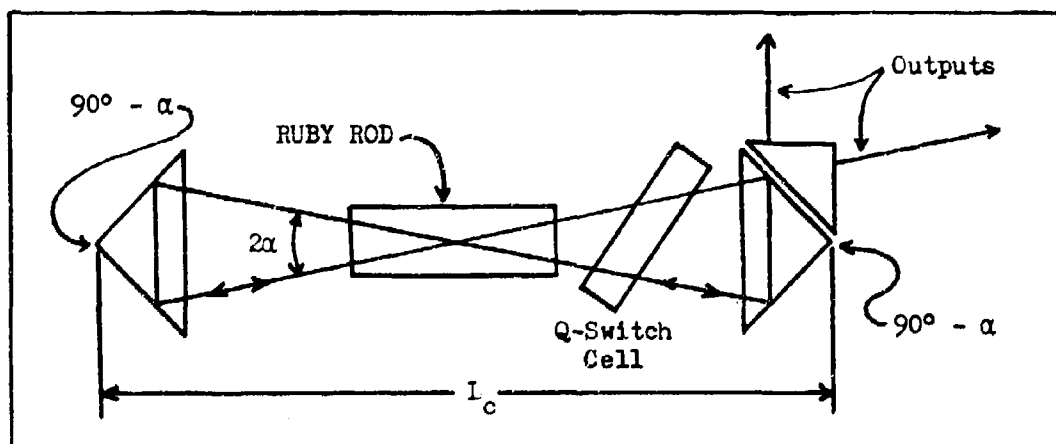


Fig. 5. Soncini and Svelto's Experiment  
(After Ref 39:262)

of the prism having been taken into account. Only the relationship between the reflecting surfaces is shown.

DeLang and Bouwhuis observed their system to lase in the different modes shown in Fig. 4(b) - (d). Significantly, the first and second of these were seen to occur simultaneously. Also, the different modes were generally seen to have the multiple outputs shown in the drawings, and these beams were noted to form interference patterns on the surface of mirror C. This implies that standing waves were present in the resonator "built up from two coherent oppositely travelling waves, which probably choose their phase relation  $\delta$  for minimum loss, e.g. in such a way that their interference pattern on the dielectric mirror has a minimum integrated intensity." (Ref 14:49) These are similar to the patterns obtained by Ledger (Ref 27) to confirm standing waves in a laser resonator.

Travelling waves were also obtained, but only in the mode of Fig. 4(b). The experimenters found this possible by deliberately spoiling the quality factor of the resonator in one direction with a wedge-shaped glass plate in optical contact with one of the prism faces.

Single Mode Operation. Roof prisms with roof angles smaller than  $90^\circ$  have also been used with solid state lasers, beginning in 1967. Soncini and Svelto (Refs 39 and 40) and Cubeddu, Polloni, Sacchi, and Svelto (Ref 11) have used pairs of  $90^\circ - \alpha$  prisms, in a parallel-roof configuration, to obtain outputs consisting of pure modes in pulsed ruby lasers. The basic experimental arrangement used by these authors is shown in Fig. 5.

In all experiments the output was found to be highly repeatable from pulse to pulse. Soncini and Svelto state, for example, that "Once a  $TEM_{00}$  mode is obtained, it is usually preserved from threshold to  $\approx 30\%$  above threshold...." and that "...the beam divergence of our  $TEM_{00}$  mode is almost diffraction limited, whereas a  $\approx 5$  mrad divergence has been measured in the case of the plane-parallel resonator." (Ref 39: 262) Using a Fabry-Perot interferometer, "it was also checked that the output beam was constituted of a single longitudinal mode." (Ref 40: 422)

The high-purity modes were explained by these authors to be due to two circumstances: (1) since the beam passes through the ruby rod twice, the cavity averages internal distortions and crystalline imperfections and (2) the spot size of the beam (half-width at  $1/e^2$  intensity points) depends on thermal lensing in the ruby rod due to pump light heating. (Ref 24:321, 338) The spot size,  $w$ , then determines a critical resonator axis length:

$$L_c \approx \frac{2w}{\alpha} \quad (1)$$

where  $\alpha$  is the variant angle of the prisms. Then "if the length  $[L]$  of the cavity is greater than  $[L_c]$ , the edges of the prisms are not involved in laser action and oscillation takes place according to the path [of Fig. 5 ]." But "If the length of the cavity is smaller than  $[L_c]$ , laser action extends over the prisms edges, no pure modes are observed and the beam becomes similar to that observed with plane or spherical mirrors." (Ref 39:262)

Recent Experiments. Since 1972, Teppo has used roof reflectors in a compact Nd:YAG laser system intended for use as an airborne target designator (Refs 42 and 43). In one experiment, a 90° roof prism was tested in a resonator with a 70% reflecting flat mirror. Thus, in Fig. 2, the right roof reflector was replaced with the flat mirror, and rotation of the left roof reflector around its roof edge showed no appreciable degradation in output energy through the flat mirror. Rotation of the roof reflector in the y-direction of Fig. 2, however, showed that it had alignment tolerances similar to a large-radius curved mirror. Teppo's experimental data is shown in Fig. 6 together with his test results of a 10 meter radius mirror for comparison.

Using the same arrangement, Teppo also measured the uniformity of the output beam of the Nd:YAG laser when operating non-Q-switched at 10pps. His results are shown in Fig. 7, where typical burn patterns are on the left and a scan trace on the right. (The scan was taken perpendicular to the roof edge and was done with an SGD-100 photodiode, with an 0.030 inch aperture, moved across the beam at 0.78 inch per minute - 0.065 inch per division on the oscilloscope trace. The scan photograph thus provides a time-averaged beam uniformity profile.) As can be seen from Fig. 7, "The roof prism tested did not lase particularly well near the roof edge, and the bimodal lasing structure normal to the roof edge is evident." (Ref 42:157) Teppo also states as a qualitative observation that "Compared with a simple end mirror, generally the roof-prism end reflector...increases the raw-beam divergence and beam non-uniformity." (Ref 42:25)

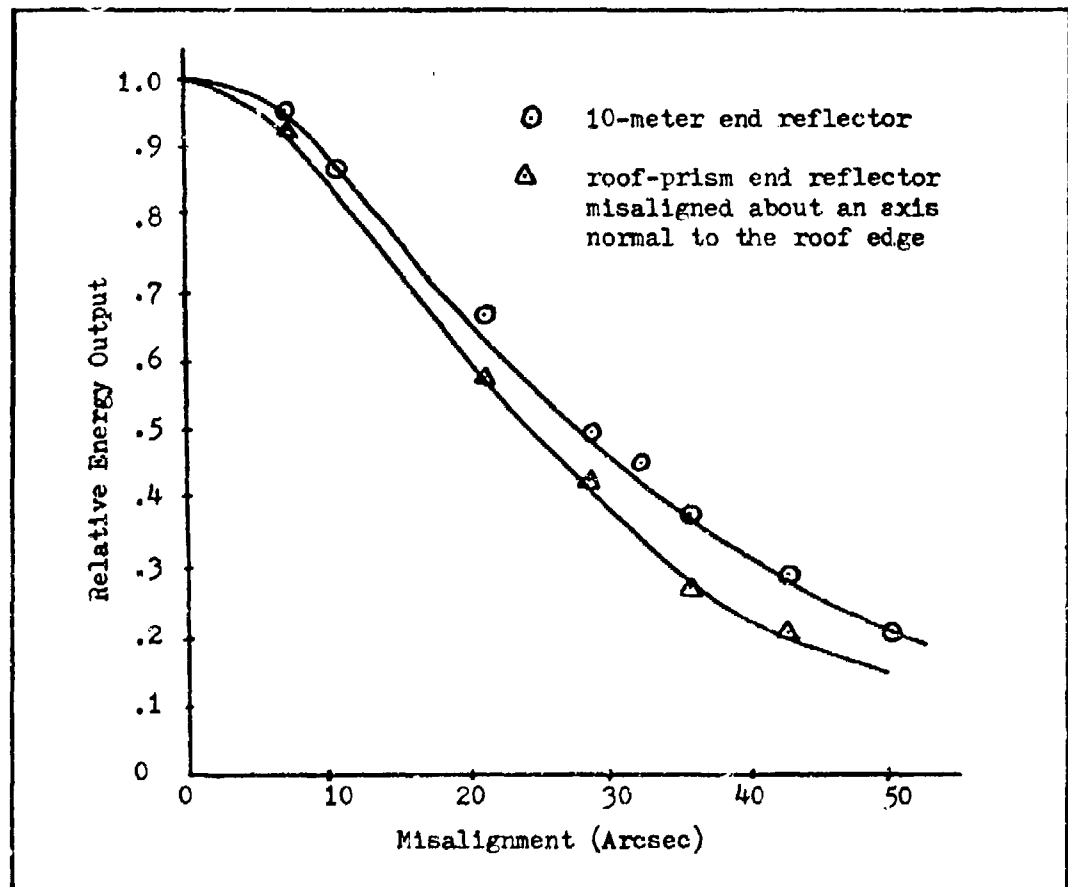


Fig. 6. Roof Reflector Misalignment Sensitivity  
(From Ref 42:28)

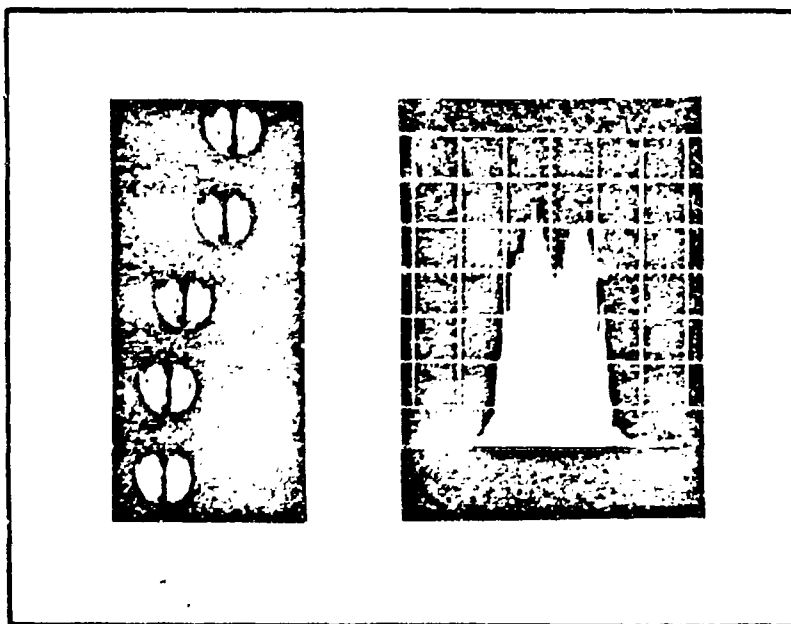


Fig. 7. Laser Output Using One  $90^\circ$  Roof Reflector (From Ref 42:162)

The roof prism used by Teppo was not a perfect specimen, but was reported to have had "several burn spots near the roof edge." (Ref 42:24) He states, however, that other experimenters obtained similar non-uniformity results with contractor-supplied prisms. (Ref 42:24) In general, the specifications on the prisms state that "The [roof] edge shall be a maximum of .002 inches wide without pits or fissures..." (Ref 43:33) Thus, the typical prism, with which the results of Fig. 7 were obtained - has a roof edge on the order of 50 wavelengths wide at optical frequencies.

#### Theoretical Papers

Methods which have been used to analyze laser resonators include (1) the geometric approach by matrix optics and (2) computer solutions for resonant modes and eigenvalues. Accordingly, some work has been done on roof reflector resonators in both areas, and is reviewed below. A procedure for calculating the eigenstates of polarization has also been given and is included under a separate heading.

Geometric Approach. Rather than roof reflectors, a paper by Kahn (Ref 21) considers the related case of dihedral reflectors. Dihedral reflectors, like roof reflectors, are made of two planar surfaces joined at an edge, but the angle is close to  $180^\circ$  rather than  $90^\circ$ . The difference between the two types of reflectors is that rays are reflected from only one surface of a dihedral reflector, while they are reflected from both surfaces of a roof reflector.

Kahn shows that if a light ray in a resonator is characterized (in two dimensions) by its distance from the axis,  $x$ , and its slope with

respect to the forward direction,  $\theta$ , and ordered as a column vector:

$$\vec{x} = \begin{bmatrix} x \\ \theta \end{bmatrix} \quad (2)$$

then it is transformed by a dihedral reflector with the transformation (Ref 21:866):

$$\begin{bmatrix} x_r \\ \theta_r \end{bmatrix} = \begin{bmatrix} A & B \\ C & D \end{bmatrix} \begin{bmatrix} x_1 \\ \theta_1 \end{bmatrix} + \begin{bmatrix} E \\ F \end{bmatrix} \quad (3)$$

where subscript r refers to the reflected ray, subscript 1 refers to the incident ray, and matrix elements A - F are characteristics of the dihedral reflector. If only paraxial rays are considered, these matrix elements are independent of ray parameters, and Eq. (3) is linear.

(Note that if  $E = F = 0$ , this is the form of the matrix transformations for thin lenses and curved mirrors.)

Using Eq. (3), Kahn shows that stable rays in dihedral reflector resonators are bounded by an envelope. This envelope is the most significant result of Kahn's geometric solution, because "such contours, which form the boundary between geometric-optically accessible and inaccessible regions are indicative of the variation in the over-all intensity distribution within the resonator." (Ref 21:867)

Another theoretical paper by Ronchi (Ref 34) uses the geometric approach to find sets of circles that fit inside the parallel-roof resonator. The circles are shown to be caustic surfaces for high-order Bessel functions chosen in such a way as to match boundary conditions on the surfaces of the roof reflectors. As in Kahn's work, the caustic surfaces separate regions of high and low fields so that the

resonant modes are exponentially low in the region of the edges of the reflectors. Thus, Ronchi shows, diffraction at the edges can be neglected.

Numerical Approach. The integral equations of laser resonator theory (Ref 16) were computer-programmed for roof reflector resonators by Pasqualetti and Ronchi in 1974 (Refs 31 and 32). The particular geometry that they studied was the parallel-roof configuration with the (equal) variant angles no larger than about five degrees. Since their work was motivated by other research in microwave theory, the dimensions used were typically small in terms of wavelengths ( $\lambda$ ): axis length  $L = 100\lambda$  and half-aperture  $a = 10\lambda$ . (Distance  $\overline{AD}$  in Fig. 1 is said to be the full aperture dimension.) Thus, the Fresnel number,  $N = \frac{a^2}{L\lambda}$ , of the resonator was on the order of 1.

Regardless of the resonator dimensions, Pasqualetti and Ronchi's numerical approach was correct for the geometry considered, and the field amplitudes and phases of the resonant modes were computed and plotted. When  $\alpha > 0^\circ$ , the resonant modes were generally found to be narrow in field distribution, and they propagate through the resonator on a path shown in Fig. 8. Of this, the authors say:

"For symmetry reasons, the beam propagating in the indicated way has to be accompanied by a beam propagating in the reverse way. An even mode is formed by two beams with the same amplitude and phase at the points of the resonator axis; for an odd mode, the phase of the two beams differ by  $\pi$  at the points of the axis. Thus, one and the same beam may form either an even or an odd mode of the roof mirror resonator. In a first approximation, apart from deformations due to diffraction, these beams should be the modal beams of a [Fabry-Perot] resonator..." (Ref 31:294)

As for diffraction, Pasqualetti and Ronchi conclude in their second paper "By noting that in a quasi-corner mirror [ $\alpha \approx 0^\circ$ ] resonator a

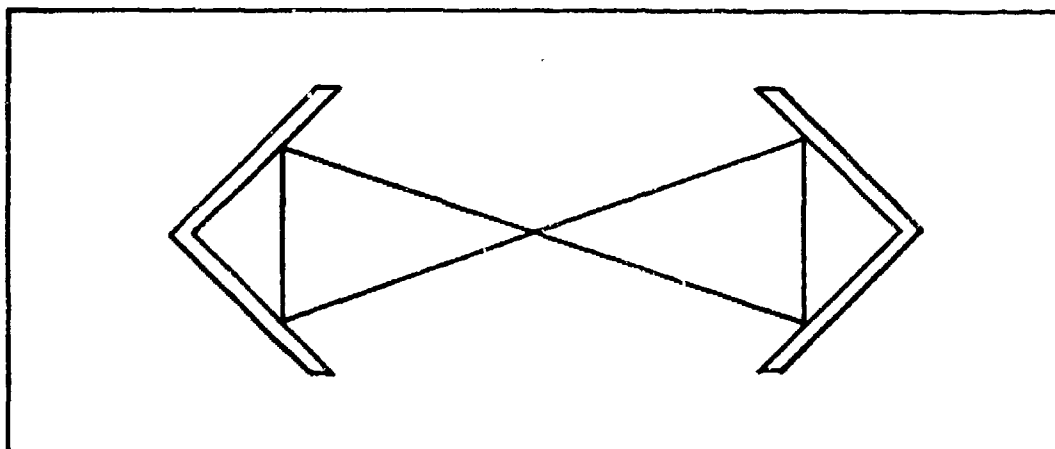


Fig. 8. Pasqualetti and Ronchi's Result For  $\alpha > 0^\circ$   
(From Ref 31:293)

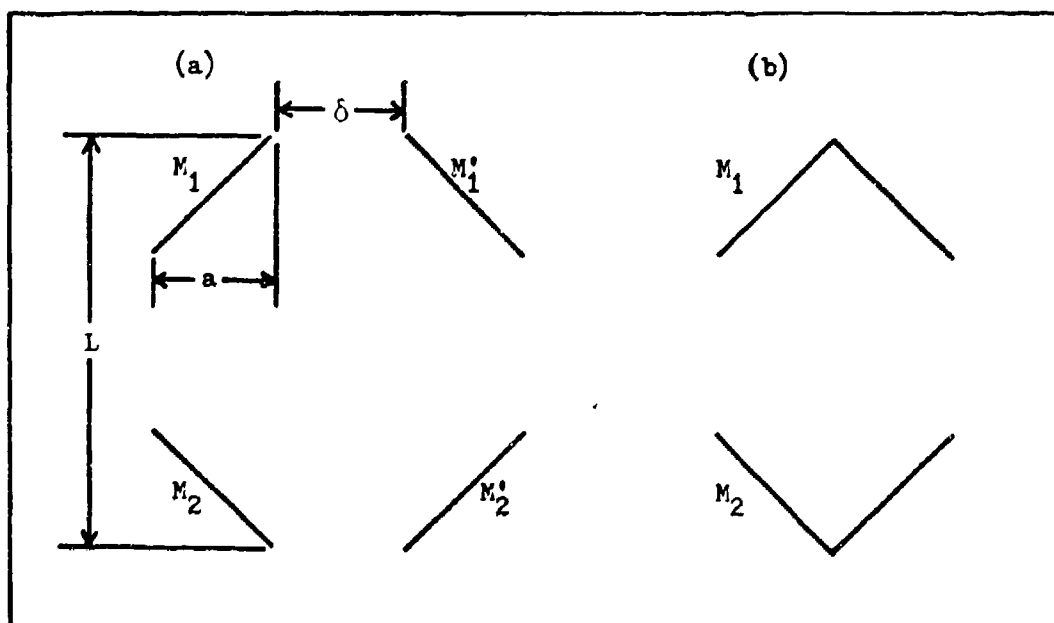


Fig. 9. Four-mirror Ring Resonator and Its Limit  
(After Ref 36:1051)

beam interacts with a mirror twice per transit, we deduce that diffraction deforms the field configurations in such a way as to diminish the losses." (Ref 32:654)

In certain instances then, Pasqualetti and Ronchi noted that their theoretical resonator appeared to operate as a four-plane-mirror resonator rather than as a two-roof-mirror resonator. This case was studied independently by Checcacci, Falciai, and Scheggi in 1974 (Refs 8 and 36). They considered the  $90^\circ$  roof reflector resonator as a limiting case of a four-plane-mirror ring resonator; the problem that these authors programmed is shown in Fig. 9, where  $\delta$  is a spacing that was variable. The dimensions considered were again motivated by microwave theory, but Fresnel numbers as large as 10 were used.

Figure 10 shows typical numerical results where the field amplitude is plotted as a function of distance perpendicular to the resonator axis. The half-aperture dimension,  $a$ , and its position is indicated in each plot, and the spacing,  $\delta$ , is also shown. It is evident that a broad, centralized field distribution - when  $\delta = 0$  - quickly separates and narrows as  $\delta$  increases. At a separation of  $\delta = 32\lambda$ , the resonator is clearly operating as a ring, and the field distribution on one side of the resonator does not disturb that on the other side, as is evidenced by the lack of interference in Fig. 10(d), compared to (b).

Polarization Calculation. A method for calculating the eigenpolarizations in a roof reflector resonator has been given by Bobroff (Ref 5). His procedure uses  $2 \times 2$  matrices to calculate the

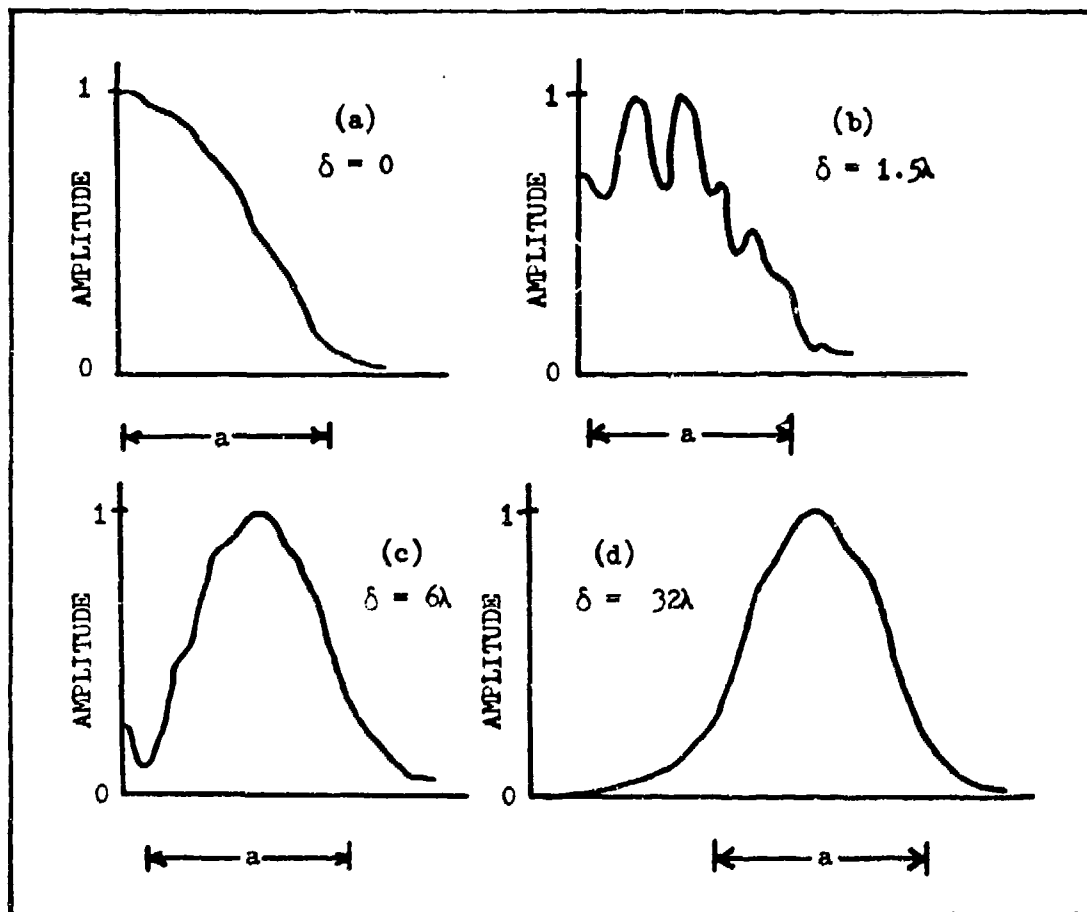


Fig. 10. Numerical Solutions for Ring Resonator  
(From Ref 36:1051)

round-trip phase changes of electric field components initially chosen parallel and perpendicular to one of the roof edges. A computation of the eigenvalues of the round-trip phase-change matrix, and its subsequent diagonalization, gives the eigenpolarizations of the resonator.

For the two special cases of roofs parallel and crossed, Bobroff's theory shows that the two eigenpolarizations are plane polarizations oriented either parallel or perpendicular to the roof edges, and the eigenvalues are unity. This can also be seen by inspection, since only plane polarizations whose plane of vibration is parallel or perpendicular to a roof edge are reflected from a roof reflector with their plane of vibration unchanged. (Ref 6:41-51)

#### Discussion

All of the above papers have been considered in the development of the present geometric theory. Primarily, the experimenters' observations on the outputs of working laser systems have been most influential.

Operation as a Ring. Geometrically speaking, the beam paths that DeLang and Bouwhuis (Fig. 4(b) ) and Soncini and Svelto (Fig. 5 ) have observed in their lasers are the same except that in the former the roof reflector is imaged by the plane mirror. These are clearly ring-type beams since rays traveling in either direction close on themselves, and this is the same behavior as the computer solutions of Pasqualetti and Ronchi (Fig. 8 ).

Even for the case of 90° roof reflectors, the burn pattern and scan trace by Teppo (Fig. 7 ) suggest that the laser is operating as a ring. This is further emphasized by the computer solutions of Checcacci, et al., (Fig. 10(d) ) where a spacing between the roof reflector surfaces of  $32\lambda$  gives ring-type operation. This spacing is the same order of magnitude as the width of the roof edges on the prism used by Teppo. So it is deduced that real roof reflector resonators operate as ring resonators, and stable rays of this type are therefore sought by this geometric theory. (A geometric theory for curved-mirror ring resonators has been given by Clark, Ref 10, and by Rigrod, Ref 33.)

Physical Modes. The modes observed by Teppo were evidently not of high purity. In his experiment, as with the roof-top ruby rod experiments and Checcacci's computer work, the roof edges are not geometrically excluded. Only in the computer solutions are the roof edges of the 90° roof reflectors perfect - the space being in effect a perfect absorber. Real devices, therefore, probably suffer from diffraction effects caused by their imperfect roof edges. (Checcacci and Scheggi - Ref 9 - built and tested a microwave model to confirm their numerical predictions. Roof edge diffraction was not observed, but the wavelength,  $\lambda = 3$  cm, was much larger than any imperfections in the apparatus.)

In contrast, Soncini and Svelto's modes are of high purity. In their case, as with the patterns drawn for DeLang and Bouwhuis' resonator, the roof edges are apparently excluded. If this is indeed the case, then Kahn's statement (see p. 19) applies and Ronchi's work

can be extended to show that diffraction by the roof edge can be neglected. This seems to be possible when roof angles less than  $90^\circ$  are considered; that is, therefore, the class of roof reflectors studied here. (Hermite-Gaussians propagating linearly are more typical at optical frequencies than Ronchi's cylindrical Bessel functions, but both are exponentially low in the region of the roof edges and the reflector edges.)

The question of counter-traveling waves also seems partly satisfied by using  $90^\circ - \alpha$  roof reflectors. When the two waves cross one another, they are apparently coupled by the lasing medium, and standing waves are formed. Standing waves were, in fact, observed to be the usual case by DeLang and Bouwhuis; so it will be assumed that the resonant modes in the resonators studied here are generally standing waves. (It will later be shown that, in the crossed-roof resonator, a single beam does not cross itself, but it is still reasonable to expect standing waves.)

Geometric Tools. Since the roof reflectors considered here are not necessarily right-angled, the mechanical stability noted by Gould, et al., is no longer generally valid. It is shown below, however, that rotation of an individual  $90^\circ - \alpha$  roof reflector around its roof edge does not affect a resonator. Thus,  $90^\circ - \alpha$  roof reflector resonators still have relaxed alignment tolerances and Gould's concept that there will always be at least one mode still applies.

To determine whether a given resonator is otherwise stable, the paper by Kahn has had the most influence on the present work. His inhomogeneous ray transformation, Eq. (3), is the primary geometric

tool that has been used here. With Eq. (3), rays can be traced through a roof reflector resonator, and established as stable ring-type rays if they close on themselves. The resonator dimensions become the determining factor as to whether this is possible and are the sought-after stability conditions. The stability conditions found in this manner are, not surprisingly, similar to the critical length, Eq. (1), computed by Soncini and Svelto.

### III. Characteristics of Roof Reflectors

The most well known characteristic of  $90^\circ$  roof reflectors is that the direction of a reflected ray remains unchanged as the reflector is rotated around its roof edge ( $\beta$ -direction in Fig. 2 ). In this chapter, it is first shown that this is true for the  $90^\circ - \alpha$  roof reflector; and second, Eq. (3) is developed for tracing rays in roof reflector resonators.

#### Rotational Invariance

To demonstrate that the direction of a reflected ray is not altered when a  $90^\circ - \alpha$  roof reflector is rotated around its roof edge, a convenient way of visualizing the reflector as "unfolded" is introduced here. Once this property is established, the physical dimensions of a  $90^\circ - \alpha$  roof reflector are used to define quantities which will be useful in later chapters.

Ray Crossing Angle. For roof reflectors with roof angle  $90^\circ - \alpha$ , it is noted that a ray is no longer retro-reflected parallel to its incident direction. Consider, for example, the roof reflector of Fig. 11 where a ray crosses itself at P after two reflections at  $B_1$  and  $B_2$ . The ray crossing angle, Angle  $B_1PB_2$ , is found by the following geometric considerations (Ref 7:178-179).

Let constructions  $\overline{FB_1}$  and  $\overline{FB_2}$  be normals to their respective surfaces. Then from quadrilateral  $B_1FB_2V$ :

$$\text{Angle } B_1FB_2 = 90^\circ + \alpha \quad (4)$$

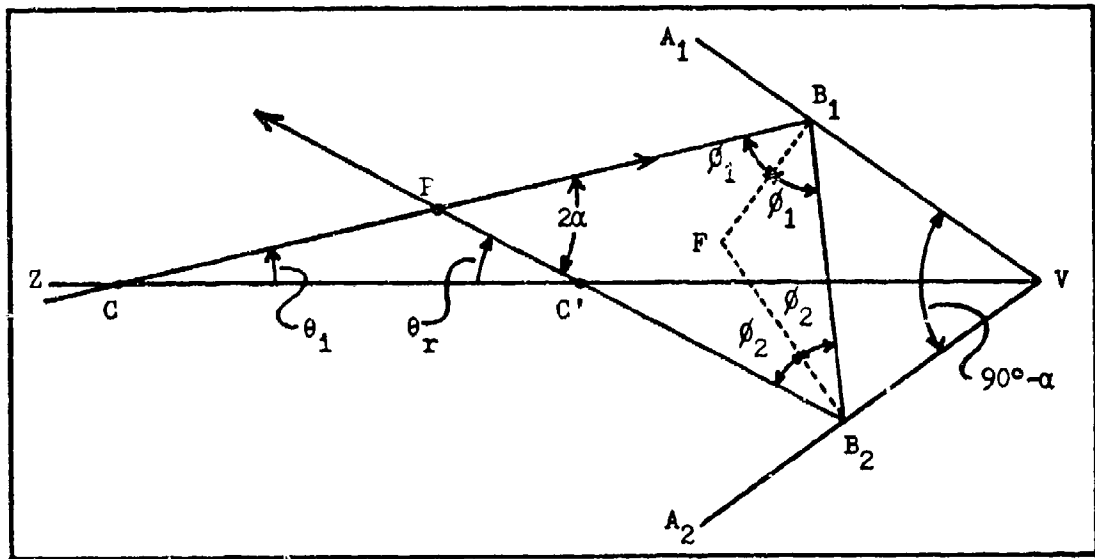


Fig. 11. Ray Crossing Angle

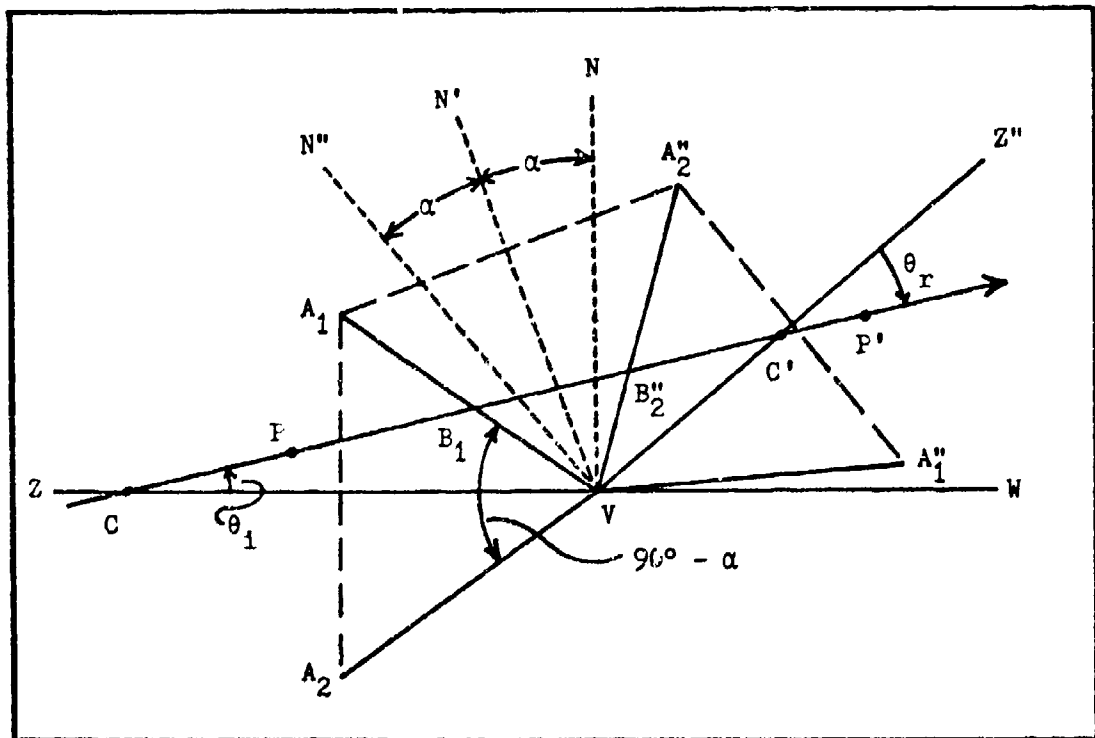


Fig. 12. Unfolded Roof Reflector

From triangle  $B_1PB_2$ , it follows that:

$$\phi_2 = 90^\circ - \alpha - \phi_1 \quad (5)$$

Then, since the reflections are specular, the result from summing the angles in triangle  $B_1PB_2$  is

$$\text{Angle } B_1PB_2 = 2\alpha \quad (6)$$

Also, since the incident ray makes an angle  $\theta_1$  with the axis of the roof reflector,  $\overline{ZV}$ , and the reflected ray makes an angle  $\theta_r$ , from triangle CPC':

$$\theta_1 + \theta_r = 2\alpha \quad (7)$$

where both ray angles are measured with respect to the forward direction of the ray.

Unfolded Roof Reflector. A construction which will be useful later is shown in Fig. 12. (Ref 45:713) In this drawing, line  $\overline{ZW}$  is the axis of roof reflector  $A_1VA_2$ , while line  $\overline{NV}$  is normal to the axis. The image of the roof reflector in its own surface,  $A_1V$ , is  $A_1VA_2''$  with axis  $\overline{N'V}$ . The second image - in surface  $A_2''V$  - is  $A_1''VA_2''$  with axis  $\overline{Z''V}$  and normal to this axis  $\overline{N''V}$ . Each of the two reflections, or "unfoldings," amounts to a rotation of the roof reflector through  $90^\circ - \alpha$  around its roof edge, V. The second image thus faces  $180^\circ - 2\alpha$  from the roof reflector's direction so that the image axis,  $\overline{Z''V}$ , makes an angle  $2\alpha$  with the real axis. Axis  $\overline{ZV}$  and its image - and normal  $\overline{NV}$  and its image,  $\overline{N''V}$  - are seen to be symmetrically positioned with respect to line  $\overline{N'V}$ , which acts the same as a plane mirror except that

the image (which has actually undergone two reflections) is inverted. Line  $\overline{N'V}$  is inclined to  $\overline{NV}$  at an angle  $\alpha$  and, in this case, is coincident with the first image axis.

A ray, such as in Fig. 11, can be unfolded into a straight line. Thus a ray from P, making an angle  $\theta_1$  with the real axis, passes through its twice reflected image point, P', and makes an angle  $\theta_r$  with the image axis. (But P' is not the reflection of P in line  $\overline{N'V}$  unless P lies on the axis, in which case  $\overline{PP'}$  is perpendicular to  $\overline{N'V}$ .) The distance  $\overline{PP'}$  is equal to the distance  $\overline{PB_1} + \overline{B_1B_2} + \overline{B_2P}$  in Fig. 11 (Ref 35:1191-1192), and the same angular relationships hold. The latter may be seen from triangle CVC' in Fig. 12. The sense of  $\theta_r$  has been inverted, however.

Rotation Around Roof Edge. If axis  $\overline{ZV}$  and direction  $\overline{N'V}$  (in Fig. 12) are thought of as fixed in space, and the roof reflector is rotated around its roof edge by an arbitrary angle  $\beta$ , Fig. 13 results. The first and second images - and the axes  $\overline{YV}$ ,  $\overline{Y'V}$ , and  $\overline{Y''V}$  as well - are seen to be rotated an angle  $\beta$  with respect to the fixed direction. Now, the first image of the fixed axis,  $\overline{Z'V}$ , is tilted  $2\beta$  with respect to its former direction, but  $\overline{Z''V}$  remains stationary. This may be demonstrated as follows:

$$\text{Angle } ZVA_1 = \frac{90^\circ - \alpha}{2} - \beta \quad (8)$$

$$\text{Angle } Z'VA_1 = \text{Angle } ZVA_1 \quad (9)$$

$$\begin{aligned} \text{Angle } Z'VA_2 &= (90^\circ - \alpha) - \text{Angle } Z'VA_1 \\ &= \frac{90^\circ - \alpha}{2} + \beta \end{aligned} \quad (10)$$

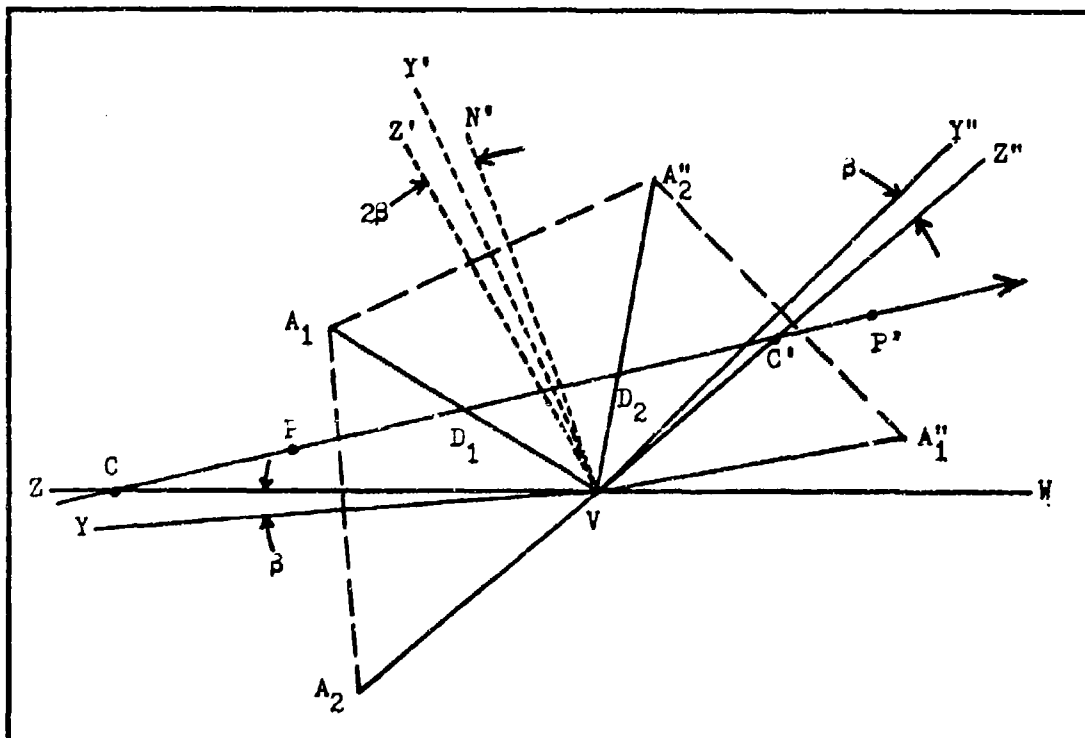


Fig. 13. Roof Reflector Rotated Around Its Roof Edge

$$\text{Angle } Z''VA''_2 = \text{Angle } Z'VA''_2 \quad (11)$$

Therefore, by summing Eqs. (8) through (11):

$$\text{Angle } ZVZ'' = 180^\circ - 2\alpha \quad (12)$$

which is independent of  $\beta$  and is the same as for a perfectly aligned roof reflector.

This demonstration could be carried out for a line from V to any arbitrary point. For the ray crossing point, P, in particular, the image point, P', unchanged; so the distance  $\overline{PP'}$  is a constant and the ray holds an invariant relationship to axes  $\overline{ZV}$  and  $\overline{Z''V}$ . Therefore, the direction of the reflected ray is unaltered and a  $90^\circ - \alpha$  roof reflector indeed has relaxed alignment tolerances as does a  $90^\circ$  roof reflector. Now that this is established, all roof reflectors in subsequent work will be considered perfectly aligned and the effects of misalignment due to vibration or mechanical stress will be neglected.

Dimensions. It is apparent from Fig. 13 that all rays which cross at a distance  $\overline{PV}$  from the roof edge can be made to appear the same by rotating the roof reflector until the axis,  $\overline{YV}$ , lies through P and the image axis,  $\overline{Y''V}$ , lies through P'. In this position, let the ray be known as the "standard ray" and it is illustrated in Fig. 14, both folded and unfolded. Now let the dimension of the roof reflector's surface,  $\overline{A_1V}$ , be  $d_0$  and the distance  $\overline{B_1V} = d$ . The ray crossing distance,  $\overline{PV} = D$ , is then:

$$D = \frac{\sqrt{2}d}{4} \left[ \frac{1}{\cos \frac{\alpha}{2}} + \frac{1}{\sin \frac{\alpha}{2}} \right] \quad (13)$$

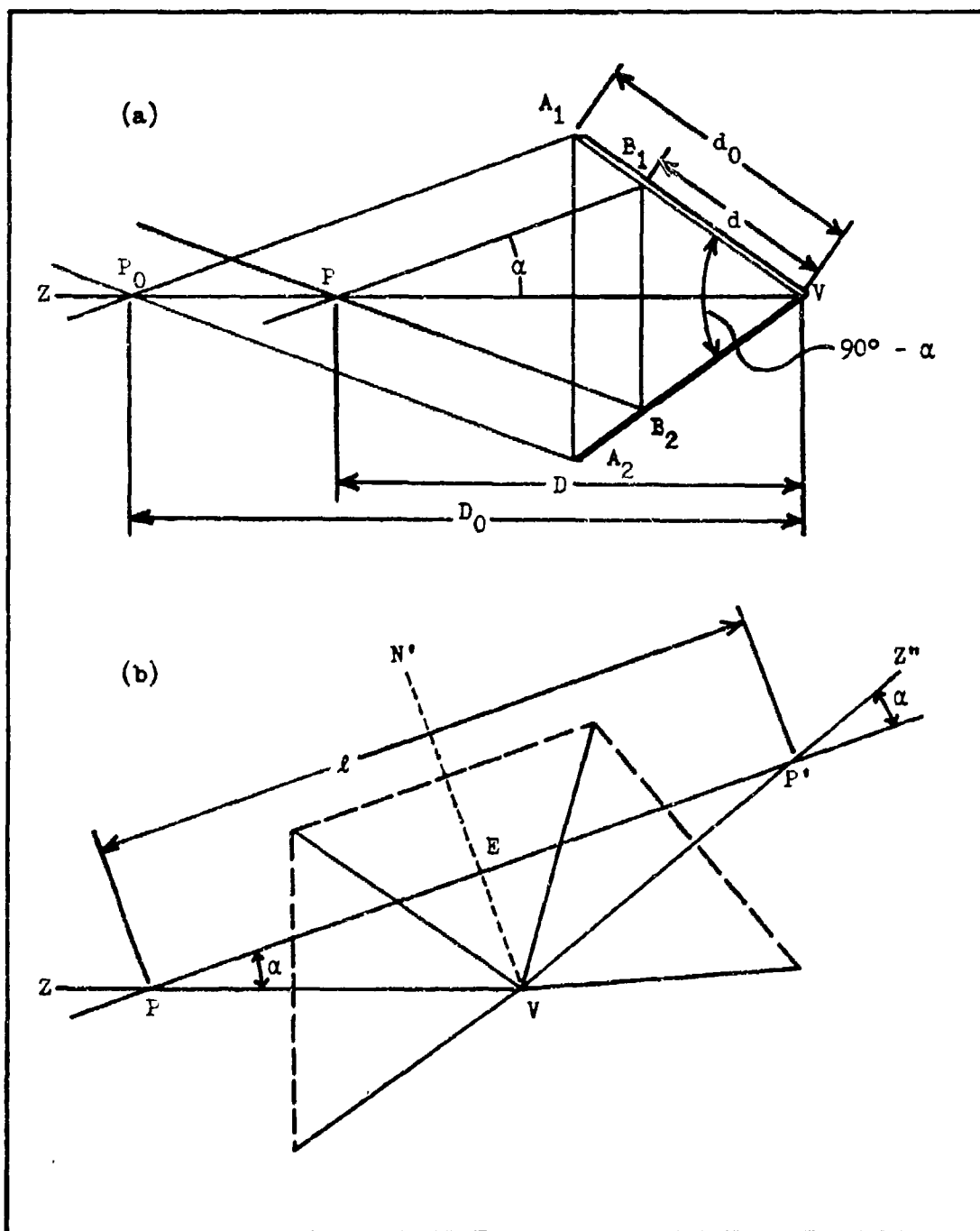


Fig. 14. The Standard Ray

If the standard ray strikes the roof reflector at  $A_1$  (that is, the aperture limit, then substituting  $d_0$  for  $d$  in Eq. (13) defines the maximum ray crossing distance,  $D_0$ . This is the greatest possible distance for which a ray can reflect from a  $90^\circ - \alpha$  roof reflector and not diverge past the aperture.

The length of the ray's path from  $P$  back to the crossing point will be important later and can easily be computed from Fig. 14(b). This distance,  $\overline{PP'} = l$ , is called the "loop length" and is

$$l = 2D \cos \alpha \quad (14)$$

For small values of the variant angle,  $\alpha \ll 1$ , first order approximations of Eqs. (13) and (14) are

$$D = \frac{\sqrt{2} d}{2\alpha} \quad (15)$$

$$l = 2D \quad (16)$$

### Roof Reflector Ray Matrix

Because roof reflector surfaces are plane mirrors, rays could be traced by considering a specular reflection at each surface. A point-imaging procedure has been worked out which does this (Ref 7:1-7), but it is more convenient to use matrix optics. This section develops the ray matrix transformation for a roof reflector.

Coordinate Transformation. Let a ray propagating through an optical system be described by the column vector of Eq. (2). Then, upon passing through an element, the input ray,  $\vec{x}_1$ , is transformed into an output ray:

$$\vec{x}_2 = \underline{M} \vec{x}_1 \quad (17)$$

where  $\underline{M}$  is a 2x2 matrix characteristic of the element. For a roof reflector, consider the plane of the transformation to be perpendicular to the optical axis through the roof edge. Then consider the input and output rays to be extended from the actual points of reflection to points  $x_1$  and  $x_2$ , respectively, as in Fig. 15(a). Thus, the input ray has coordinates  $(x_1, \theta_1)$  in the transformation plane, and the output ray has coordinates  $(x_2, \theta_2)$ . The transformation between these coordinates is

$$x_2 = - \frac{x_1 \cos \theta_1}{\cos(\theta_1 - 2\alpha)} \quad (18)$$

$$\theta_2 = - \theta_1 + 2\alpha \quad (19)$$

Optical systems involving mirrors - such as resonators - are frequently unfolded into a series of equivalent elements aligned on an axis. This is done by reflecting the output rays of the mirrors through their transform planes. Performing this operation on a roof reflector results in Fig. 15(b), where the ray is obviously discontinuous. Inverting the image in Fig. 15(c) (that is  $\vec{x}_2 \rightarrow -\vec{x}_2$ ) emphasizes the relationship between ray slopes and nearly aligns the position coordinates. One more operation - rotating the inverted image through  $2\alpha$  in Fig. 15(d) - recovers the unfolded reflector picture.

The input and output rays have now become continuous, but the optic axis is no longer straight (thus, the position coordinate,  $-x_2$ , is measured along  $\overline{N''V}$ ). From the figure, a better choice for the transform plane would apparently be  $\overline{N'V}$ , where the position coordinates

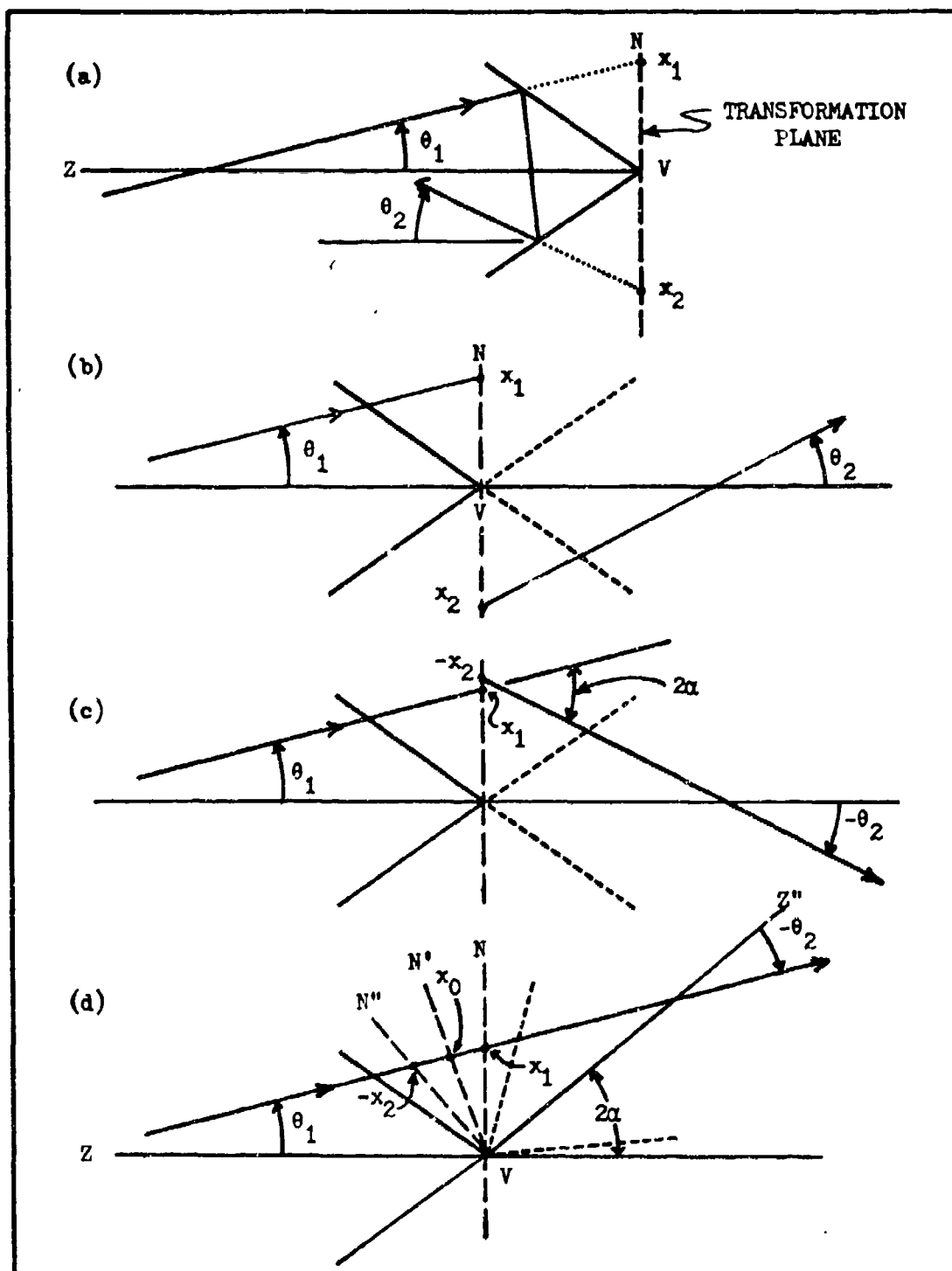


Fig. 15. Ray Coordinate Transformation

coincide at  $x_0$ . If  $\alpha$  is small and only paraxial rays are considered,  $x_1$  and  $-x_2$  approach  $x_0$ , and the transformation becomes simply:

$$x_2 = -x_1 \quad (20)$$

$$\theta_2 = -\theta_1 + 2\alpha \quad (19)$$

Homogeneous Matrix. This transformation cannot be put into the form of Eq. (17) except in the special cases of  $\alpha = 0$  or  $\theta_1 = \alpha$ .

In the first case:

$$\underline{M} = \begin{bmatrix} -1 & 0 \\ 0 & -1 \end{bmatrix} \quad (21)$$

While in the second:

$$\underline{M} = \begin{bmatrix} -1 & 0 \\ 0 & 1 \end{bmatrix} \quad (22)$$

Equation (21) has been given for 90° roof reflectors by Maitland and Dunn (Ref 29:111), except that they define the sense of the slope with respect to a fixed direction (not always the forward direction of the ray). Equation (22) is seen to be the correct transformation for the standard ray only. In either of these cases, the transformation,  $\underline{M}$ , is not particularly useful. (For another approach to the homogeneous matrix transformation, see Appendix A.)

Inhomogeneous Matrix. Ray coordinate transformation Eqs. (19) and (20) (for the small angle approximation) can be written in the linear form of Eq. (3). The transformation is thus inhomogeneous (that is, the additive constant is non-zero), and the ray matrix transformation

for a roof reflector becomes:

$$\begin{bmatrix} x_2 \\ \theta_2 \end{bmatrix} = \begin{bmatrix} -1 & 0 \\ 0 & -1 \end{bmatrix} \begin{bmatrix} x_1 \\ \theta_1 \end{bmatrix} + \begin{bmatrix} 0 \\ 2\alpha \end{bmatrix} \quad (23)$$

This is extremely simple, but is not the usual sort of matrix transformation encountered in the analysis of laser resonators. But as pointed out by Kahn (see p. 19), it is independent of the ray parameters because of the paraxial approximations made.

Nonlinearity. Transformation Eq. (23) has been derived assuming that the input ray is incident on the roof reflector above the axis, as the ray labeled A in Fig. 16. Consider ray B in that figure, which is incident with the same slope as A, but below the axis. Both rays cross themselves at  $2\alpha$ , but the correct transformation for ray B is

$$x_2 = - \frac{x_1 \cos \theta_1}{\cos(\theta_1 + 2\alpha)} \quad (24)$$

$$\theta_2 = - \theta_1 - 2\alpha \quad (25)$$

Evidently, then, the correct expression for the inhomogeneous matrix transformation, for small angles must be:

$$\begin{bmatrix} x_2 \\ \theta_2 \end{bmatrix} = \begin{bmatrix} -1 & 0 \\ 0 & -1 \end{bmatrix} \begin{bmatrix} x_1 \\ \theta_1 \end{bmatrix} \pm \begin{bmatrix} 0 \\ 2\alpha \end{bmatrix} \quad (26)$$

where the "±" sign is a "nonlinearity" because it is a discrete function (this was noted by Kahn for thin diamond-shaped prisms - Ref 21:867). Apparently, the choice of sign must be the same as that of  $x_1$ . In unfolding ray B, the image axis would be angled downward by  $2\alpha$ ,

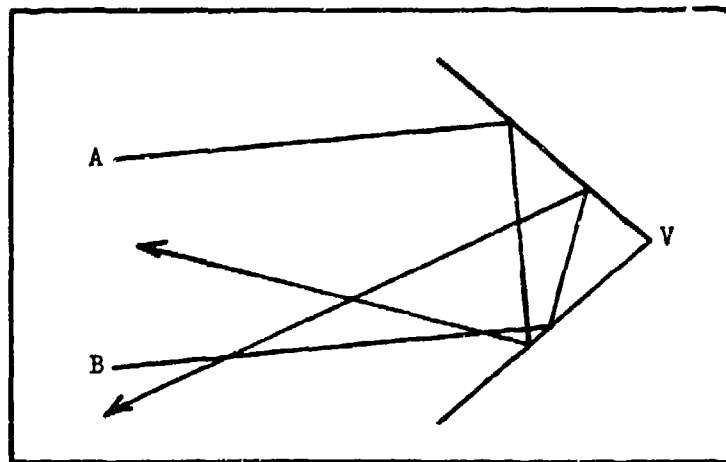


Fig. 16. Discrete Nonlinearity

and the transformation plane,  $\overline{N'V}$ , tilted  $-\alpha$ . Otherwise, the unfolded reflector is the same.

If ray A were held at the same incident slope, but translated downward in Fig. 16, its reflected direction would not change smoothly as it moved across the roof edge. In theory, the ray could be moved as close to the roof edge as desired - from either top or bottom - until reflection exactly from the roof edge took place in some limiting process. But the direction of this reflected ray is meaningless because (1) geometric optics is invalid when distances approach a few wavelengths and (2) real roof reflectors do not have perfect roof edges anyway. The roof edge is to be geometrically avoided.

Equation (26) then becomes the most important idea in this chapter, and will be used extensively in the following theory. The unfolded roof reflector, also developed in this chapter, will be used in an equivalent waveguide to decide whether the plus or minus sign is to be used in any individual transformation.

#### IV. Resonators With Roofs Parallel

The first resonator to be considered is with opposite roof edges contained in a plane and parallel. This resonator may be represented by a two-dimensional drawing as in Fig. 17. There are no restrictions on the y-dimension of the reflectors, of course, but only rays which are contained in the xz-plane can stay in the resonator.

##### Stable Rays

The standard geometric approach for analyzing laser resonators in two-dimensions is to trace a ray through a round-trip using matrices. Eigenvalues of the round-trip system matrix then determine whether stable rays exist. This approach cannot be used with a roof reflector resonator because the ray transformation matrix, Eq. (26), for a roof reflector - and subsequently the round-trip system matrix - is inhomogeneous (Ref 30:249). Also, there is a choice of signs when applying Eq. (26). This problem can be conveniently solved with the equivalent waveguide developed below.

Equivalent Waveguide. Stable rays in laser resonators can also be thought of as propagating through an equivalent lens waveguide, as in Fig. 18(a). There is no equivalent "lens" for a roof reflector, but an equivalent waveguide could be drawn using Fig. 15(b). This has been done in Fig. 18(b), but the ray is discontinuous. As has been seen in Chapter III, the ray can be straightened out if the roof reflector is unfolded - Fig. 15(d) - however the axis no longer appears as a straight line, but is bent up or down by  $2\alpha$ .

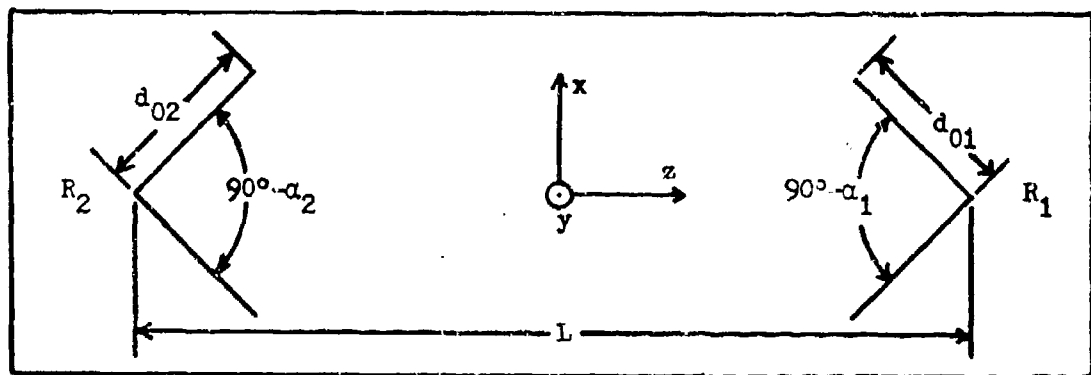


Fig. 17. Resonator with Roofs Parallel

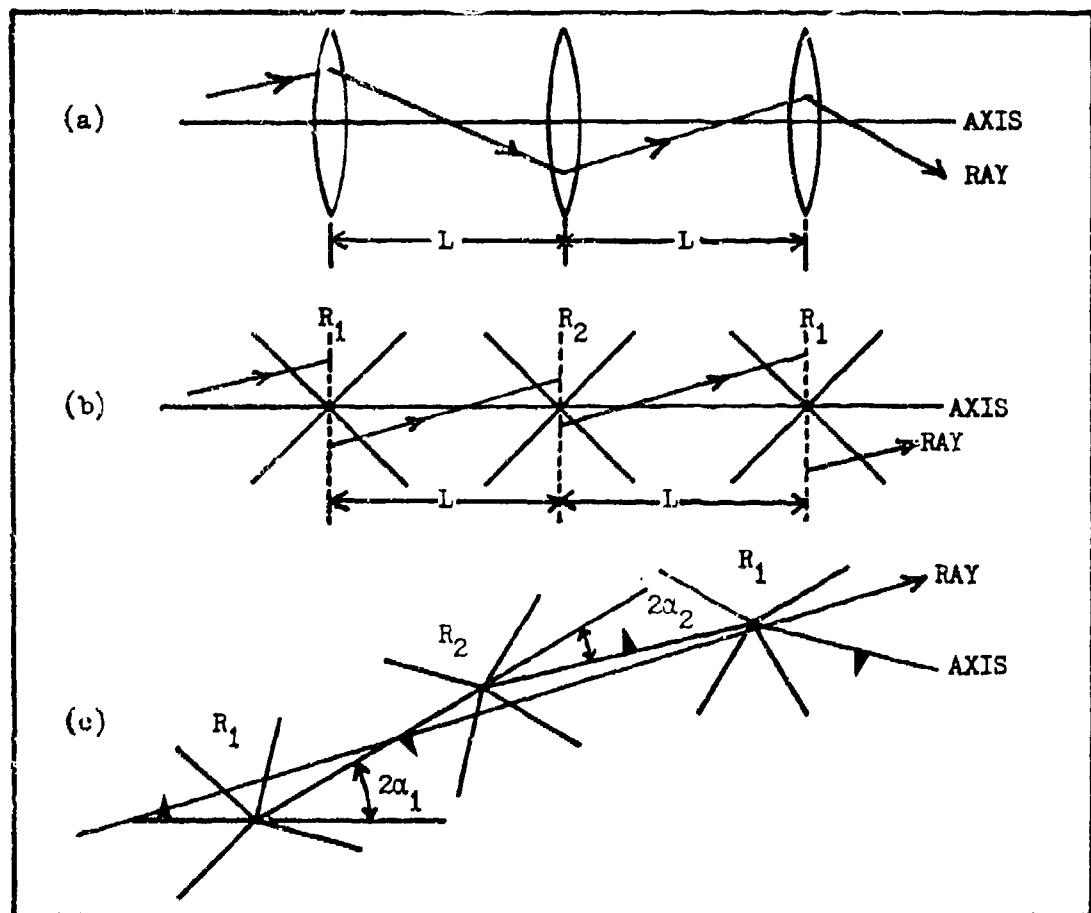



Fig. 18. Equivalent Waveguides

An equivalent waveguide - using unfolded roof reflectors - is thus drawn in Fig. 18(c). In this figure, the variant angles -  $\alpha_1$  and  $\alpha_2$  - are relatively large to emphasize the bends. The direction the axis bends depends on the ray that is being traced, but the rule for constructing the equivalent waveguide is simple: the axis always bends toward the ray.

An unconventional feature of this equivalent waveguide must be pointed out. When a roof reflector is unfolded, the image is inverted (see pp. 30-31). Thus, every other section of the waveguide in Fig. 18(c) is actually inverted. As a reminder, arrowheads () are drawn on each section of axis indicating which way is "up."

The equivalent waveguide just constructed is a valuable aid in visualizing the way in which rays can be analytically traced with matrices. If a ray is incident on a roof reflector on the same side of the axis as the arrowhead, then the "+" sign is to be chosen when applying transformation Eq. (26), and conversely.

First Pattern. Stable rays (ring-type like those in Fig. 5 or Fig. 8) in the equivalent waveguide developed here are those where the axis oscillates periodically around the ray. In terms of analytically tracing a ray, this is the equivalent of one round-trip: two reflector transformations and translation through two axis lengths ( $2L$ ).

In Fig. 18(c), the third section of waveguide axis makes an angle of  $2(\alpha_1 - \alpha_2)$  with the axis of the first section. If an equivalent waveguide were drawn with alternating up and down bends, this angle would be repeated every other section. No ray can be contained in such a waveguide unless  $2(\alpha_1 - \alpha_2) = 0$ . The two cases of  $\alpha_1 \neq \alpha_2$  and

$\alpha_1 = \alpha_2 = \alpha$  are illustrated in Fig. 19(a) and 19(b), respectively, where only the axis and ray are drawn for simplicity. In Fig. 19(a), the ray crosses the axis once between each bend - but at an angle different by  $2(\alpha_1 - \alpha_2)$  each time - and diverges. In Fig. 19(b), however, the ray always crosses the axis at the same angle. By inspection, only a ray making an angle  $\alpha$  with the axis is stable, and this ray is called the "first pattern" for later convenience.

To generate the system matrix for one round-trip, assume for the moment that  $\alpha_1 \neq \alpha_2$  and that the reference plane is chosen at mid-axis ( $L/2$ ). Then, starting with a ray  $(x_0, \theta_0)$ , the sequence of matrix operations is worked out here for illustration, and reference to Fig. 19(a), shows that "+" signs are chosen in the reflector transformations. First, translate to  $R_1$ :

$$\begin{bmatrix} x_1 \\ \theta_1 \end{bmatrix} = \begin{bmatrix} 1 & \frac{L}{2} \\ 0 & 1 \end{bmatrix} \begin{bmatrix} x_0 \\ \theta_0 \end{bmatrix} \quad (27)$$

Second, transform through  $R_1$ :

$$\begin{aligned} \begin{bmatrix} x_2 \\ \theta_2 \end{bmatrix} &= \begin{bmatrix} -1 & 0 \\ 0 & -1 \end{bmatrix} \begin{bmatrix} x_1 \\ \theta_1 \end{bmatrix} + \begin{bmatrix} 0 \\ 2\alpha_1 \end{bmatrix} \\ &= \begin{bmatrix} -1 & \frac{L}{2} \\ 0 & -1 \end{bmatrix} \begin{bmatrix} x_0 \\ \theta_0 \end{bmatrix} + \begin{bmatrix} 0 \\ 2\alpha_1 \end{bmatrix} \end{aligned} \quad (28)$$

Third, translate to  $R_2$ :

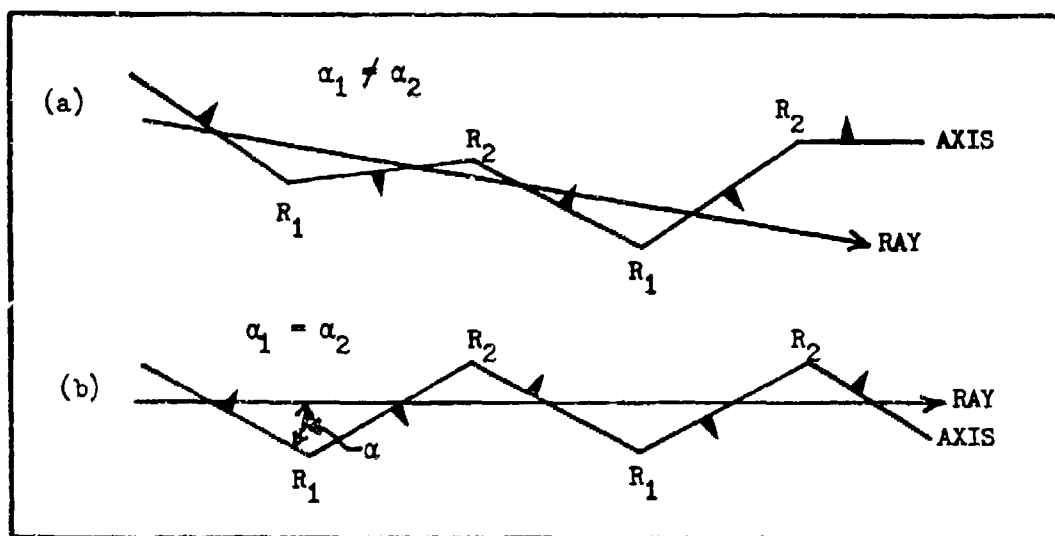


Fig. 19. Ray propagating through Equivalent Waveguide - First Pattern

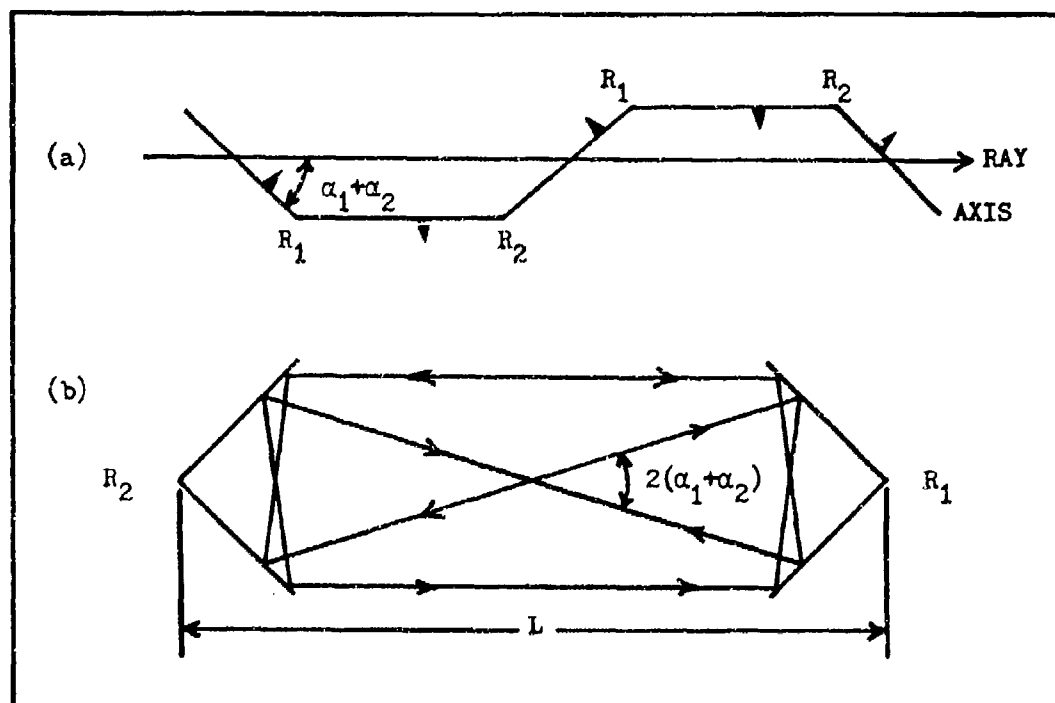


Fig. 20. Second Pattern

$$\begin{aligned}
 \begin{bmatrix} x_3 \\ \theta_3 \end{bmatrix} &= \begin{bmatrix} 1 & 0 \\ 0 & 1 \end{bmatrix} \begin{bmatrix} x_2 \\ \theta_2 \end{bmatrix} \\
 &= \begin{bmatrix} -1 & -\frac{3L}{2} \\ 0 & -1 \end{bmatrix} \begin{bmatrix} x_0 \\ \theta_0 \end{bmatrix} + \begin{bmatrix} 2La_1 \\ 2a_1 \end{bmatrix}
 \end{aligned} \tag{29}$$

Fourth, transform through  $R_2$ :

$$\begin{aligned}
 \begin{bmatrix} x_4 \\ \theta_4 \end{bmatrix} &= \begin{bmatrix} -1 & 0 \\ 0 & -1 \end{bmatrix} \begin{bmatrix} x_3 \\ \theta_3 \end{bmatrix} + \begin{bmatrix} 0 \\ 2a_2 \end{bmatrix} \\
 &= \begin{bmatrix} 1 & \frac{3L}{2} \\ 0 & 1 \end{bmatrix} \begin{bmatrix} x_0 \\ \theta_0 \end{bmatrix} + \begin{bmatrix} -2La_1 \\ -2(a_1 - a_2) \end{bmatrix}
 \end{aligned} \tag{30}$$

Finally, translate to the reference plane:

$$\begin{aligned}
 \begin{bmatrix} x_5 \\ \theta_5 \end{bmatrix} &= \begin{bmatrix} 1 & \frac{L}{2} \\ 0 & 1 \end{bmatrix} \begin{bmatrix} x_4 \\ \theta_4 \end{bmatrix} \\
 &= \begin{bmatrix} 1 & 2L \\ 0 & 1 \end{bmatrix} \begin{bmatrix} x_0 \\ \theta_0 \end{bmatrix} + \begin{bmatrix} -3La_1 + La_2 \\ -2(a_1 - a_2) \end{bmatrix}
 \end{aligned} \tag{31}$$

Or:

$$x_5 = x_0 + 2L\theta_0 - 3La_1 + La_2 \tag{32}$$

$$\theta_5 = \theta_0 - 2(a_1 - a_2) \tag{33}$$

By now setting  $x_5 = x_0$  and  $\theta_5 = \theta_0$  for the first pattern, Eqs. (33) and (32), respectively, may be satisfied only for:

$$a_1 = a_2 \tag{34}$$

$$\theta_0 = a_1 \tag{35}$$

Thus the stable ray found by inspection is confirmed analytically.

(The fact that  $x_0$  is unspecified indicates that the ray is not unique but that a family, or packet, of rays exists.)

Second Pattern. There are other stable ring-type rays which close on themselves after more than one round-trip, so the equivalent waveguide picture becomes more useful as the number of roof reflector transformations increases. (In general, after  $p$  round-trips with two transformations each, there are  $2^{2p}$  possible sign sequences.) For two round trips, the number of axis bends is four. The equivalent waveguide is drawn in Fig. 20(a); the stable ray is shown as it appears in the resonator in Fig. 20(b).

The system matrix may be worked out as above. Using the same mid-axis reference plane, Fig. 20(a) indicates that the sequence of signs that must be used in applying Eq. (26) is  $+, -, -, +$ . After these four transformations and translation along the axis four times ( $4L$ ), the resulting ray is

$$\begin{bmatrix} x_9 \\ \theta_9 \end{bmatrix} = \begin{bmatrix} 1 & 4L \\ 0 & 1 \end{bmatrix} \begin{bmatrix} x_0 \\ \theta_0 \end{bmatrix} + \begin{bmatrix} -4L(\alpha_1 + \alpha_2) \\ 0 \end{bmatrix} \quad (36)$$

This shows that  $\theta_9 = \theta_0$  so that for rays of this, the second pattern, it is thus required that:

$$\theta_0 = \alpha_1 + \alpha_2 \quad (37)$$

to satisfy Eq. (36). Stable rays, therefore, are only those which cross the axis at this angle; but note, however, that the restriction that  $\alpha_1 = \alpha_2$  - in the case of the first pattern - is removed.

Higher-order Patterns. In general, let  $p_2$  denote the pattern number - which is the number of round-trips that a ray makes before repeating the same path in the two-dimensional resonator - so that the first pattern is henceforth designated  $p_2 = 1$ . Not all of the patterns are independent of one another, as will now be shown.

Consider a resonator with two roof reflectors of equal aperture and having  $\alpha_1 = \alpha_2 = \alpha$ , but with the axis length,  $L$ , being variable. Fig. 21(a) then shows a standard ray associated with the right-hand reflector diverging past the edges of the left-hand reflector. As  $L$  is decreased, a  $p_2 = 1$  pattern becomes stable in Fig. 21(b). This pattern disappears as  $L$  is further shortened (Fig. 21(c) and (d)), until a  $p_2 = 3$  pattern appears in Fig. 21(e). Evidently the axis could be further shortened until higher-order odd-numbered patterns appear. This same demonstration could be carried out starting with  $p_2 = 2$ , and all even-numbered patterns would be seen to be similarly related by the variation of axis length.

Drawings of high-order patterns become complex, but the equivalent waveguide picture gives an easy way to visualize the patterns.

Patterns  $p_2 = 3$  through  $p_2 = 6$  are unfolded in Fig. 22 where the sign to be applied to each roof reflector transformation is also shown. Extending both odd and even patterns to the general case, the sign sequences are (there are  $2p_2$  signs in each sequence):

(1) for  $p_2$  odd:

$$\begin{array}{c} \boxed{+ \quad - \quad + \quad \dots \quad +} \quad \boxed{+ \quad - \quad + \quad \dots \quad +} \\ p_2 \text{ signs} \qquad \qquad p_2 \text{ signs} \end{array} \quad (38)$$

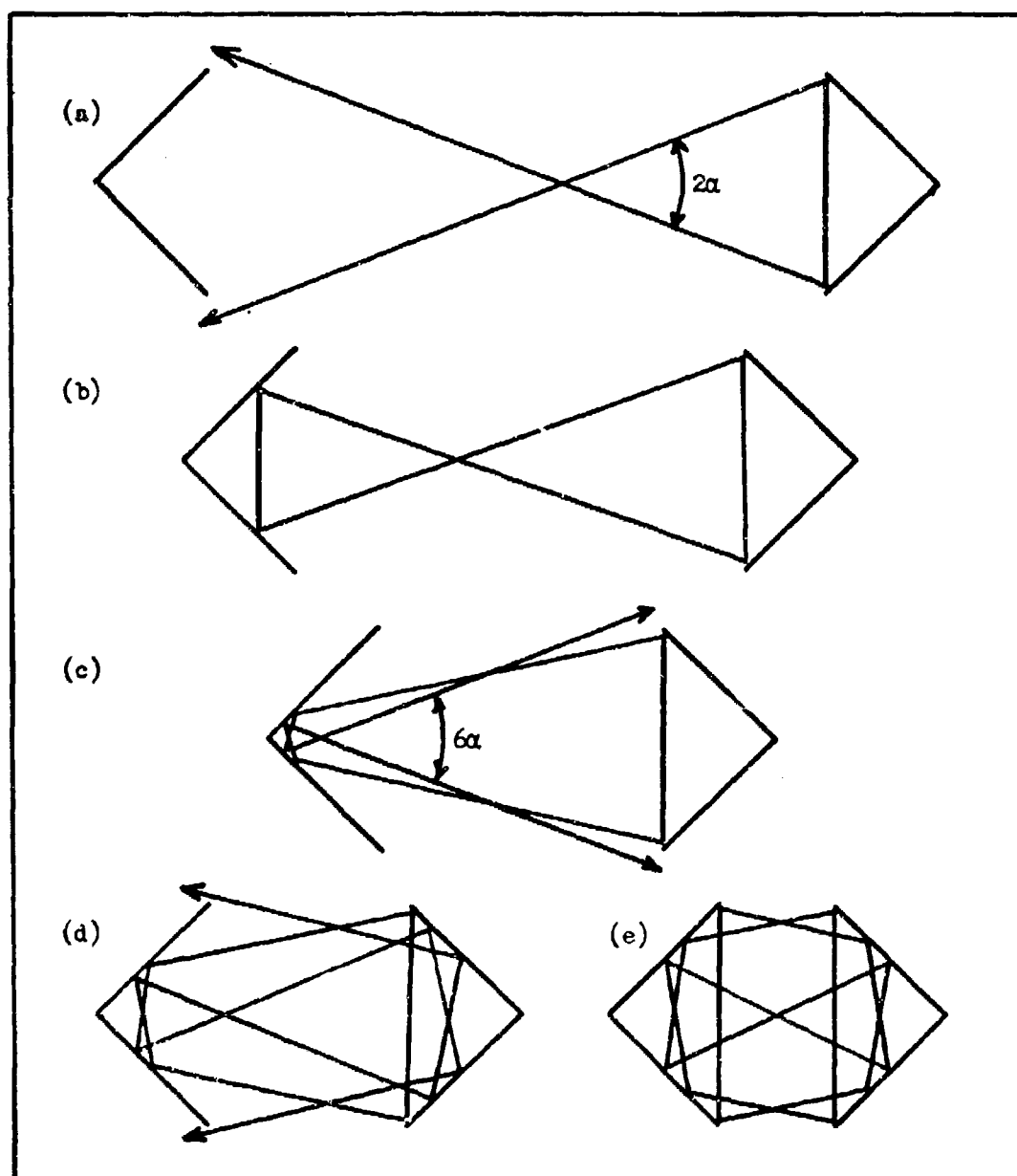


Fig. 21. Relation of First and Third Patterns

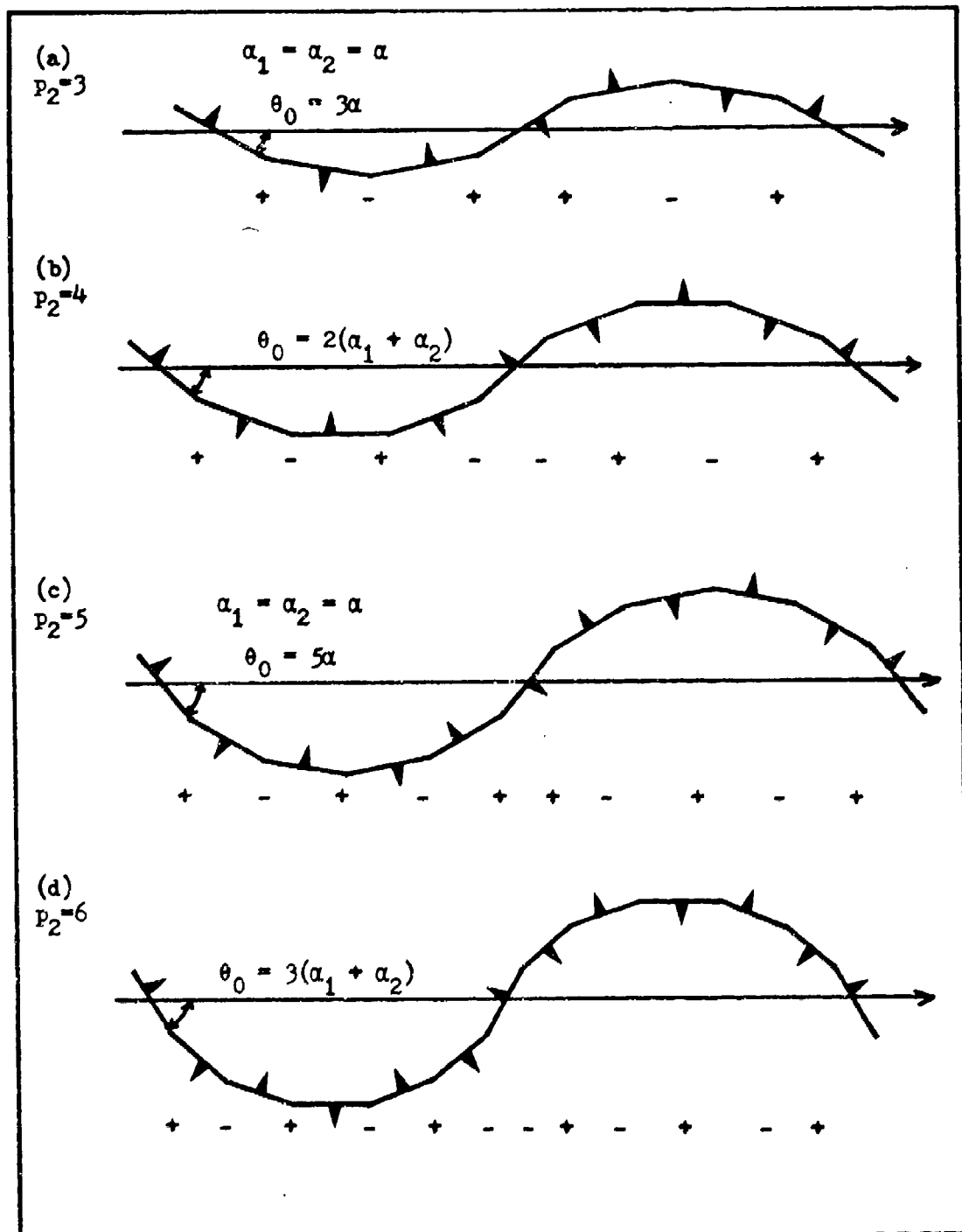


Fig. 22. Equivalent Waveguides for Higher-Order Patterns  
 (If a ray is incident on a roof reflector on the same side of the axis as the arrowhead, then the "+" sign is to be chosen when applying Eq. (26), and conversely.)

(2) for  $p_2$  even:

$$\begin{array}{c} \boxed{+ \quad - \quad + \quad \dots \quad -} \quad \boxed{- \quad + \quad - \quad \dots \quad +} \\ p_2 \text{ signs} \quad \quad \quad p_2 \text{ signs} \end{array} \quad (39)$$

Applying these sign rules to tracing a ray through  $p_2$  round-trips (starting and ending at mid-axis), the general form of the system matrices are

(1) for  $p_2$  odd:

$$\begin{bmatrix} x_{4p_2+1} \\ \theta_{4p_2+1} \end{bmatrix} = \begin{bmatrix} 1 & 2p_2L \\ 0 & 1 \end{bmatrix} \begin{bmatrix} x_0 \\ \theta_0 \end{bmatrix} + \begin{bmatrix} -p_2L[p_2(\alpha_1 + \alpha_2) + 2(\alpha_1 - \alpha_2)] \\ -2(\alpha_1 - \alpha_2) \end{bmatrix} \quad (40)$$

(2) for  $p_2$  even:

$$\begin{bmatrix} x_{4p_2+1} \\ \theta_{4p_2+1} \end{bmatrix} = \begin{bmatrix} 1 & 2p_2L \\ 0 & 1 \end{bmatrix} \begin{bmatrix} x_0 \\ \theta_0 \end{bmatrix} + \begin{bmatrix} -p_2^2L(\alpha_1 + \alpha_2) \\ 0 \end{bmatrix} \quad (41)$$

It is seen that if  $\alpha_1 = \alpha_2$  (which is indeed required for ring-type rays to exist when  $p_2$  is odd), then Eqs. (40) and (41) become identical. In either case, however, the initial angle which the stable rays make with the axis is

$$\theta_0 = \frac{p_2}{2} (\alpha_1 + \alpha_2) \quad (42)$$

This angle is indicated in Fig. 22.

One more feature of the patterns illustrated in Fig. 22 is their increasing distance from the axis with pattern number. But for small variant angles, the distance a ray travels before closing,  $P_{p_2}$ , is approximately the same as the axis length for the same number of round-trips:

$$P_{p_2} = 2 p_2 L \quad (43)$$

Since the ray transfer matrices used to derive Eqs. (40) and (41) are themselves only good to first order, it is not surprising that this length appears as the upper right element of the 2x2 matrix in these equations.

Importance of the patterns. The importance of the different stable ray patterns is that they are essentially separated in space, aside from a finite number of crossing points. The patterns that can exist depend on axis length and roof reflector aperture as is evident from Fig. (21). This dependence is discussed below under stability conditions, but for now let it be said that different patterns could operate simultaneously. Patterns  $p_2 = 1, 2$ , and 3 were in fact observed in the resonator of DeLang and Bouwhuis. They remark that the different patterns were observed to be operating simultaneously (see p. 13 and Fig. 4 ).

When  $\alpha_1 = \alpha_2 = 0$  for a  $90^\circ$  roof reflector, both Eqs. (40) and (41) become homogeneous and are automatically satisfied by a ring-type ray of any pattern number. Thus there is always a stable ray in this case, and Eq. (42) indicates that it is parallel to the axis.

#### Stability Conditions

Now that stable ring-type rays have been found, the parallel-roof resonator dimensions that allow them to exist - the stability conditions - can be determined.

Variant Angle Conditions. From the solutions of the general ray transfer Eqs. (40) and (41), restrictions which must be imposed on the

roof reflector variant angles - for stable rays to exist - are

(1) for  $p_2$  odd:

$$\alpha_1 = \alpha_2 \quad (34)$$

(2) for  $p_2$  even:

$$(\text{No restriction on variant angles}) \quad (44)$$

Thus it is easy to build a practical device which will not operate in any odd pattern, simply by choosing  $\alpha_1 \neq \alpha_2$ .

Axis Length and Aperture Conditions. The dependence of roof reflector aperture and resonator axis length - held over from the discussion of Fig. 21. - will now be quantified. In Fig. 23, let the two roof reflectors be identical with surface dimension  $d_0$ . The upper drawing shows the maximum axis length that just allows the  $p_2 = 1$  stable rays to fit in the resonator - using the full apertures of the reflectors. The lower drawing shows the same condition for the  $p_2 = 3$  pattern.

The odd patterns have previously been shown to be related, and that is again evident here. In Fig. 23(b), two standard rays (filling the apertures) for the right and left reflectors - virtually crossing at  $Q'$  and  $Q''$  - are each reflected by the opposite reflector and join at  $Q$ . The total path length for three round-trips in the  $p_2 = 3$  pattern is thus the same as the path length for one round-trip in the  $p_2 = 1$  pattern:

$$P = 2l \quad (46)$$

where  $l$  is the standard ray loop length defined by Eq. (16). The path length is, in fact, a constant for all odd-numbered patterns by

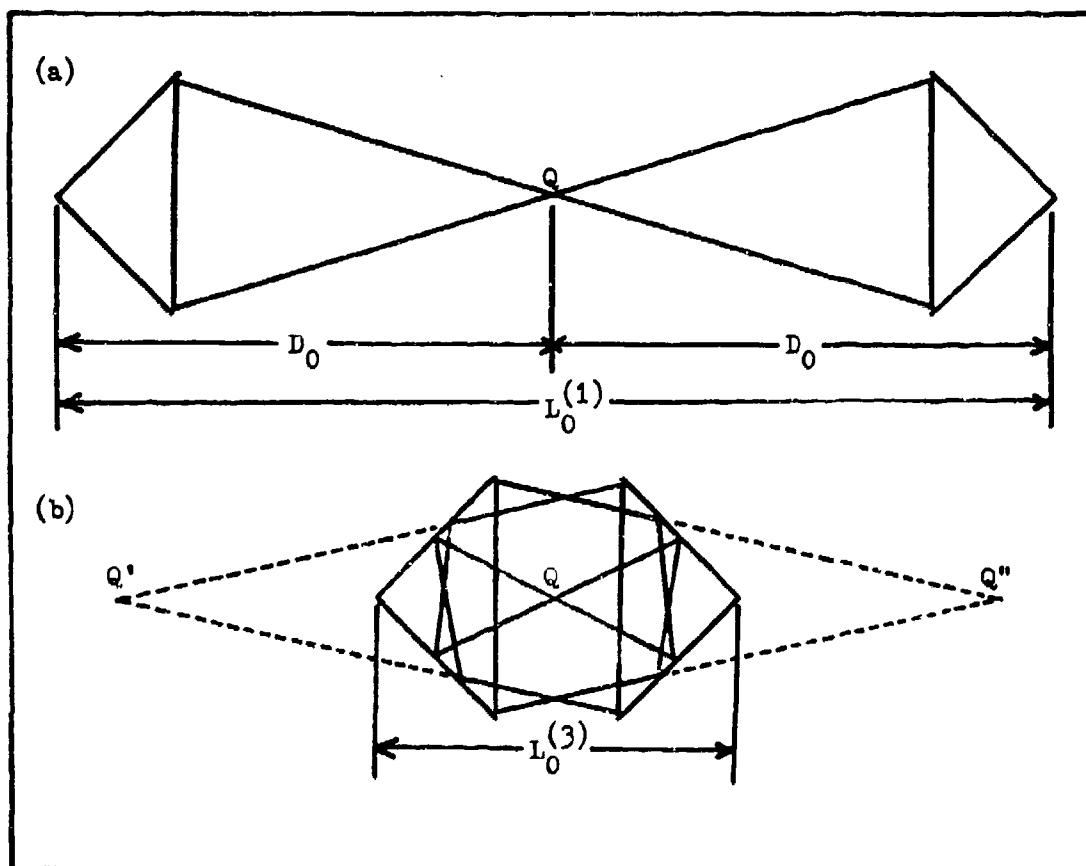


Fig. 23. Dependence of Odd Patterns on Axis Length and Aperture

the demonstration of Fig. 21. Using the relations of Chapter III - and considering the maximum path length when filling the apertures for threshold conditions as in Fig. 23 - this becomes, to first order:

$$\begin{aligned} P &= 4 D_0 \\ &= \frac{2 \sqrt{2} d_0}{\alpha} \end{aligned} \quad (46)$$

Total path length for even patterns has a similar relationship, shown in Fig. 24. Here  $\alpha_1 \neq \alpha_2$  with  $\alpha_1 < \alpha_2$ . Fig. 24(a) shows an unsuccessful attempt to construct a  $p_2 = 2$  pattern where a ray from the left reflector, with virtual crossing at  $S'$ , diverges from the resonator after reflection from the right reflector. This is because  $D_R$ , the crossing distance for the right reflector, is less than that for the left,  $D_L$ . Fig. 24(b) shows a  $p_2 = 2$  pattern successfully constructed when the ray crossing points,  $T'$  and  $T''$ , for the right reflector have been reflected by the left reflector to join at  $T$ . Thus the total path length is again twice the loop length from  $T$ , and - since all even patterns are related - this is true in general. For small angles, the ray crossing distance in Fig. 24(b) is approximately  $D_0$ , so (to first order) for even patterns:

$$\begin{aligned} P &= 4 D_0 \\ &= \frac{2 \sqrt{2} d_0}{\alpha} \end{aligned} \quad (46)$$

which is identical to the expression for odd-numbered patterns, but the larger of  $\alpha_1$  and  $\alpha_2$  must be used.

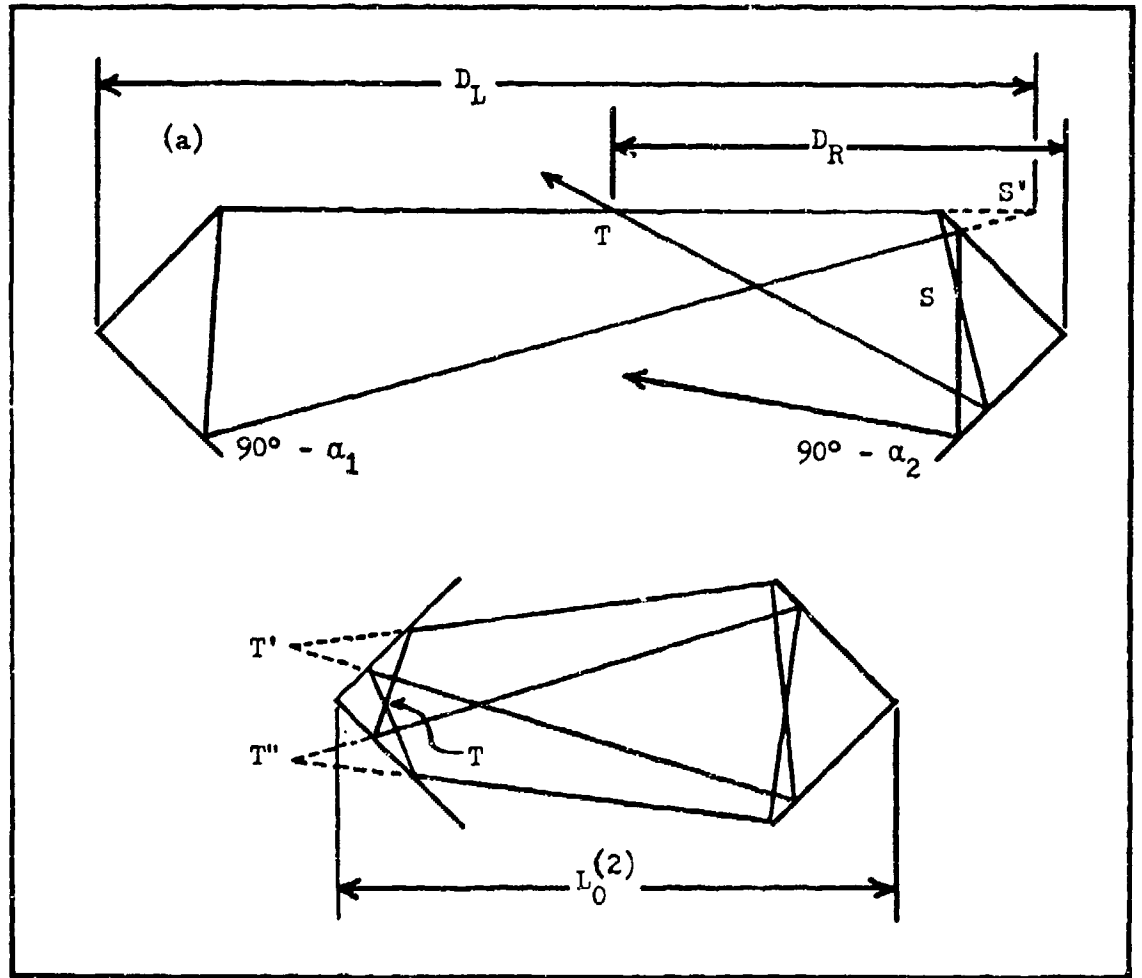


Fig. 24. Dependence of Even Patterns on Axis Length and Aperture

Total path length has also been given in terms of axis length for odd and even patterns by Eq. (43), correct also to first order. If  $L_0^{(p)}$  is the maximum axis length that will permit stable rays in pattern  $p_2$ , then it is seen that the conditions for stability are

(1) for  $p_2$  odd:

$$L \leq L_0^{(p)} = \frac{2 D_0}{p_2} = \frac{\sqrt{2} d_0}{p_2 \alpha} \quad (47)$$

(2) for  $p_2$  even:

$$L \leq L_0^{(p)} = \frac{2 D_0}{p_2} = \frac{\sqrt{2} d_0}{p_2 \alpha} \quad (47)$$

where the larger variant angle must be used.

Significance. The significance of the above result is that if  $L$  is greater than  $L_0^{(p)}$ , then stable rays of pattern number  $p_2$  and higher do not exist. For example, if  $L = 1.1 D_0$ , which is greater than  $L_0^{(2)} = D_0$ , then only stable rays of the first pattern will exist. Thus, by appropriately choosing  $L$ , it is possible to select only low-order patterns. As a further example, if  $L = 0.7 D_0$ , then only  $p_2 = 1$  and  $p_2 = 2$  could operate, but if  $\alpha_1 \neq \alpha_2$ , then  $p_2 = 1$  is excluded.

Pattern Area. If  $L$  is less than  $L_0^{(p)}$ , then there is no unique stable ray, but an entire "packet." For example, the dependence of the ray packet, for  $p_2 = 1$ , on  $L$  is shown in Fig. 25. From the figure, the following facts can be generalized which are valid for both odd and even pattern ray packets:

(1) For  $L_0^{(p)} > L > L_0^{(p)}/2$  the ray packets are limited by the apertures of the roof reflectors and the roof edges are geometrically excluded.

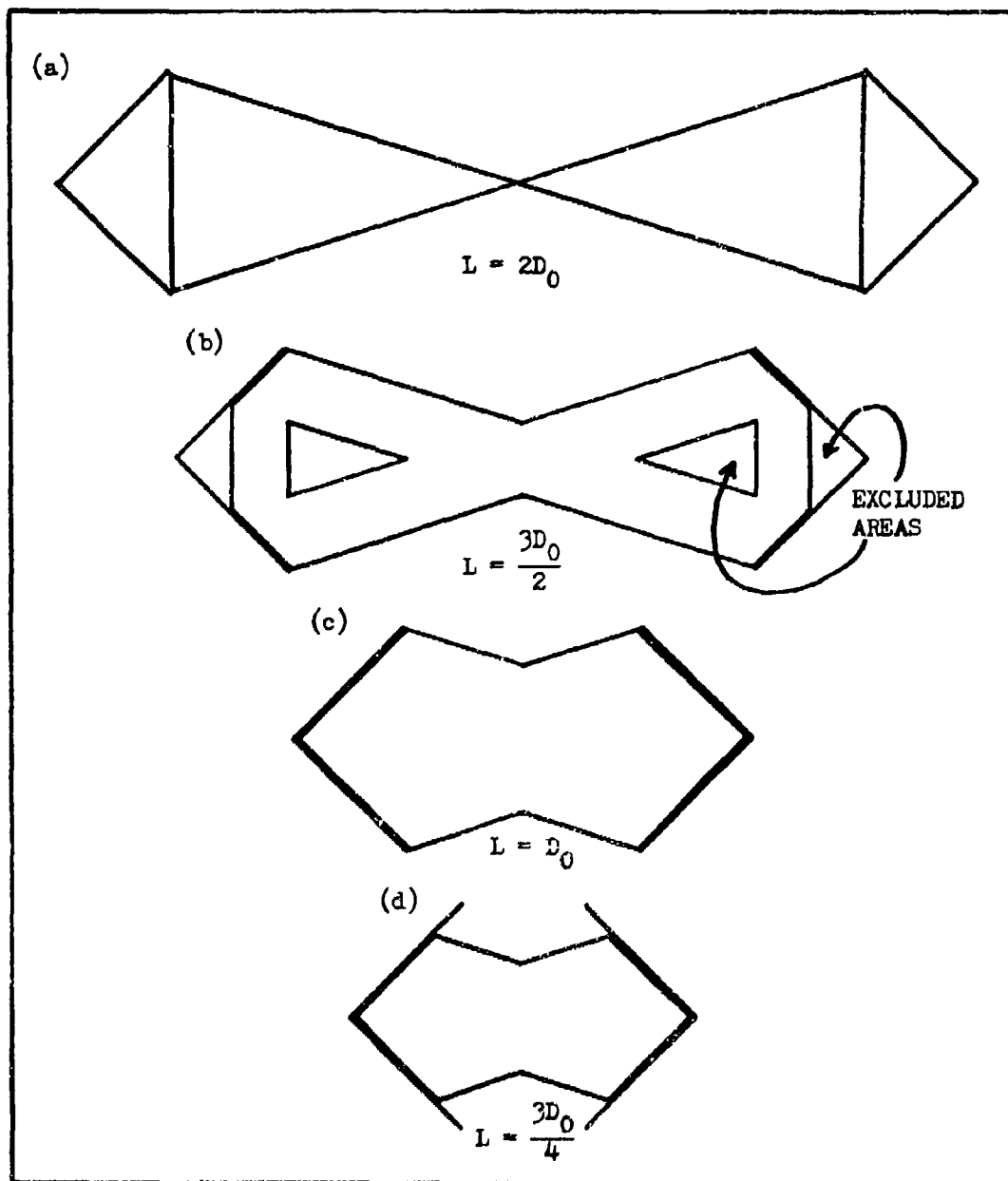


Fig. 25. Dependence of  $p_2 = 1$  Ray Packet on  $L$

- (2) For  $L \approx L_0^{(p)} / 2$  the area covered by the ray packet is a maximum, and the pattern approaches the roof edges.
- (3) For  $L < L_0^{(p)} / 2$  the ray packets are no longer aperture limited, but do diffract from the roof edges.

For small angles, the maximum area covered by the ray packets is given by the approximate expressions:

- (1) for  $p_2$  odd:

$$A_{\max} = \frac{d_0^2}{\alpha p_2^2} \left( p_2 - \alpha p_2^2 - \frac{1}{4} + \alpha p_2 \right) \quad (48)$$

- (2) for  $p_2$  even:

$$A_{\max} = \frac{d_0^2}{\alpha p_2^2} \left( p_2 - \alpha p_2^2 \right) \quad (49)$$

Fig. (26) is a plot of geometric pattern area as a function of axis length. The peak values have been computed from Eqs. (48) and (49) using  $d_0 = 1$  cm and  $\alpha = 0.01$  rad (which gives  $D_0 = 71.1$  cm).

### Resonant Modes

The stable geometric ray "patterns" just developed are not to be confused with resonant "modes." Resonant modes are the electromagnetic fields in a resonator which, at a discrete frequency, spatially reproduce themselves in amplitude and phase as they reflect back and forth. The patterns provide a way of predicting the physical distribution of the fields in the resonator. This follows from the statement in Kahn's paper, quoted on p. 19. Thus, for example, in Fig. 25(b) the area of the resonator covered by the ray packet could be expected to have large field amplitudes while the excluded areas have small field amplitudes (or none).

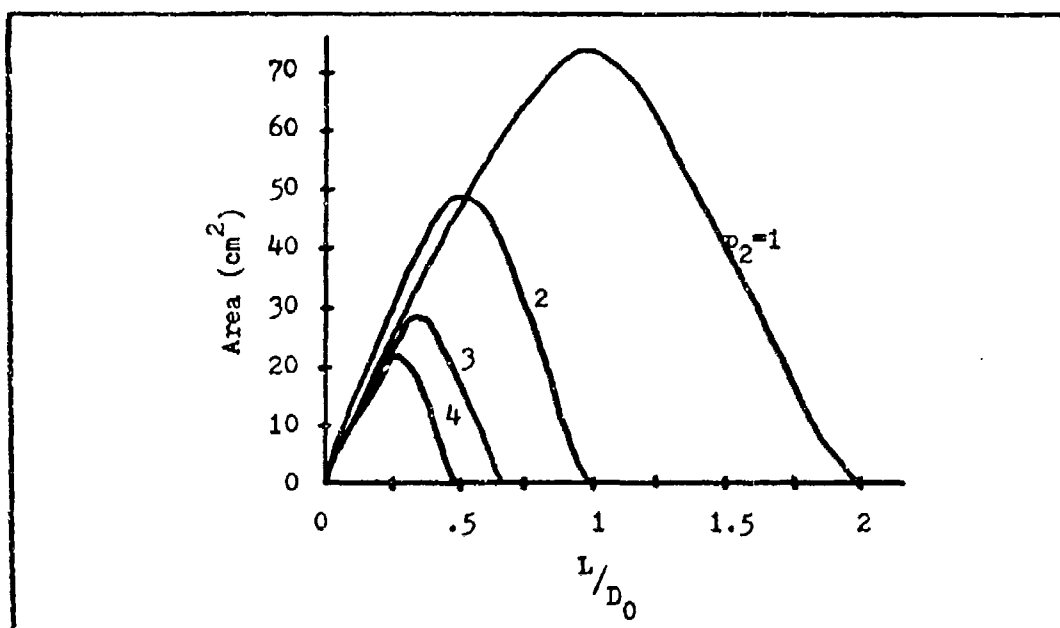


Fig. 26. Dependence of Pattern Area on Axis Length

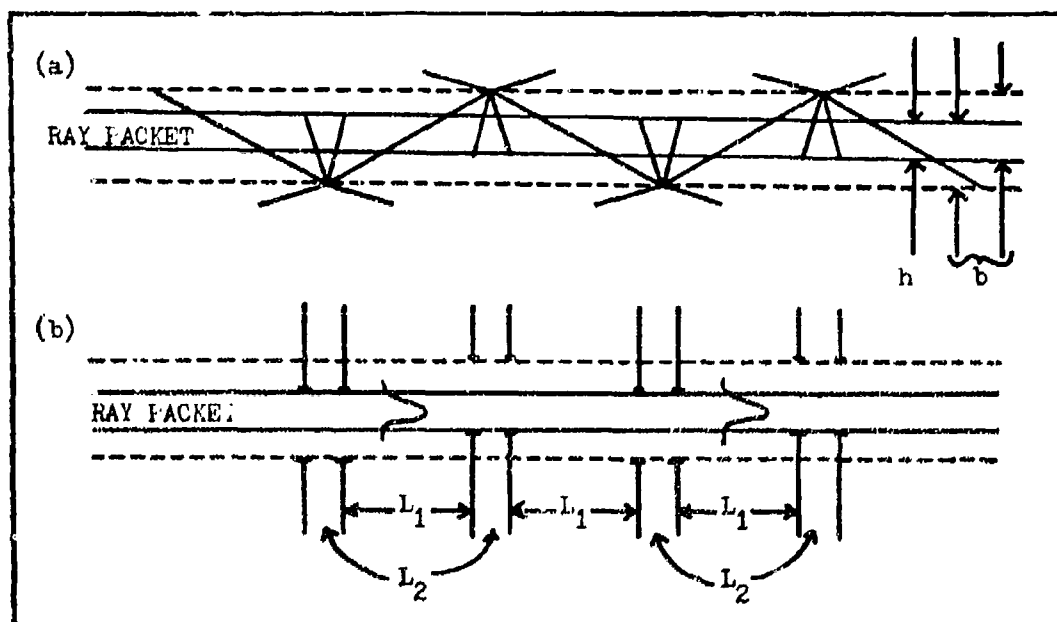


Fig. 27. Roof Reflector Aperture-Equivalent Waveguide

Gaussian Modes. Particular field distributions which are known to be self-reproducing in laser resonators (with rectangular reflectors) are Hermite-Gaussian modes. Therefore, it is reasonable to assume that the resonant modes of roof reflector resonators are Hermite-Gaussian. However, these modes are predicted to exist only in cases where the resonator is designed to operate in a particular pattern not approaching the roof edges. Otherwise, diffraction by the roof edges becomes important and the resonant modes are no longer pure Gaussians.

Steier (Ref 41) has shown that a Gaussian beam can be described by an equivalent packet of rays. According to his work: "the position of the beam center, the beam spot size, and the phase front curvature can be found for a Gaussian beam passing through any sequence of perfect, large-aperture lenses or flat dielectric interfaces." (Ref 41:1229) Although in the present case, "perfect, large-aperture lenses or flat dielectric interfaces" are not involved, Steier shows that if rays can be traced through an optical system having an inhomogeneous system matrix like Eqs. (40) and (41), then the quoted properties of a Gaussian beam will be carried by the equivalent ray packet (Ref 41:1231).

The fact that Steier's theory necessitates large apertures remains, however. If the ray packet patterns in a roof reflector resonator are to be equivalents of Gaussian beams, they are obviously aperture-limited. A quantitative relationship between the aperturing effect and the dimension (spot size) of the ray packet that should be chosen as a Gaussian beam equivalent is beyond the scope of this study, but the following qualitative argument shows that, indeed, a Gaussian beam can propagate in roof reflector resonators.

Fox and Li (Refs 16 and 28) have shown that plane mirrors in laser resonators can be treated as apertures in equivalent waveguides. Thus, self-reproducing modes can be found which propagate through a waveguide of equally spaced apertures. Now for roof reflectors, the reflecting surfaces are plane mirrors, and Fig. 27(a), for example, is Fig. 19(b) redrawn with these plane mirrors in place. The effect of aperturing on the ray packet is evident in this figure, where, for small angles, the height of the ray packet is

$$h = \frac{\sqrt{2} d_0}{2} - \alpha L \quad (50)$$

while the aperture of the mirror surfaces normal to the direction of propagation is

$$b = \frac{\sqrt{2} d_0}{2} \quad (51)$$

Since the reflecting surfaces are stigmatic (Ref 20:94) they could be replaced at once by apertures normal to the direction of propagation, but it must be required that  $h < b$  to geometrically exclude the roof edges. If this condition is satisfied, Fig. 27(b) follows - showing apertures replacing the roof reflectors. Unlike the waveguide representation of a Fabry-Perot resonator, the spacing between apertures is not uniform, nor are the apertures aligned. The spacings in Fig. 27(b) are

$$L_1 = L - \sqrt{2} d_0 \quad (52)$$

$$L_2 = \sqrt{2} d_0 \quad (53)$$

Figure 27(b) also shows a sketch of a wavefront which, after four apertures, is a self-reproducing Gaussian - even though the apertures

are offset. This latter does not prevent the predicted modes from being Gaussian because, if the spot size (full width at the  $1/e$  amplitude points) is less than  $h$ , the amplitude in the offset regions is negligible. Thus, the paper by Ronchi is applicable in this regard (see pp. 19-20).

From Chapter II, there is evidence that the Gaussian modes predicted here are correct: the output from ruby by Soncini and Svelto was reported to be pure Gaussian. (Their critical resonator axis length, Eq. (1), appears to be similar to Eq. (47) developed here, with  $p_2 = 1$ . From their discussion, however, it is clear that they mean  $L_c \approx L_0^{(1)}/2$ , but their description of axis length longer or shorter than  $L_c$  is backwards compared to this theory. Here,  $L < L_c$  indicates that it is roof edge diffraction that spoils the output beam, whereas Soncini and Svelto thought  $L < L_c$  meant the pattern was spilling past the apertures. See p. 14.)

Axial Mode Frequency Interval. Figure 27(a) points out another important feature of the resonator patterns. Since every stable ray crosses the axis at exactly the same angle, every ray of a particular pattern has the same length for a closed path. To first order, this distance is  $P_{p_2} = 2p_2L$ , from Eq. (43).

The frequency interval between resonant axial, or longitudinal, modes can then be computed as follows. Let a ray packet be the equivalent of a Gaussian mode (according to Steier) with resonant frequency:

$$f_q = \frac{c}{\lambda_q} \quad (54)$$

where  $c$  is the velocity of light and  $\lambda_q$  is the wavelength of the  $q^{\text{th}}$  axial mode. Then the requirement that the mode be self-reproducing (standing waves) establishes the condition:

$$2q\pi = 2\pi \frac{2p_2 L}{\lambda_q} + \Phi \quad (55)$$

or

$$2q\pi = 2\pi \frac{2p_2 L}{c} f_q + \Phi \quad (56)$$

where  $\Phi$  is a phase shift due to reflection from the surfaces of the roof reflectors. The same requirement on the next higher allowed frequency is

$$2(q+1)\pi = 2\pi \frac{2p_2 L}{c} f_{q+1} + \Phi \quad (57)$$

Subtracting Eq. (56) from (57) gives the axial mode frequency interval, which is an expected result:

$$\Delta f_q = \frac{c}{2p_2 L} \quad (58)$$

Transverse Mode Frequency Interval. Since an infinite set of Hermite-Gaussian modes is mathematically possible for every pattern, the resonant frequency,  $f_{qmn}$  (for rectangular reflectors) depends on the orders,  $m$  and  $n$ , of the Hermite polynomials. This is given by (Ref 1:190):

$$2q\pi = 2\pi \frac{2p_2 L}{c} f_{qmn} - (m+n+1)\cos^{-1} \frac{A+D}{2} \quad (59)$$

where  $A$  and  $D$  are elements of the homogeneous round-trip ray matrix:

$$\begin{bmatrix} x \\ \theta \end{bmatrix} = \begin{bmatrix} A & B \\ C & D \end{bmatrix} \begin{bmatrix} x_0 \\ \theta_0 \end{bmatrix} \quad (60)$$

This is from the theory of Arnaud where, it is pointed out, stable rays which close on themselves satisfy Eq. (60) only if:

$$A = D = 1 \quad \text{and} \quad B = C = 0 \quad (61)$$

In the present case, the closed path patterns are known to be solutions of Eqs. (40) and (41); and consequently, they also satisfy the homogeneous Eq. (60) with the restrictions of Eq. (61). Therefore,  $A + D = 2$  and  $\cos^{-1} \frac{A + D}{2} = 0$  in Eq. (59), and for any change in  $m$  or  $n$ , the transverse mode frequency interval is given by:

$$\Delta f_{mn} = 0 \quad (62)$$

Losses in the Unstable Region. All laser resonators suffer losses as energy is diffracted past the apertures of the reflectors, but this geometric theory is not capable of predicting them. (A geometric theory of diffraction has been given by Keller, Ref 23, but is not used here.) However, a simple geometric construction has been devised for estimating losses in the  $p_2 = 1$  pattern when the resonator is unstable, that is  $\alpha_1 \neq \alpha_2$ .

An equivalent waveguide for the  $p_2 = 1$  pattern and  $\alpha_1 \neq \alpha_2$  is shown in Fig. 19(a) - with succeeding alternate sections rotated an additional angle  $2(\alpha_1 - \alpha_2)$  with respect to the first section. If this waveguide is drawn through many sections, it would eventually curve through an entire circle of radius approximately given by:

$$r = \frac{L}{\alpha_1 - \alpha_2} \quad (63)$$

(This is the radius of the cylindrical Bessel functions given by Ronchi.) A ray cannot remain inside this waveguide, but the maximum

distance a ray can travel can be estimated by calculating the chord length in Fig. (28):

$$z \approx \left[ \frac{\sqrt{2} L d_0}{(\alpha_1 - \alpha_2)} \right]^{1/2} \quad (64)$$

In terms of the number of (one-way) trips or reflections that the ray makes in the resonator, this is

$$M = \frac{z}{L} = \left[ \frac{\sqrt{2}}{\alpha_1 - \alpha_2} \frac{d_0}{L} \right]^{1/2} \quad (65)$$

If a packet of rays is then considered to be launched through the waveguide, all rays will be lost after M reflections, so the geometric loss,  $\delta_g$ , can be approximated by:

$$\delta_g = \frac{1}{M} = \left[ \frac{\alpha_1 - \alpha_2}{\sqrt{2}} \frac{L}{d_0} \right]^{1/2} \quad (66)$$

This expression is in qualitative agreement with what would be expected for the  $p_2 = 1$  pattern in an actual device (larger  $d_0$ , less loss).

Eigenpolarizations. As has been noted in Chapter II, only those plane polarizations oriented parallel or perpendicular to the roof edge of a roof reflector are reflected with their planes of vibration unchanged. Strictly speaking, the theory of Bobroff (Ref 5), which shows that these are the self-reproducing polarizations (eigenpolarizations) in a  $90^\circ$  roof reflector resonator (roofs either parallel or crossed), assumes that polarized wavefronts propagate parallel to the axis in the resonator. The direction of propagation in the  $90^\circ - \alpha$  parallel-roof resonator is not necessarily parallel to the axis, but the plane of incidence (xz-plane in Fig. 17) is nevertheless perpendicular to the roof edges. This is sufficient to show that these

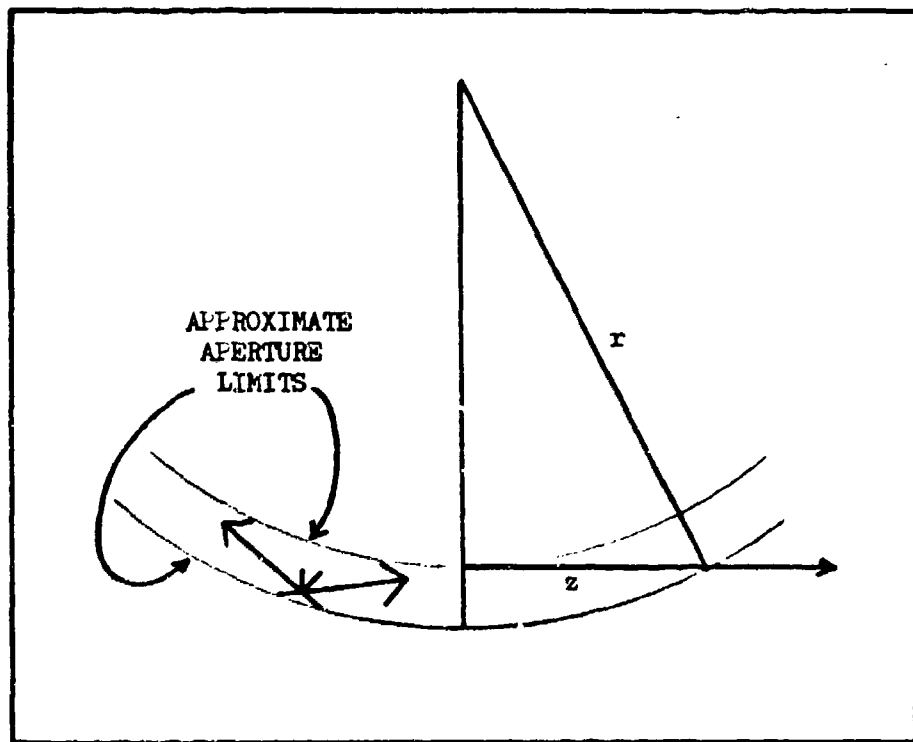


Fig. 28. Estimate of Maximum Ray Length

two plane polarizations are still the eigenpolarizations of this resonator.

In a laser system using a parallel-roof resonator, the eigenpolarization that would be dominant depends on two factors. First is the presence of other surfaces, such as Brewster windows on a gas tube or the Q-switch cell shown in Fig. 5. Second is the loss for each polarization at the four roof reflector surfaces. For metal front-surfaced reflectors, for example, these losses could be computed from the Fresnel formulas given by Born and Wolf (Ref 6:628-629).

## V. Resonators With Roofs Crossed

The resonator considered in this chapter is similar to the one studied by Gould, et al., shown in Fig. 2. Here, the right-hand reflector,  $R_1$ , has variant angle  $\alpha_1$  and roof edge horizontal (parallel to the y-axis), and the left-hand reflector,  $R_2$ , has variant angle  $\alpha_2$  and roof edge vertical (parallel to the x-axis). As in Chapter IV, the variant angles are considered to be small, so the apertures of the two reflectors are considered equal and (approximately) square. The resonator axis is of length  $L$  so that when the roof reflectors are perfectly aligned, the axis joins the midpoints of the roof edges.

The crossed-roof resonator can be considered as a three-dimensional superposition of two two-dimensional resonators. This is shown in Fig. 29 where a vertical cross-section of the resonator - called the "elevation" - is shown to contain the profile of  $R_1$  and the roof edge of  $R_2$ . A horizontal cross-section - called the "plan" - is shown to contain the profile of  $R_2$  and the roof edge of  $R_1$ . This decomposition suggests that stable rays in the crossed-roof resonator can be found from superpositions of the patterns of Chapter IV. This is indeed the case, as will be shown after some preliminary work.

### Three-Dimensional Ray Tracing

Before considering the general case of both variant angles non-zero in a crossed-roof resonator, the basic geometric tool for ray tracing will be worked out and applied to two simpler examples.

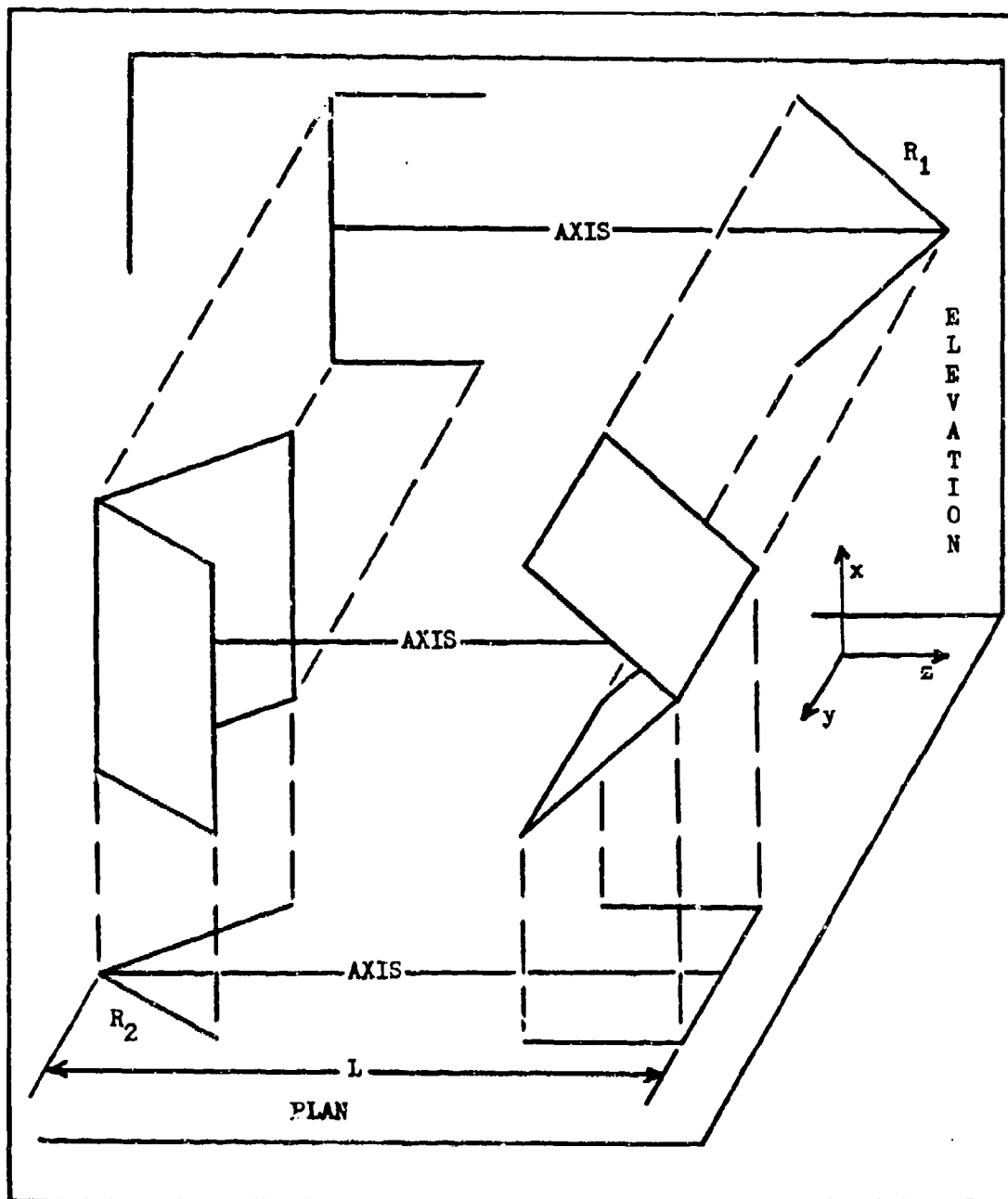


Fig. 29. Three-Dimensional Roof Reflector Resonator as a Superposition of Two-Dimensional Resonators

4x4 Matrix Transformations. In three-dimensions, as in two, rays can be described analytically with column vectors. This may be done by projecting a ray into two orthogonal planes; then two coordinates - position and slope - are required in each plane, as in Fig. 30. Thus:

$$\vec{x} = \begin{bmatrix} x \\ \theta \\ y \\ \phi \end{bmatrix} \quad (67)$$

where the x- and y-displacements are independent of one another, as are the angles  $\theta$  and  $\phi$ . As in two-dimensions, the forward direction of the ray determines the sense of the angles  $\theta$  and  $\phi$ . (Ref 22:502-504)

The propagation of three-dimensional rays is similar to that of two-dimensional rays. Since the two projections are independent, the familiar translation matrix of first-order optics can be used when suitably arranged in a partitioned 4x4 form. For example, to translate a ray through a distance L, the matrix equation is

$$\begin{bmatrix} x_1 \\ \theta_1 \\ y_1 \\ \phi_1 \end{bmatrix} = \begin{bmatrix} 1 & L & 0 & 0 \\ 0 & 1 & 0 & 0 \\ \hline 0 & 0 & 1 & L \\ 0 & 0 & 0 & 1 \end{bmatrix} \begin{bmatrix} x_0 \\ \theta_0 \\ y_0 \\ \phi_0 \end{bmatrix} \quad (68)$$

where the zeros in the upper-right and lower-left quadrants clearly indicate that the x- and y-directions are uncoupled.

The 4x4 ray transformation matrix for a roof reflector is also a partitioned form of 2x2 matrices and - in the general case of non-zero

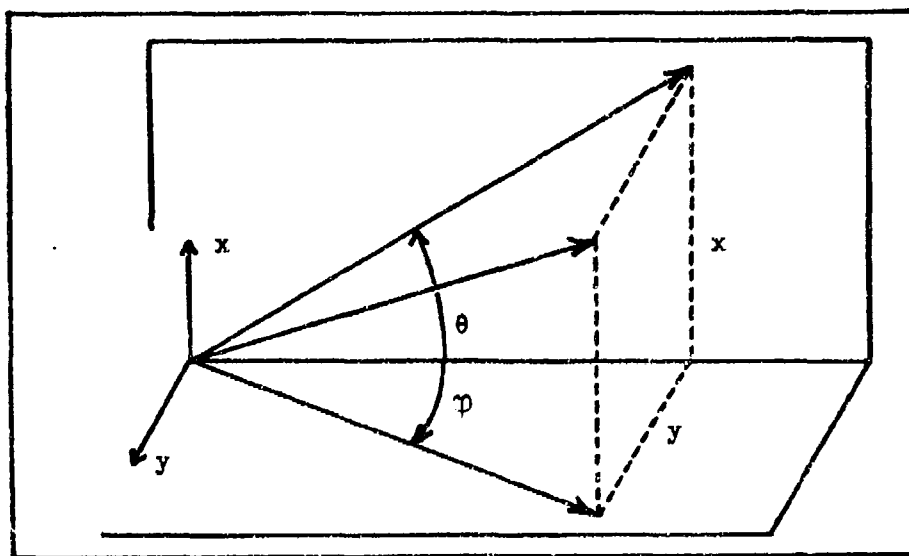


Fig. 30. Three-Dimensional Ray Coordinates

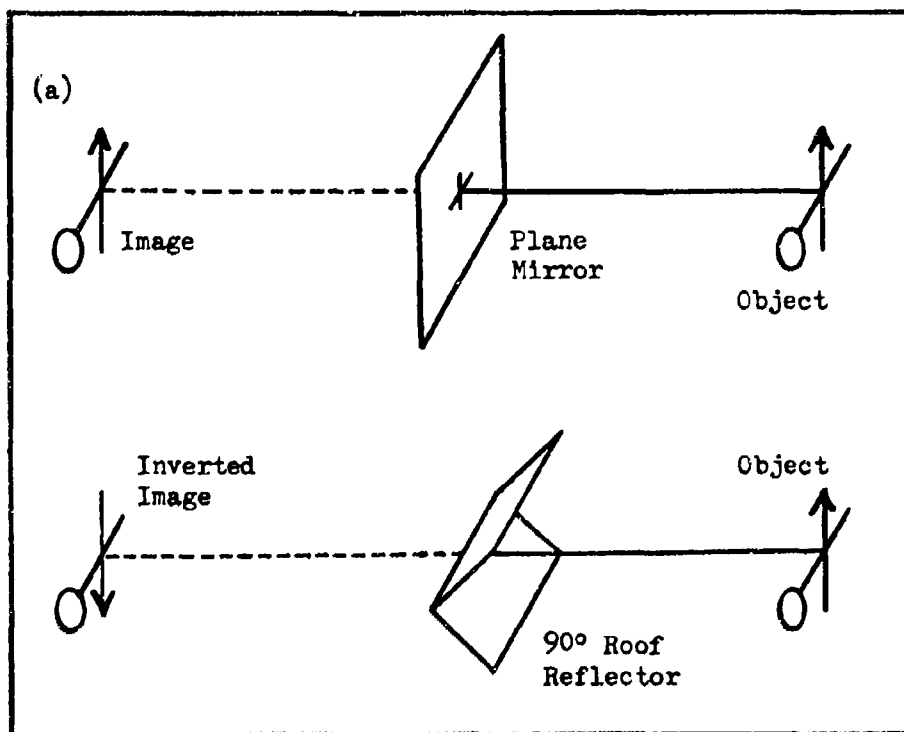


Fig. 31. Image Inversion by a Roof Reflector

variant angles - follows from the inhomogeneous transformation of Chapter III. To develop this three-dimensional transformation, first consider reflection by a plane mirror as in Fig. 31(a). Since an image is neither inverted nor reversed, the transformation for a plane mirror is an identity matrix:

$$\begin{bmatrix} x_1 \\ \theta_1 \\ y_1 \\ \phi_1 \end{bmatrix} = \begin{bmatrix} 1 & 0 & 0 & 0 \\ 0 & 1 & 0 & 0 \\ 0 & 0 & 1 & 0 \\ 0 & 0 & 0 & 1 \end{bmatrix} \begin{bmatrix} x_0 \\ \theta_0 \\ y_0 \\ \phi_0 \end{bmatrix} \quad (69)$$

For a 90° roof reflector, however, the image is inverted while left-and-right remain the same as in Fig. 31(b). The transformation for this roof reflector is then:

$$\begin{bmatrix} x_1 \\ \theta_1 \\ y_1 \\ \phi_1 \end{bmatrix} = \begin{bmatrix} -1 & 0 & 0 & 0 \\ 0 & -1 & 0 & 0 \\ 0 & 0 & 1 & 0 \\ 0 & 0 & 0 & 1 \end{bmatrix} \begin{bmatrix} x_0 \\ \theta_0 \\ y_0 \\ \phi_0 \end{bmatrix} \quad (70)$$

Thus, considering only roof reflectors whose roof edges are in the x- or y-directions, the minus signs (which signify inversion) go with the ray projection in the plane perpendicular to the roof edge.

Extending the transformation Eq. (70) to the case of non-zero variant angles, the ray transformation is as given by Eq. (26) in the projection perpendicular to the roof edge. Using Fig. 29 as an example, the transformation for a ray incident on  $R_1$  is given by:

$$\begin{bmatrix} x_1 \\ \theta_1 \\ y_1 \\ \varphi_1 \end{bmatrix} = \begin{bmatrix} -1 & 0 & 0 & 0 \\ 0 & -1 & 0 & 0 \\ \hline 0 & 0 & 1 & 0 \\ 0 & 0 & 0 & 1 \end{bmatrix} \begin{bmatrix} x_0 \\ \theta_0 \\ y_0 \\ \varphi_0 \end{bmatrix} \pm \begin{bmatrix} 0 \\ 2\alpha_1 \\ 0 \\ 0 \end{bmatrix} \quad (71)$$

where the "+" sign is to be taken when the ray is incident on the upper surface of  $R_1$ , and conversely. For  $R_2$ , the transformation is

$$\begin{bmatrix} x_1 \\ \theta_1 \\ y_1 \\ \varphi_1 \end{bmatrix} = \begin{bmatrix} 1 & 0 & 0 & 0 \\ 0 & 1 & 0 & 0 \\ \hline 0 & 0 & -1 & 0 \\ 0 & 0 & 0 & -1 \end{bmatrix} \begin{bmatrix} x_0 \\ \theta_0 \\ y_0 \\ \varphi_0 \end{bmatrix} \pm \begin{bmatrix} 0 \\ 0 \\ 0 \\ 2\alpha_2 \end{bmatrix} \quad (72)$$

where now the "+" sign goes with a ray incident on the front surface, and conversely.

Right-angled Crossed-Roof Resonator. As a simple example of three-dimensional ray tracing, the ray shown in Fig. 2 is particularly easy to follow. Here,  $\alpha_1 = \alpha_2 = 0$  - so Eqs. (71) and (72) are both homogeneous - and the ray makes two round-trips before closing on itself. To trace this ray, consider a starting point in a plane at mid-axis. The ray then translates a total of four times the length of the axis and four transformations before returning to the reference point. Following this ray around, it is not surprising to find that the system matrix is

$$\begin{bmatrix} x_g \\ \theta_g \\ y_g \\ \varphi_g \end{bmatrix} = \begin{bmatrix} 1 & 4L & 0 & 0 \\ 0 & 1 & 0 & 0 \\ \hline 0 & 0 & 1 & 4L \\ 0 & 0 & 0 & 1 \end{bmatrix} \begin{bmatrix} x_0 \\ \theta_0 \\ y_0 \\ \varphi_0 \end{bmatrix} \quad (73)$$

Equation (73) is just the result expected from tracing a ray through one round-trip in a plane mirror resonator of length  $2L$ . Since the stable ray solutions are parallel to the resonator axis ( $\theta_0 = \varphi_0 = 0$ ), they are not restricted from approaching the roof edges, and the resonant modes should therefore be expected to be the same as for a Fabry-Perot resonator except for diffraction by the imperfect roof edges. (It has been suggested by Weichel, Ref 44, that computer solutions for the modes of a  $90^\circ$  crossed-roof resonator could be done by replacing the roof reflectors with apertures and approximating the roof edges with thin wires across the apertures.)

One Variant Angle Non-zero. The second example to be considered is for one variant angle non-zero. With  $\alpha_1 \neq 0$  and  $\alpha_2 = 0$ , the resonator is similar to one roof reflector,  $R_1$  in Fig. 2, facing a plane mirror, except that left-and-right become interchanged by  $R_2$ . To trace a ray through two round-trips, the order of signs to be used when applying transformation Eq. (71) at  $R_1$  is the same as for a  $p_2 = 1$  pattern from Chapter IV. The result is

$$\begin{bmatrix} x_9 \\ \theta_9 \\ y_9 \\ \varphi_9 \end{bmatrix} = \begin{bmatrix} 1 & 4L & 0 & 0 \\ 0 & 1 & 0 & 0 \\ \hline 0 & 0 & 1 & 4L \\ 0 & 0 & 0 & 1 \end{bmatrix} \begin{bmatrix} x_0 \\ \theta_0 \\ y_0 \\ \varphi_0 \end{bmatrix} + \begin{bmatrix} -4L\alpha_1 \\ 0 \\ 0 \\ 0 \end{bmatrix} \quad (74)$$

and, for closed path rays, the solutions are  $\theta_0 = \alpha_1$  and  $\varphi_0 = 0$ .

A solution ray is illustrated in Fig. 32 where the actual crossing point,  $K$ , is imaged at  $K'$  by the front surface of  $R_2$ . The image point,  $K'$ , is also shown to be projected onto the roof edge in

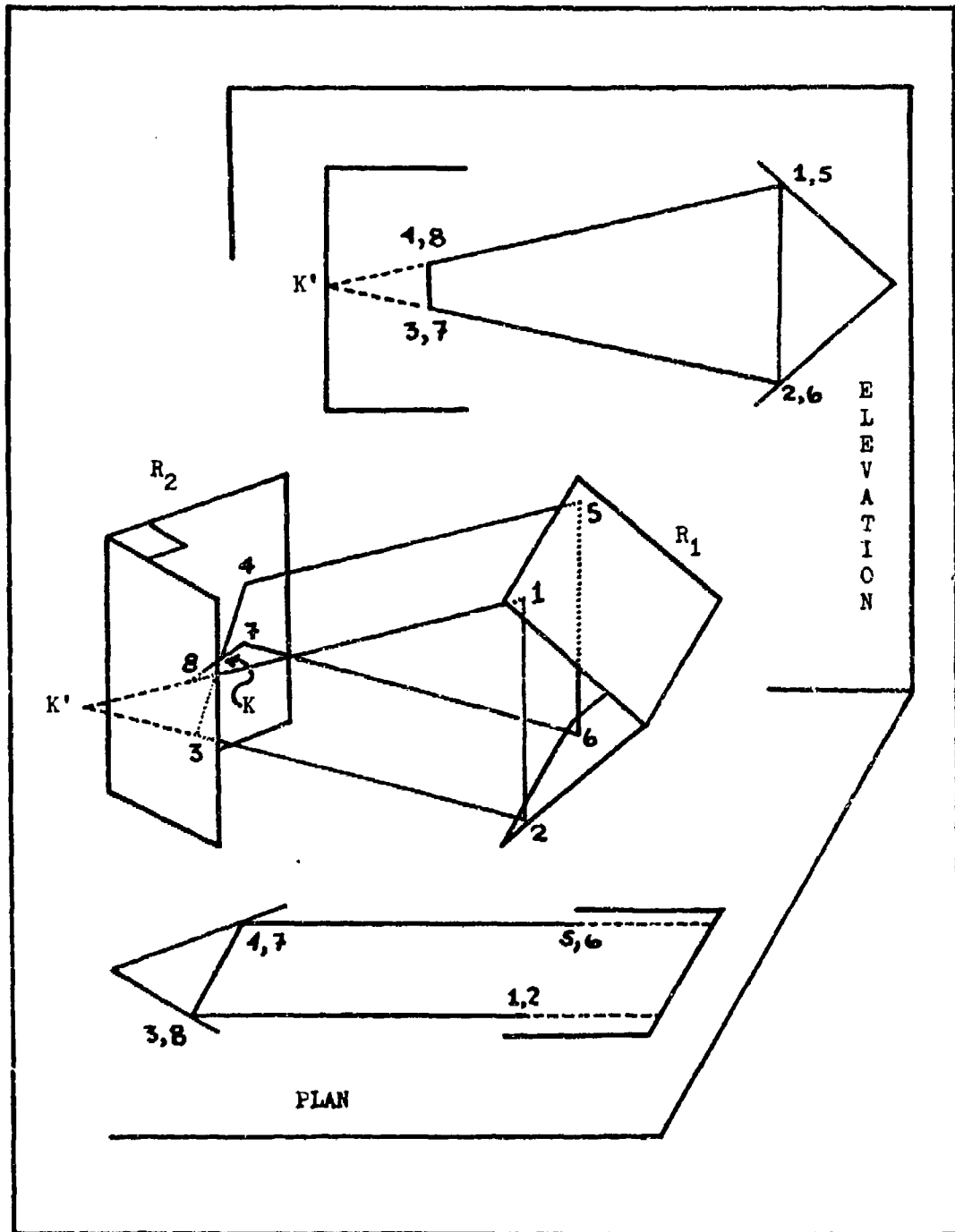


Fig. 32. Stable  $p_3 = 1$  Ray in Crossed-Roof Resonator With One Non-zero Variant Angle

the elevation, which is seen to be (half of) a  $p_2 = 1$  pattern. In the plan projection, the ray of Fig. 32 is seen to be a pattern of the  $90^\circ$  parallel-roof resonator, and is not restricted, geometrically, from approaching the roof edge of  $R_2$ .

Although Fig. 32 shows a  $p_2 = 1$  pattern in elevation, it should be clear that other patterns become possible as the resonator axis length decreases, as in Chapter IV. All the results of Chapter IV, in fact, apply if the pattern number is defined:

$$p_3 = \frac{\{\text{\# of round-trips}\}}{2} \quad (75)$$

The general ray-trace matrix through an even number of round-trips then becomes:

$$\begin{bmatrix} x_{8p_3+1} \\ \theta_{8p_3+1} \\ y_{8p_3+1} \\ \phi_{8p_3+1} \end{bmatrix} = \begin{bmatrix} 1 & 4p_3L & 0 & 0 \\ 0 & 1 & 0 & 0 \\ 0 & 0 & 1 & 4p_3L \\ 0 & 0 & 0 & 1 \end{bmatrix} \begin{bmatrix} x_0 \\ \theta_0 \\ y_0 \\ \phi_0 \end{bmatrix} + \begin{bmatrix} -4p_3^2L\alpha_1 \\ 0 \\ 0 \\ 0 \end{bmatrix} \quad (76)$$

Closed path rays of a particular pattern exist when the axis length is less than:

$$L_0^{(F)} = \frac{D_0}{p_3} \quad (77)$$

where  $D_0$  is calculated for the right-hand reflector. The stable rays are characterized by:

$$\theta_0 = p_3\alpha_1 \quad \text{and} \quad \phi_0 = 0 \quad (78)$$

and they fill the maximum volume in the resonator when:

$$L \approx \frac{L_0^{(p)}}{2} = \frac{D_0}{2 p_3} \quad (79)$$

The optical path length is

$$P_{p_3} = 4 p_3 L \quad (80)$$

The importance of these patterns is not in their existence in a physical device, but as a logical step in developing the more general theory that follows. It is seen that crossed-roof resonators with only one non-zero variant angle are probably not desirable because the roof edge of the 90° reflector is geometrically accessible.

#### The General Case

The most general case of crossed-roof resonators can now be considered: both variant angles non-zero. As in the second example just considered, the patterns of the three-dimensional resonator are superpositions of the patterns in Chapter IV.

When the two-dimensional resonator was studied in Chapter IV, the sequences of signs that were developed, Eq. (38) and Eq. (39), for applying Eq. (26) in tracing a ray through  $p_2$  round-trips all began with "+". The sequences could equally well have begun with "-" and have followed the same alternating scheme; but all these sequences are identical to the former - they just trace a ray through the resonator in reverse. While the individual elevation and plan projections considered in this chapter are, indeed, identical whether traced forward or backward, it will now become important which direction the tracing proceeds as the two are combined in the three-dimensional resonator.

First Pattern. The first demonstration that the order of signs is important comes in tracing what should be expected to be the  $p_3 = 1$  pattern - two round-trips in a crossed-roof resonator with  $\alpha_1 \neq 0$  and  $\alpha_2 \neq 0$ . Again starting at mid-axis and first translating to the right, the sequence in which the roof reflectors is encountered is

$$\text{right} / \text{left} / \text{right} / \text{left} \quad (81)$$

Since the right and left reflectors determine the patterns that are projected into the elevation and plan, respectively, two-dimensional  $p_2 = 1$  patterns are expected in these two planes, with sign sequences either  $+, +$  or  $-, -$  for either reflector. Substituting these independent sequences into the above transformation order, there are four possibilities:

$$\begin{array}{ll} (1) & \begin{array}{c} \overbrace{+ / + / + / +}^{\text{right}} \\ \underbrace{\phantom{+ / + / + / +}}_{\text{left}} \end{array} \\ (2) & \begin{array}{c} \overbrace{+ / - / + / -} \\ \underbrace{\phantom{+ / - / + / -}} \end{array} \\ (3) & \begin{array}{c} \overbrace{- / + / - / +} \\ \underbrace{\phantom{- / + / - / +}} \end{array} \\ (4) & \begin{array}{c} \overbrace{- / - / - / -} \\ \underbrace{\phantom{- / - / - / -}} \end{array} \end{array} \quad (82)$$

Not all of these sign sequences lead to distinct stable ray solutions, however. The same comment as above about tracing a ray forward or backward applies, and the first and fourth sequences describe the same ray, as do the second and third.

Applying the first sequence of signs to trace a ray through two round-trips, the resultant system matrix is

$$\begin{bmatrix} x_9 \\ \theta_9 \\ y_9 \\ \varphi_9 \end{bmatrix} = \begin{bmatrix} 1 & 4L & 0 & 0 \\ 0 & 1 & 0 & 0 \\ 0 & 0 & 1 & 4L \\ 0 & 0 & 0 & 1 \end{bmatrix} \begin{bmatrix} x_0 \\ \theta_0 \\ y_0 \\ \varphi_0 \end{bmatrix} + \begin{bmatrix} -4La_1 \\ 0 \\ -4La_2 \\ 0 \end{bmatrix} \quad (83)$$

which will have stable ray solutions characterized by:

$$\theta_0 = a_1 \quad \text{and} \quad \varphi_0 = a_2 \quad (84)$$

Applying the second sequence of signs, the resultant system matrix is

$$\begin{bmatrix} x_9 \\ \theta_9 \\ y_9 \\ \varphi_9 \end{bmatrix} = \begin{bmatrix} 1 & 4L & 0 & 0 \\ 0 & 1 & 0 & 0 \\ 0 & 0 & 1 & 4L \\ 0 & 0 & 0 & 1 \end{bmatrix} \begin{bmatrix} x_0 \\ \theta_0 \\ y_0 \\ \varphi_0 \end{bmatrix} + \begin{bmatrix} -4La_1 \\ 0 \\ +4La_2 \\ 0 \end{bmatrix} \quad (85)$$

which will have stable ray solutions characterized by:

$$\theta_0 = a_1 \quad \text{and} \quad \varphi_0 = -a_2 \quad (86)$$

The two rays characterized by Eqs. (84) and (86) are drawn in Figs. 33 and 34, respectively, where the individual reflections are numbered as an aid to tracing the rays. It is easy to see that following the rays in reverse leads to the sequences of signs that were claimed to be identical to those taken to develop Eqs. (83) and (85). More important, however, is that the two stable rays are independent and do not coincide within the resonator, except at a finite number of crossing points. (Assuming the losses are equal, it is assumed that

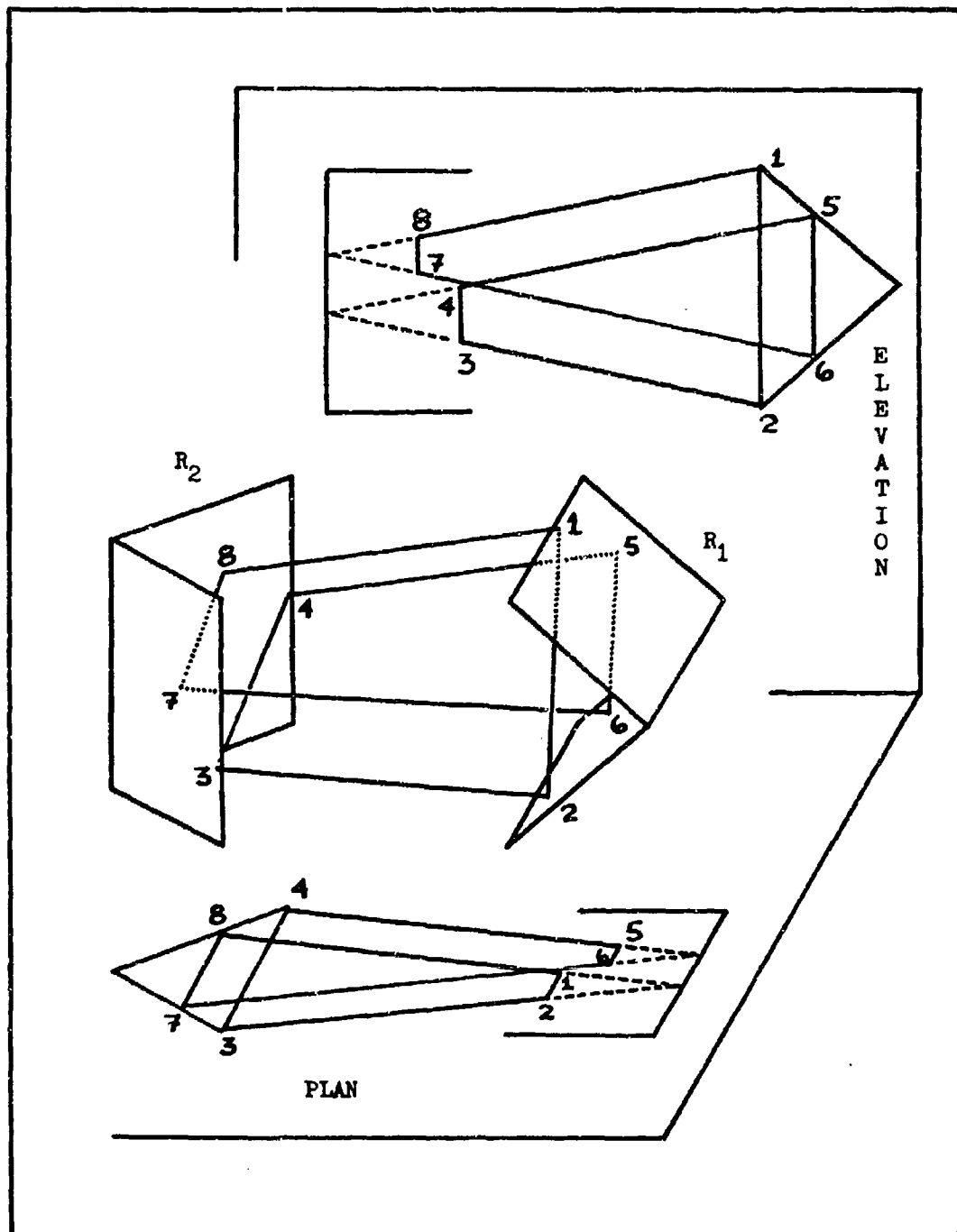


Fig. 33. First Crossed-Roof  $p_3 = 1$  Pattern

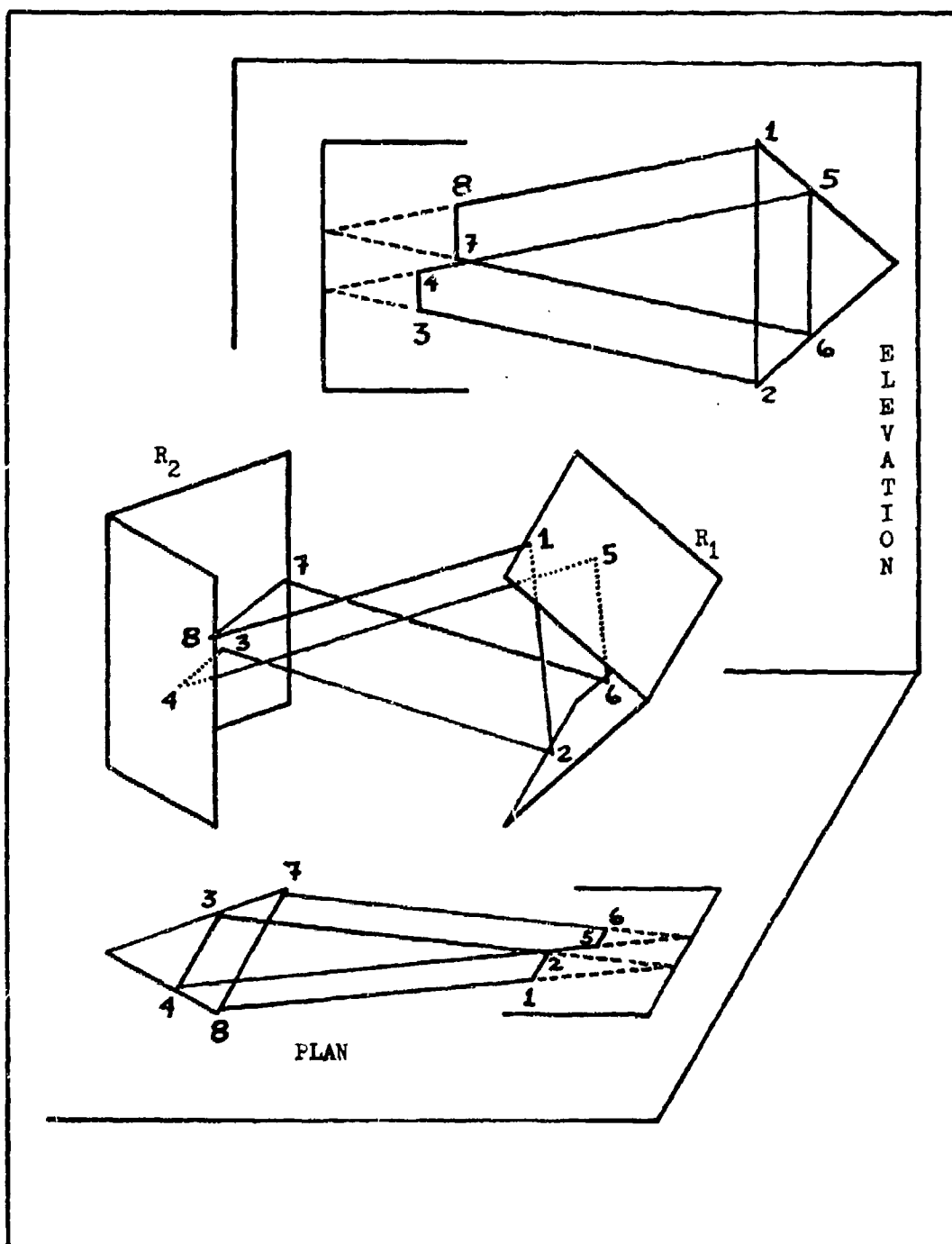


Fig. 34. Second Crossed-Roof  $p_3 = 1$  Pattern

the rays are sufficiently coupled by the lasing medium at the crossing points to form standing waves. See p. 26.)

Central Rays and First Pattern Volume. The rays drawn in Figs. 33 and 34 are not the only possible stable rays of the first pattern. As in Chapter IV, the maximum axis length (stability condition) for this pattern is

$$L_{\max} = D_0 \quad (87)$$

where  $D_0$  is computed for the reflector having the larger variant angle. When the axis length is less than this value, a packet of rays in both projections can be combined in the three-dimensional resonator to form a geometric tube with rectangular cross-section. This has been done in Figs. 35 and 36 where the geometrically accessible areas on the roof reflector surfaces are rectangular. The dimensions of the tube cross-sections are given by the ray packet heights in the two projections,  $h_1$  and  $h_2$ , which may be computed from Eq. (50).

The tubes of rays in Figs. 35 and 36 have interesting properties. A ray which defines one corner of the tube traces through two round-trips before closing on itself. Thus, starting at A in Fig. 35, after one round-trip the ray is at A' on the opposite corner of the tube cross-section; and after two round-trips it is back to A. This is true for any ray in the interior of the tube (except for the central ray which is discussed below). This feature of the ray tubes is reminiscent of the Moebius strip which is a two-dimensional figure but has only one surface and one edge. Here, the ray tube similarly

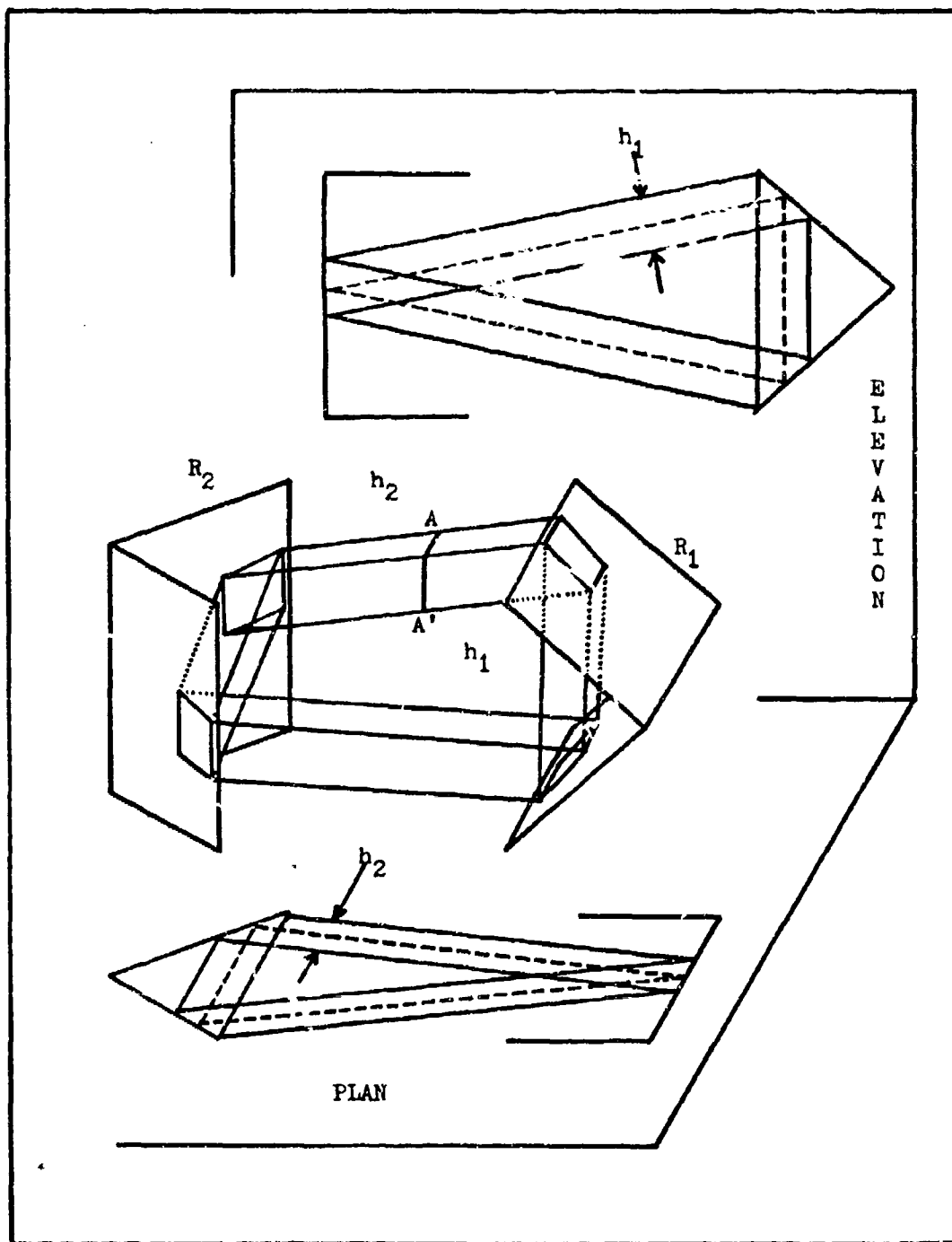


Fig. 35. First Geometric Tube of Rays for  $p_3 = 1$  Pattern

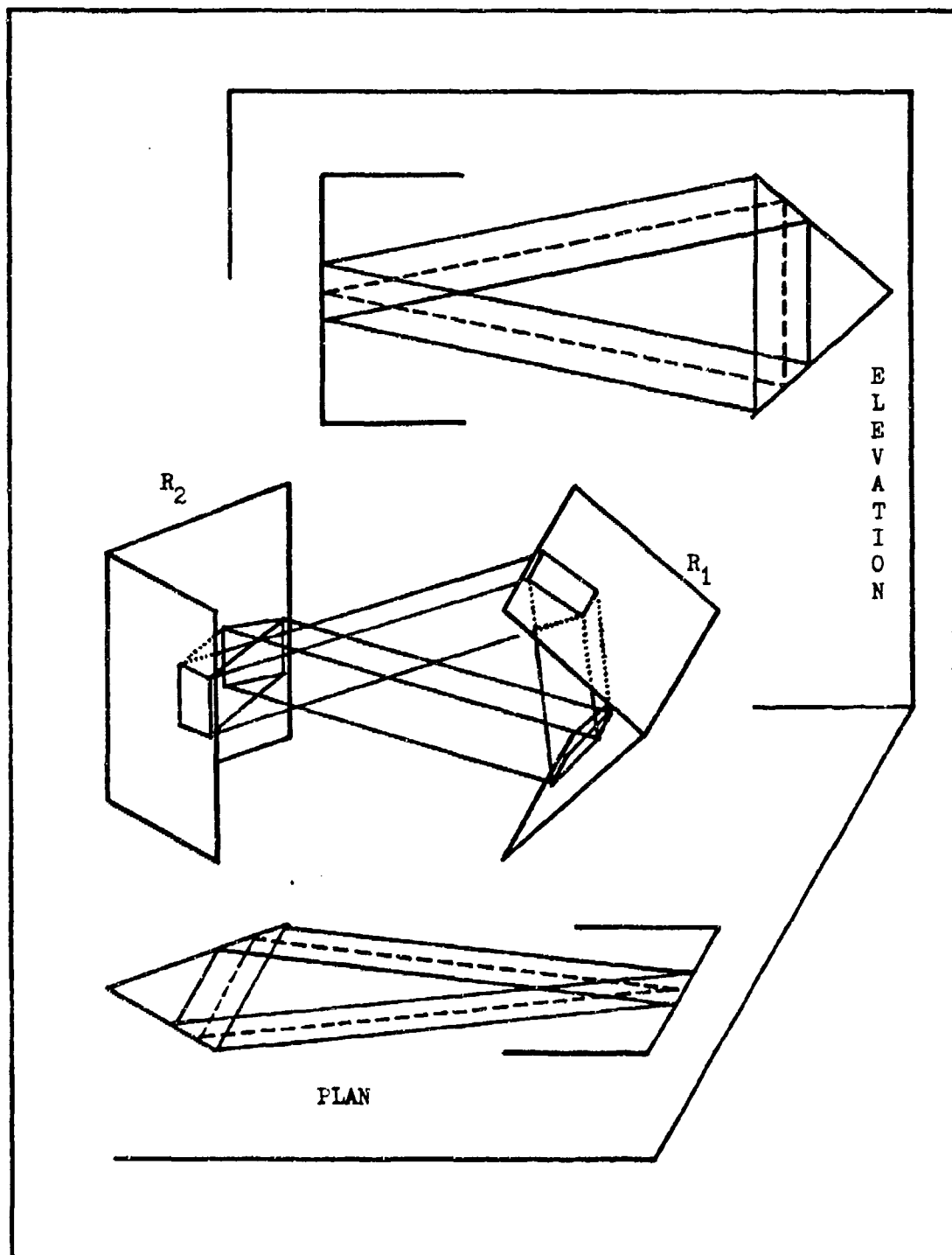


Fig. 36. Second Geometric Tube of Rays for  $p_3 = 1$  Pattern

makes a half-twist in joining on itself, but is a three-dimensional figure with a single two-dimensional surface.

In either Fig. 35 or Fig. 36, it is seen that there is a central ray in both the plan and elevation that makes only one round-trip before closing on itself. (These are shown as dashed lines in the figures and still represent  $p_2 = 1$  patterns.) Figure 37 shows these two central rays in the crossed-roof resonator, and correspond to the ray tubes of Figs. 35 and 36. The central rays still are a part of the  $p_3 = 1$  pattern, but are apparently degenerate in that the same path is traced twice. Analytically tracing the central rays through one round-trip (again starting at mid-axis), it is found for the one corresponding to Fig. 35:

$$\begin{bmatrix} x_5 \\ \theta_5 \\ y_5 \\ \varphi_5 \end{bmatrix} = \begin{bmatrix} -1 & -2L & 0 & 0 \\ 0 & -1 & 0 & 0 \\ 0 & 0 & -1 & -2L \\ 0 & 0 & 0 & -1 \end{bmatrix} \begin{bmatrix} x_0 \\ \theta_0 \\ y_0 \\ \varphi_0 \end{bmatrix} + \begin{bmatrix} 3La_1 \\ 2a_1 \\ La_2 \\ 2a_2 \end{bmatrix} \quad (88)$$

and for the other:

$$\begin{bmatrix} x_5 \\ \theta_5 \\ y_5 \\ \varphi_5 \end{bmatrix} = \begin{bmatrix} -1 & -2L & 0 & 0 \\ 0 & -1 & 0 & 0 \\ 0 & 0 & -1 & -2L \\ 0 & 0 & 0 & -1 \end{bmatrix} \begin{bmatrix} x_0 \\ \theta_0 \\ y_0 \\ \varphi_0 \end{bmatrix} + \begin{bmatrix} 3La_1 \\ 2a_1 \\ -La_2 \\ -2a_2 \end{bmatrix} \quad (89)$$

As expected, the central rays are unique solutions of these equations. The ray that satisfies Eq. (88) is

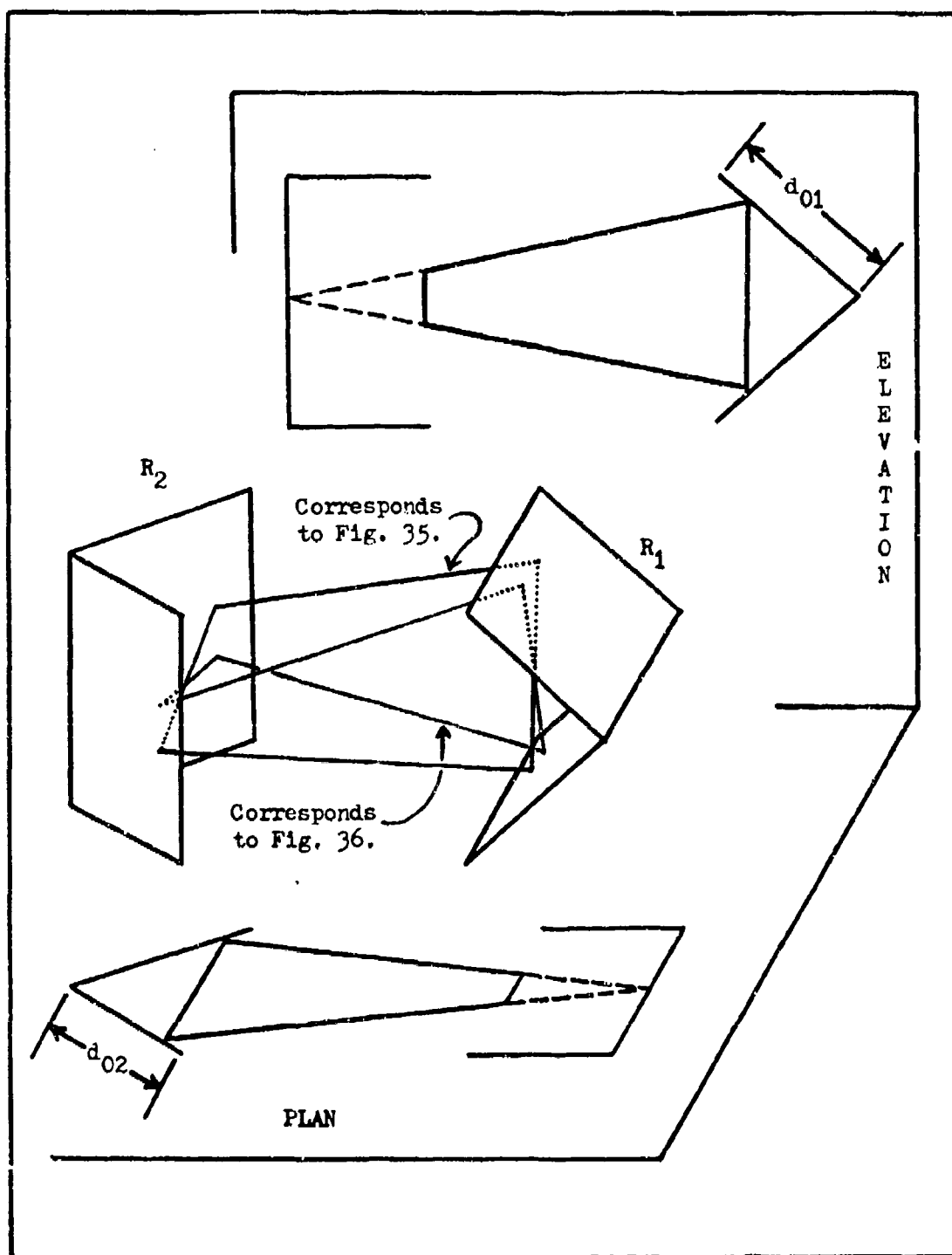


Fig. 37. Central Rays

$$\begin{aligned}
 x_0 &= \frac{L a_1}{2} \\
 \theta_0 &= a_1 \\
 y_0 &= \frac{L a_2}{2} \\
 \phi_0 &= a_2
 \end{aligned}
 \tag{90}$$

and the ray that satisfies Eq. (89) is

$$\begin{aligned}
 x_0 &= \frac{L a_1}{2} \\
 \theta_0 &= a_1 \\
 y_0 &= \frac{L a_2}{2} \\
 \phi_0 &= -a_2
 \end{aligned}
 \tag{91}$$

It is seen that the two rays do not cross between the reflectors, but do cross between the surfaces of an individual reflector.

There is an important similarity between the two central rays in Fig. 37. Both have the same path length for one round-trip. By inspection of Eqs. (88) and (89), this path length is

$$F = 2 L \tag{92}$$

The volume of the  $p_3 = 1$  pattern (for one of the central rays) is thus approximately given by

$$\begin{aligned}
 V &\approx 2 L h_1 h_2 \\
 &\approx 2 L d_{01} d_{02} \left[ 2 + \sqrt{2} L \left[ \frac{a_1}{d_{01}} + \frac{a_2}{d_{02}} \right] \right]
 \end{aligned}$$

where  $d_{01}$  and  $d_{02}$  are the dimensions of the surfaces of  $R_1$  and  $R_2$ , respectively. Since there are the two possible central rays, the entire volume that is geometrically accessible by the  $p_3 = 1$  pattern is approximately twice that given by Eq. (93). There is some overlap between the two ray tubes near the reflector surfaces.

Higher-order Patterns. As with the two-dimensional resonator, stable patterns are possible in which rays make a multiple of two round-trips. As the pattern number increases, the number of independent solutions that can be found increases due to the different ways of combining elevation and plan sign sequences. In actual devices, each independent ray would produce an output beam in a different direction, so patterns higher than  $p_3 = 1$  are probably undesirable. Accordingly, the general system matrices for higher order patterns are not given here, but a method for finding the different independent rays is illustrated in the following example for  $p_3 = 2$ .

Tracing a ray through four round-trips, it is reasonable to expect  $p_2 = 2$  patterns to be projected into the elevation and plan as the ray undergoes eight roof reflector transformations. In either projection, the sequence of signs could be either  $+, -, -, +$  or  $-, +, +, -$  from Eq. (39). (the two sequences are equivalent, however, so only one need be considered. This may be seen by writing two successive  $p_2 = 2$  sequences - starting with either a plus or minus sign - and noting that it is an alternating pattern of pairs of like signs.) If the alternating sequence:

$$\text{right} / \text{left} / \text{right} / \text{left} / \text{right} / \text{left} / \text{right} / \text{left} \quad (94)$$

is considered, there are four ways in which the  $p_2 = 2$  sign sequences can be combined. They are listed here, and a ray corresponding to the first sequence is drawn in Fig. 38:

$$\begin{array}{lcl}
 (1) & \begin{array}{c} \text{+ / + / - / - / - / - / + / +} \\ \text{+ / + / - / - / - / - / + / +} \end{array} & \begin{array}{l} \text{right} \\ \text{left} \end{array} \\
 (2) & \begin{array}{c} \text{+ / + / - / + / - / - / - / + / -} \\ \text{+ / + / - / + / - / - / - / + / -} \end{array} & \\
 (3) & \begin{array}{c} \text{+ / - / - / + / - / + / + / + / -} \\ \text{+ / - / - / + / - / + / + / + / -} \end{array} & \\
 (4) & \begin{array}{c} \text{+ / - / - / - / - / - / + / + / +} \\ \text{+ / - / - / - / - / - / + / + / +} \end{array} & 
 \end{array} \tag{95}$$

In addition to independent rays for these sequences, it is also possible to mix different patterns from the two projections. While the projection of a  $p_3 = 2$  ray in the elevation could be a  $p_2 = 2$  pattern, for instance, its projection in the plan could be a  $p_2 = 1$  pattern that is traced around twice for once in the elevation. Different combinations of these patterns give rise to other distinct sequences such as these:

$$\begin{array}{lcl}
 (5) & \begin{array}{c} \text{+ / + / + / - / + / - / + / +} \\ \text{+ / + / + / - / + / - / + / +} \end{array} & \\
 (6) & \begin{array}{c} \text{+ / + / - / + / - / - / + / +} \\ \text{+ / + / - / + / - / - / + / +} \end{array} & 
 \end{array} \tag{96}$$

In general, the number of independent rays of the first type (both elevation and plan pattern numbers equal to  $p_3$ ) that can be found is thought to be  $2p_3$ . The number of possible rays of the second type (elevation and plan pattern numbers different) obviously increases as  $p_3$  increases, but a general expression for their number has not been worked out.

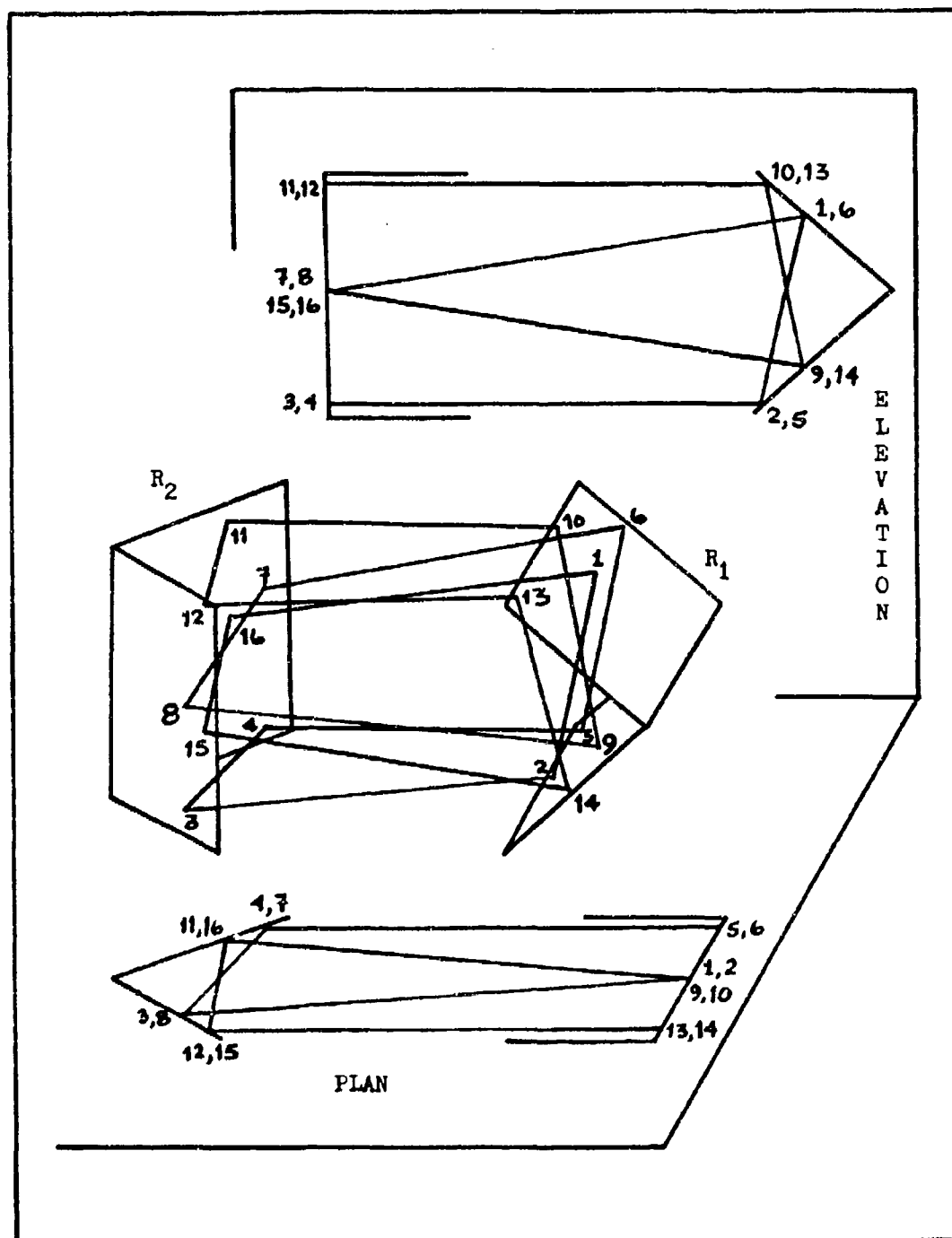


Fig. 38. A Possible  $p_3 = 2$  Pattern

Significance. The most important feature of the crossed-roof resonator patterns is that they are superpositions of the two projections. The results of Chapter IV apply to the two projections independently. Thus Eq. (47) can be modified and the stability condition for stable rays of pattern  $p_2$  to exist in either plan or elevation is

$$L \leq \frac{L_0^{(p)}}{2} = \frac{D_0}{p_2} = \frac{\sqrt{2} d_0}{2 p_2 \alpha} \quad (97)$$

(There is no restriction on the variant angle.) The same condition also holds that, in order for the roof edge to be geometrically excluded, the axis length must be greater than  $L_0^{(p)}/2$  computed for that roof reflector. It must be noted, however, that in order for the crossed-roof resonator to have any stable rays, both elevation and plan must have stable patterns simultaneously, so Eq. (97) is the general stability condition for  $p_3 = 1$  or higher when  $p_2 = 1$ , and  $D_0$  is computed for the larger variant angle.

The combination of the two independent patterns can get quite complicated if the individual pattern numbers are high. This is due to the fact that if the axis length is such as to permit, say, a  $p_2 = 4$  pattern in elevation, then  $p_2 = 3, 2$ , and  $1$  are also stable and may combine with the plan patterns. Some of these elevation patterns may approach the roof edges and, consequently, resonant modes free of diffraction effects would not be expected. (This is possibly why  $\approx 90^\circ$  crossed-roof resonators with extremely small variant angles - manufacturing tolerances - are noted to have poor beam divergence. The pattern numbers can be very large in these cases. See p. 15.)

### Resonant Modes of the First Pattern

For exactly the same arguments as were given in Chapter IV, it is reasonable to expect that Hermite-Gaussian modes can be supported by the crossed-roof resonator when the roof edges are geometrically excluded. If the tube of rays in either Fig. 35 or Fig. 36 is drawn out straight and the effect of aperturing by the roof reflector surfaces is considered, a picture such as Fig. 39 results. Here it has been assumed that each reflector surface can be replaced with a rectangular aperture normal to the ray tube. Each aperture limits the ray tube on only one side; but after travelling a distance  $2L$ , the tube has been restricted on all four sides.

From the point of view of either Fig. 35 or 36, the tube of rays appears to close on itself after one round-trip, so it is reasonable to expect that a wavefront could propagate a distance  $2L$  through the apertures of Fig. 39 and be self-reproducing. This is indeed possible for Hermite-Gaussian wavefronts, and a careful consideration of the phase relationships indicates that both odd and even modes are allowed.

Odd and Even Modes. Consider a cross-section of the ray tube as in Fig. 40. The central ray pierces the cross-section in the center and any other ray pierces the cross-section twice at  $A$  and  $A'$ . These two points are symmetric with respect to the central ray. On this cross-section, let the phase of a wavefront - propagating either direction along the ray tube - be  $\phi_{A_0}$  at  $A_0$  and  $\phi_{A'_0}$  at  $A'_0$ . Also, let the difference in phase between points  $A_0$  and  $A'_0$  be  $\phi_0$ , so that:

$$\phi_{A'_0} = \phi_{A_0} + \phi_0 \quad (98)$$

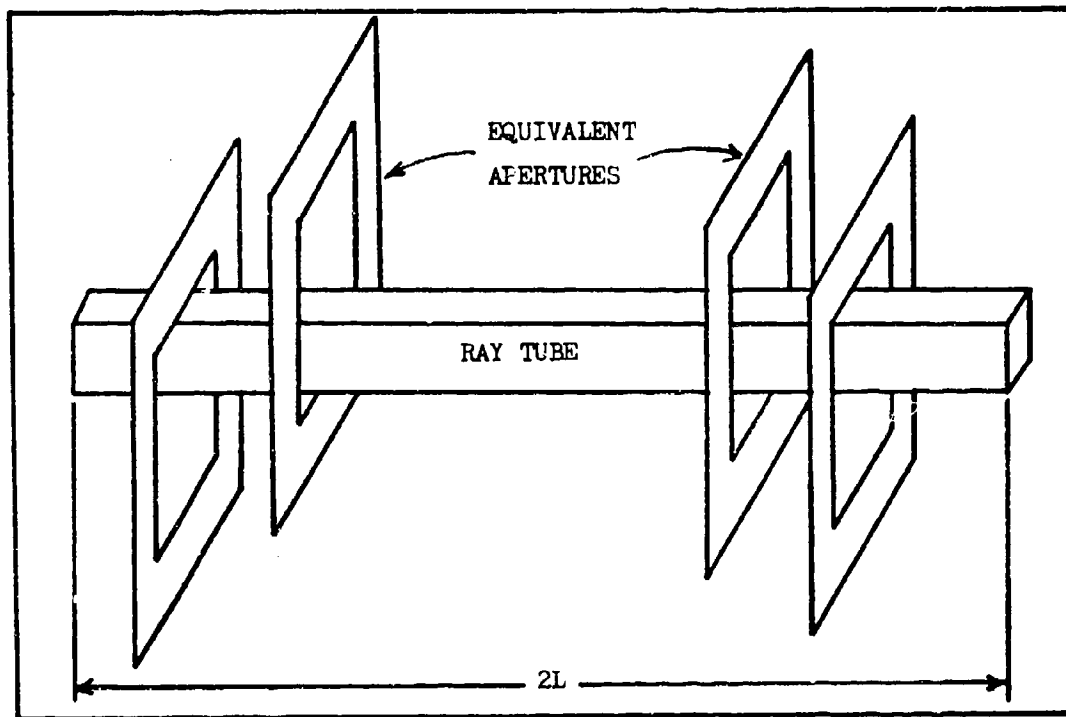


Fig. 39. Aperture Effects on  $p_3 = 1$  Ray Tube

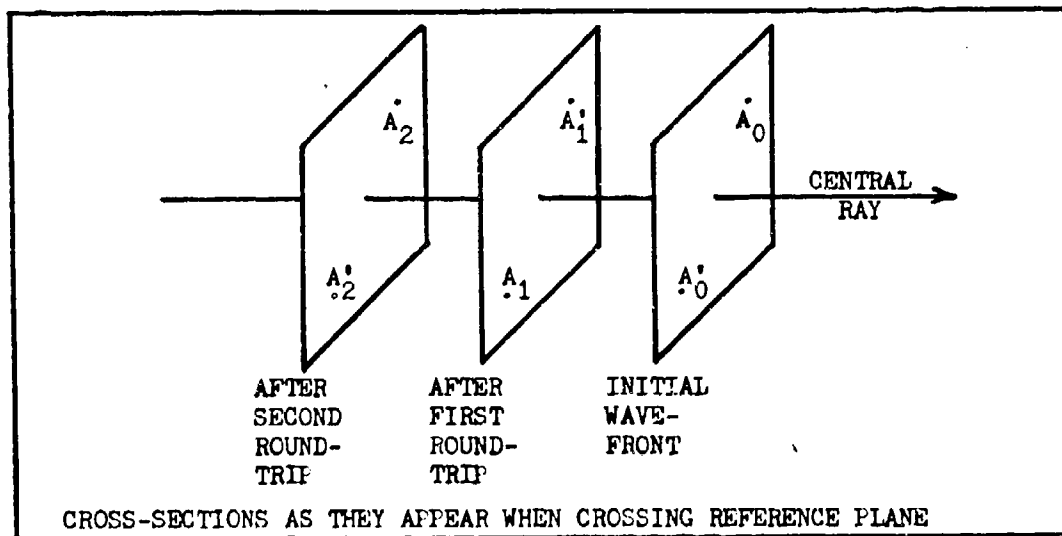


Fig. 40. Ray Tube Cross-Section

After the wavefront has propagated through one round-trip, the ray that started at  $A_0$  is now at  $A_1$ , but is spatially coincident with  $A'_0$ ; and conversely for the ray starting at  $A'_0$ . The phase at  $A_1$  is

$$\phi_{A_1} = \phi_{A_0} + 2\pi \frac{2L}{\lambda} + \Phi \quad (99)$$

where the second term in the sum is the phase shift due to the propagation through distance  $2L$  and  $\Phi$  is the phase shift due to reflection from the roof reflector surfaces. Now let the wavefront propagate through a second round-trip, and  $A$  and  $A'$  interchange again.

The phase at  $A_2$  is now:

$$\begin{aligned} \phi_{A_2} &= \phi_{A_1} + 2\pi \frac{2L}{\lambda} + \Phi \\ &= \phi_{A_0} + 2(2\pi \frac{2L}{\lambda} + \Phi) \end{aligned} \quad (100)$$

Then assuming that standing waves are formed (from the discussion of the first pattern), the requirement that the phase be self-reproducing in two round-trips is certainly reasonable:

$$\begin{aligned} \phi_{A_2} - \phi_{A_0} &= 2(2\pi \frac{2L}{\lambda} + \Phi) \\ &= 0 \quad (\text{mod } 2\pi) \end{aligned} \quad (101)$$

This implies that:

$$2\pi \frac{2L}{\lambda} + \Phi = 0 \quad \text{or} \quad \pi \quad (\text{mod } 2\pi) \quad (102)$$

which is the same as  $\phi_{A_1} - \phi_{A_0}$  from Eq. (99). But also Eq. (98) can be subtracted from Eq. (99) to get:

$$\phi_{A_1} - \phi_{A'_0} = (2\pi \frac{2L}{\lambda} + \Phi) - \phi_0 \quad (103)$$

Since these two phases,  $\phi_{A_1}$  and  $\phi_{A_0}$ , occur at the same point in space, they must be the same for self-reproducibility, and Eq. (103) must therefore be set equal to zero (mod  $2\pi$ ). Then substitution from Eq. (102) into Eq. (103) yields:

$$\phi_0 = 0 \quad \text{or} \quad \pi \quad (104)$$

The importance of this result is that wavefronts propagating through the ray tubes are allowed to be either even or odd with respect to the center of the mode pattern. The familiar Hermite-Gaussians (for the rectangular cross-section of the ray tube) indeed display this characteristic.

Axial Mode Frequency Interval. If  $\phi_0 = 0$ , self-consistency Eq. (103) can be rewritten as:

$$2\pi \frac{2L}{\lambda_q} + \phi = 2q\pi \quad (105)$$

where  $q$  is the number of wavelengths that can be fit into one round-trip. As was done in Chapter IV, the expression for the axial mode frequency interval follows at once:

$$\Delta f_q = \frac{c}{2L} \quad (106)$$

If  $\phi = \pi$ , Eq. (103) becomes:

$$2\pi \frac{2L}{\lambda_q} + \phi - \pi = 2q\pi \quad (107)$$

and the same result - Eq. (106) - again is obtained.

Intuitively,  $\Delta f_q = c/4L$  might have been a more expected result since rays travel a distance  $4L$  before closing on themselves. If this

were true, however, the central ray would be a null if there happened to be an odd number of wavelengths in two round-trips - that is the wavefront is out of phase with itself by  $\pi$  after one round-trip. This is not satisfying physically, since it is also reasonable to expect that the fundamental - or 00 - Hermite-Gaussian mode has the lowest loss and is therefore dominant. This mode is definitely non-zero at its center.

Transverse Mode Frequency Interval. The same arguments as were used in Chapter IV for the transverse mode frequency interval also apply here. The only difference is that the closed path rays satisfy a 4x4 matrix equation rather than a 2x2 matrix equation. For any closed path, this is given by Eq. (69) which is nothing more than an identity transformation. It is therefore expected that the transverse mode frequency interval is

$$\Delta f_{mn} = 0 \quad (62)$$

## VI. Conclusion

The geometric theory of roof reflector resonators has been developed for the two cases of (1) parallel-roof resonators (Fig. 17 ) and (2) crossed-roof resonators (Fig. 29 ). The assumptions that were made are listed in Chapter I, and the basic mathematical tool for ray tracing - an inhomogeneous ray transformation matrix - is derived in Chapter III. This chapter summarizes the important results of the theory and recommends areas for further study.

### Summary of Stability Conditions

Stability conditions are the physical dimensions of a resonator that allow stable rays to exist. Stable rays in roof reflector resonators have been shown in Chapters IV and V to be only those which close on themselves - that is, ring-type rays. Stability conditions for parallel-roof and crossed-roof resonators are given separately below.

Parallel-Roof Resonator. Stable rays can be found in the parallel-roof resonator that make any number of round-trips and are designated as "patterns" with a pattern number,  $p_2$ , defined as the number of round-trips a ray makes before closing on itself. There are two sets of stability conditions depending on whether  $p_2$  is odd or even:

(1) for  $p_2$  odd:

$$\alpha_1 = \alpha_2 = \alpha \quad (34)$$

$$L \leq L_0^{(p)} = \frac{\sqrt{2} d_0}{p_2 \alpha} \quad (47)$$

where  $\alpha_1$  and  $\alpha_2$  are the variant angles,  $L$  is the resonator axis length,  $L_0^{(p)}$  is the maximum length for pattern  $p_2$  to exist, and  $d_0$  is the surface dimension (see Fig. 14(a)).

(2) for  $p_2$  even:

(No restriction on variant angles) (44)

$$L \leq L_0^{(p)} = \frac{\sqrt{2} d_0}{p_2 \alpha} \quad (47)$$

where  $\alpha$  is the larger of the two variant angles.

Remarks are in order concerning these stability conditions.

First, Eq. (47) implies that if the resonator axis length is chosen less than, say,  $L_0^{(3)}$ , then either (1) stable rays of patterns  $p_2 = 3, 2$ , or 1 could exist if Eq. (34) is satisfied, or (2) stable rays of only  $p_2 = 2$  could exist if  $\alpha_1 \neq \alpha_2$ . Second, it is possible for different patterns to exist simultaneously - in which case they are spatially separated except at a finite number of crossing points. They are not unique rays, but entire bundles of parallel rays called "packets." Third, the number of possible patterns is theoretically infinite as  $L \rightarrow 0$ , but is practically limited in a real device. And, if  $\alpha_1 = \alpha_2 \rightarrow 0$ , then there is no defined maximum axis length, implying that there is always a stable ray in a  $90^\circ$  parallel-roof resonator.

Crossed-Roof Resonator. The stable rays that can exist in the crossed-roof resonator are shown, in Chapter V, to be superpositions of two parallel-roof patterns in orthogonal planes (see Fig. 33, for example). The pattern number,  $p_3$ , for a stable ray is defined as:

$$p_3 = \frac{[\# \text{ of round-trips}]}{2} \quad (75)$$

The condition that stable rays exist in the crossed-roof resonator is that stable patterns must exist in both of the projections. Accordingly, there are no restrictions on the variant angles, and the minimum condition that stable rays of any pattern number to exist is

$$L \leq \frac{\sqrt{2} d_0}{2 \alpha} \quad (108)$$

where  $\alpha$  is the larger variant angle.

The above remarks concerning patterns which can exist in the parallel-roof resonator also apply to the crossed-roof resonator, but one additional comment is necessary. This geometric theory predicts that, for any given  $p_3$ , there will be more than one stable ray packet, and these will generally be spatially separated and not parallel. Their number increases in a complicated way as the pattern number increases.

#### Major Predictions of This Thesis

The stated purpose of this thesis has been fulfilled with the above listing of the stability conditions, but the most important conclusion is the prediction that can be made based on the stability conditions. This conclusion is of extreme interest to the designer of successful laser systems using roof reflectors.

Use of 90° -  $\alpha$  Roof Reflectors. From the geometric theory, it is concluded that 90° -  $\alpha$  roof reflectors are more desirable than 90° roof reflectors in laser resonators. This is an extremely simple conclusion and is motivated by the prediction of the resonant modes, discussed below. Basically, the reason why 90° -  $\alpha$  roof reflectors are desirable

is because the roof edges can be geometrically excluded. This is fully discussed in Chapters IV and V for parallel-roof and crossed-roof resonators, respectively.

It is also important, for the purpose of design, that  $90^\circ - \alpha$  roof reflectors preserve the relaxed mechanical alignment tolerances of  $90^\circ$  roof reflectors. This is demonstrated in Chapter III.

Resonant Modes. When the roof edges of the reflectors are geometrically excluded, it is predicted that roof reflector resonators can support pure Gaussian modes. This is argued in both Chapters IV and V, and there is evidence in the literature that this prediction is correct (reviewed in Chapter II). For the parallel-roof resonator, the axial mode frequency interval is predicted to be:

$$\Delta f_q = \frac{c}{2 p_2 L} \quad (58)$$

while for the  $p_3 = 1$  pattern in the crossed-roof resonator:

$$\Delta f_q = \frac{c}{2 L} \quad (106)$$

For both resonators, the transverse modes are claimed to be frequency degenerate:

$$\Delta f_{mn} = 0 \quad (62)$$

An Example. The desirability of  $90^\circ - \alpha$  roof reflector resonators can be further emphasized with a simple example. Suppose a laser is to be designed for field use in a high-vibration environment. The crossed-roof configuration is then desired for mechanical stability, and  $90^\circ - \alpha$  roof reflectors are to be used to obtain a pure mode

output. The beam divergence will then be less than if 90° roof reflectors were used since roof edge diffraction will be avoided.

Now suppose that precision-built roof reflectors are not available, but that two approximately matched items can be found. The first reflector has a side dimension  $d_{01} = 1$  cm, variant angle  $\alpha_1 = 31' = 0.0090$  rad, and a roof edge 0.5 mm wide. The second reflector has  $d_{02} = 1$  cm,  $\alpha_2 = 29' = 0.0084$  rad, and roof edge 0.5 mm wide. From Eq. (15):

$$D_{01} = \frac{\sqrt{2} d_{01}}{2 \alpha_1} = 78.4 \text{ cm} \quad (109)$$

$$D_{02} = \frac{\sqrt{2} d_{02}}{2 \alpha_2} = 83.8 \text{ cm} \quad (110)$$

In order for the resonator to be stable, the axis length must be chosen less than the smaller of these two, by Eq. (108). In order to exclude the roof edges with the  $p_3 = 1$  pattern, however,  $L$  must be greater than one-half of the larger (from the discussion on p. 93). Thus, if:

$$41.9 \text{ cm} < L < 78.4 \text{ cm} \quad (111)$$

the resonator will operate only in the  $p_3 = 1$  mode.

Let  $L = 50$  cm be a convenient axis length, then by Eq. (50) the cross-sectional dimensions of the  $p_3 = 1$  ray tube are

$$h_1 = \frac{\sqrt{2} d_{01}}{2} - \alpha_1 L = 0.26 \text{ cm} \quad (112)$$

$$h_2 = \frac{\sqrt{2} d_{02}}{2} - \alpha_2 L = 0.29 \text{ cm} \quad (113)$$

It is also easy to calculate that the size of the geometrically excluded area at the roof edge of the first reflector (measured

perpendicular to the axis) is approximately 3.8 mm, and for the second 2.6 mm. Thus the geometrically excluded areas are clearly much larger than the size of the roof edge width, so roof edge quality need not be of great concern. Also, the conditions have been satisfied which, according to the predictions of this theory, permit the resonator to support the desired pure modes.

#### Recommendations for Further Study

Many questions have arisen in the course of developing this theory, and not all have been answered. Listed below are recommended areas for further study which either (1) logically extend the work presented here or (2) involve designing practical devices.

Extending the Theory. This geometric theory is thought to be the first of its kind for roof reflector resonators, and has only been a beginning in the study of these devices. The following topics are recommended as areas for research to extend the theory, listed in order of increasing sophistication. Possible methods for solution are also suggested.

(1) Arbitrarily aligned roof edges. The two configurations examined in this thesis are, admittedly, only special cases of the general  $90^\circ - \alpha$  roof reflector resonator. Kahn and Nemt (Ref 22) provide a  $4 \times 4$  rotation matrix which could be used to extend the work of Chapter V to find stable rays in the general case.

(2) Computer solutions for resonant modes. Self-reproducing wavefronts could be found using iterative methods to substantiate the predicted resonant modes. These numerical results would also provide

calculations of diffraction losses that cannot be given by geometric theory.

(3) Thermal lensing by lasing medium. Soncini and Svelto (Ref 39) partly attribute the pure modes they observed to thermal lensing in their ruby rod. This is a topic for study by computer that could be added on to (2) above. A paper by Kurauchi and Kahn (Ref 26) addresses the problem of focusing media in resonators having stable ray envelopes as the roof reflector resonator certainly does.

(4) Polarization analysis. Although a method of determining the eigenpolarizations in roof reflector resonators has been given by Bobroff (Ref 5), it is noted that the direction of propagation of the ray tubes in the crossed-roof resonator is not parallel to the axis and, hence, the plane of incidence at each reflection is neither parallel nor perpendicular to the roof edge. The eigenpolarizations of this resonator are thus thought not to be so simple as in the 90° roof reflector case treated by Bobroff (or the parallel-roof resonator of Chapter IV ). In order to take into account the vectorial nature of light, the eigenpolarizations need to be more closely studied for this resonator. DeLang (Ref 13:1-20) discusses the interaction of polarized beams with active laser media, and a possible method for computing is the polarization transfer function given by Azzam and Bashara (Ref 2).

Designing Practical Devices. Before operating lasers can be built, there are a number of design problems which must be dealt with. Three of these which seem to be of immediate interest to the designer are recommended as areas for advanced study.

(1) Stable or unstable operation. Apparently the crossed-roof configuration is preferable where mechanical stability and relaxed alignment tolerances are needed. Then it would also seem to be most advantageous to design for  $p_3 = 1$  operation only. On the other hand, unstable operation may be more desirable as in high-energy laser applications. Then perhaps a parallel-roof resonator would be better with  $\alpha_1 \neq \alpha_2$  and, say, the roof edges aligned with the gas flow in a gas-dynamic laser.

(2) Best method for outcoupling. The traditional methods of extracting energy from a laser resonator are through a partially reflecting mirror if the resonator is stable, or allowing energy to diffract past the mirrors if it is unstable (Ref 38). Both of these methods are possible with roof reflector resonators, but there are other methods which have been proposed, or used on a limited basis, that require further evaluation: (a) frustrated total internal reflection has been used by Soncini and Svelto (Ref 39), (b) less than total internal reflection on one surface of a roof prism was used by Farkas (Ref 15) in a high-power ruby laser, (c) a beamsplitter was inserted into a resonator using a  $90^\circ$  -  $\alpha$  roof reflector on one end by Dahlstrom (Ref 12), and (d) a birefringent crystal was placed in a  $90^\circ$  crossed-roof resonator by Teppo (Ref 43) to outcouple one of the eigen-polarizations.

(3) Multiple beams. Another problem facing the designer of practical devices is the possibility of multiple beams predicted in the crossed-roof resonator. A reasonable solution would be to eliminate all but one by internal aperturing. Or possible multiple beams may be

desired, in high-energy lasers for instance, and some clever arrangement of reflectors outside the resonator could be used to focus them onto a common target.

Regardless of the above design problems, the advantages of roof reflector resonators - mechanical stability and pure mode outputs - are felt to be worthy of the effort to design working lasers using them. Due to their simplicity alone - and the possible savings in cost and fabrication time - roof reflector resonators are seen to offer a practical alternative to curved mirrors in laser systems of the future.

### Bibliography

1. Arnaud, J. A. "Degenerate Optical Cavities." Applied Optics, 8:189-195 (January 1969).
2. Azzam, R. M. A. and N. M. Bashara. "Separability of Amplitude, Phase, and Polarization Information in the Jones Calculus." Optical Communications, 7:317-319 (April 1973).
3. Bergstein, L., W. Kahn, and C. Shulman. "A Total-Reflection Solid-State Optical-Maser Resonator." Proceedings of the IRE, 50:1833 (August 1962).
4. Bertolotti, M., L. Muzii, and D. Sette. "On Cavity Termination of Ruby Laser." Nuovo Cimento, 26:401-402 (16 October 1962).
5. Bobroff, D. L. "Modes of Optical Maser Cavities With Roof-Top and Corner-Cube Reflectors." Applied Optics, 3:1485-1487 (December 1964).
6. Born, M. and E. Wolf. Principles of Optics (2<sup>nd</sup> Rev. Ed.). Oxford, England: Pergamon Press, 1964.
7. Brouwer, W. Matrix Methods in Optical Instrument Design. New York: W. A. Benjamin, Inc., 1964.
8. Checcacci, P. F., R. Falciai, and A. M. Scheggi. "Ring and 90° Roof Open Resonators." Proceedings of the IEEE, 62:1611-1613 (November 1974).
9. Checcacci, P. F. and A. M. Scheggi. "Microwave Model of a 90° Roof Resonator." Proceedings of the Symposium on Modern Optics (Microwave Research Institute Symposia Series, J. Fox, Ed.), 17:481-489. New York: Polytechnic Press of the Polytechnic Institute of Brooklyn, 1967.
10. Clark, F. O. "Multireflector Optical Resonators." Proceedings of the IEEE, 51:949-950 (June 1963).
11. Cubeddu, R., R. Polloni, C. A. Sacchi, and O. Svelto. "Femtosecond Pulses, TEM<sub>00</sub> Mode, Mode-Locked Ruby Laser." IEEE Journal of Quantum Electronics, QE-5:470-471 (September 1969).
12. Dahlstrom, L. "A New Passive Non-Linear Output Coupler for Mode-Locked High Power Lasers." Optical Communications, 4:214-219 (November 1971).

13. DeLang, H. "Polarization Properties of Optical Resonators Passive and Active." Philips Research Reports, Supplement 8 (1967).
14. DeLang, H. and G. Bouwhuis. "A Gas Laser With a Non-Degenerate Configuration of Three Plane Mirrors." Physics Letters, 5:48-50 (1 June 1963).
15. Farkas, G. "Roof Prism Output Coupler for Gigawatt Laser Pulses." Optics and Laser Technology, 2:204-205 (November 1970).
16. Fox, A. G. and T. Li. "Resonant Modes in a Maser Interferometer." Bell System Technical Journal, 40:453-488 (March 1961).
17. Gibbs, W. E. K. and R. E. Whitcher. "Polarization Effects in a Roof-Top Ruby Laser." Applied Optics, 4:1034-1035 (August 1965).
18. Gould, G., S. Jacobs, P. Rabinowitz, and T. Shultz. "Crossed Roof Prism Interferometer." Applied Optics, 1:533-534 (July 1962).
19. Grotbeck, R. An Experimental Investigation of the Resonant Modes of a Roof-Top Laser. Master's thesis. Wright-Patterson Air Force Base, Ohio: Air Force Institute of Technology, December, 1976.
20. Jenkins, F. A. and H. E. White. Fundamentals of Optics (3<sup>rd</sup> Ed.). New York: McGraw-Hill Book Company, Inc., 1957.
21. Kahn, W. K. "Dihedral Optical Resonators and Prism Beam Waveguides." Applied Optics, 6:865-872 (May 1967).
22. Kahn, W. K. and J. T. Nemit. "Ray Theory of Astigmatic Resonators and Beam Waveguides." Proceedings of the Symposium on Modern Optics (Microwave Research Institute Symposia Series, J. Fox, Ed.), 17:501-526. New York: Polytechnic Press of the Polytechnic Institute of Brooklyn, 1967.
23. Keller, J. B. "Geometrical Theory of Diffraction." Journal of the Optical Society of America, 52:116-130 (February 1962).
24. Kogelnik, H. "Modes in Optical Resonators." in Lasers. Vol. 1., pp. 295-347 (A. K. Levine, Ed.). New York: Marcel Dekker, Inc., 1966.
25. Kogelnik, H. and T. Li. "Laser Beams and Resonators." Applied Optics, 5:1550-1567 (October 1966). Simultaneously published in Proceedings of the IEEE, 54:1312-1329 (October 1966).
26. Kurauchi, N. and W. K. Kahn. "Rays and Ray Envelopes Within Stable Optical Resonators Containing Focusing Media." Applied Optics, 5:1023-1029 (June 1966).

27. Ledger, A. M. "Experimental Confirmation of Standing Waves in Laser Resonators." Applied Optics, 5:476-477 (March 1966).
28. Li, T. "Mode Selection in an Aperture-Limited Concentric Maser Interferometer." Bell System Technical Journal, 42:2609-2620 (November 1963).
29. Maitland, A. and M. H. Dunn. Laser Physics. New York: American Elsevier Publishing Company, Inc., 1969.
30. Mathews, J. and R. L. Walker. Mathematical Methods of Physics. New York: W. A. Benjamin, Inc., 1965.
31. Pasqualetti, F. and L. Ronchi. "Integral Equation for a 90° or a Quasi-90° Roof-Mirror Optical Resonator." Journal of the Optical Society of America, 64:289-295 (March 1974).
32. ----- "Roof-Mirror Resonators." Journal of the Optical Society of America, 65:649-654 (June 1975).
33. Rigrod, W. W. "The Optical Ring Resonator." Bell System Technical Journal, 44:907-916 (May 1965).
34. Ronchi, L. "Low-Loss Modes and Resonances in a Quasi-90°-Roof Mirror Resonator." Applied Optics, 12:93-97 (January 1973).
35. Rothstein, J. "Isocles Total Internal Reflectors as Optical Elements." Applied Optics, 2:1191-1194 (November 1963).
36. Scheggi, A. M., P. F. Checcacci, and R. Falciai. "Modes and Modes Degeneracy in 90° and in Quasi-90° Roof Open Resonators." Journal of the Optical Society of America, 65:1050-1053 (September 1975).
37. Siegman, A. E. An Introduction to Lasers and Masers. New York: McGraw-Hill Book Company, Inc., 1971.
38. ----- "Unstable Optical Resonators." Applied Optics, 13:353-367 (February 1974).
39. Soncini, G. and O. Svelto. "Single Transverse Mode Pulsed Ruby Laser." Applied Physics Letters, 11:261-263 (15 October 1967).
40. ----- "Single Mode Passive Q-Switched Ruby Laser." IEEE Journal of Quantum Electronics, QE-4:422 (June 1968).
41. Steier, W. H. "The Ray Packet Equivalent of a Gaussian Light Beam." Applied Optics, 5:1229-1233 (July 1966).

42. Teppo, E. A. Nd:YAG Laser Lab Experiments. NWC Technical Note 4051-2. China Lake, California: Naval Weapons Center, February 1972.
43. ----- Nd:YAG Laser Technology. NWC Technical Memorandum 2534. China Lake, California: Naval Weapons Center, August 1975.
44. Weichel, H. Private communication. 6 August 1976.
45. Williamson, D. E. "Cone Channel Condenser Optics." Journal of the Optical Society of America, 42:712-715 (October 1952).

## Appendix A

### Similarities Between Roof Reflectors and Spherical Mirrors

Roof Reflectors with roof angle  $90^\circ - \alpha$ , where  $\alpha$  is small and positive, are noted to have a "focusing" effect; that is, incident rays are reflected back and converge on their former direction, crossing at an angle of  $2\alpha$  (see Fig. 11). This focusing is remarkably similar to the familiar results of first-order optics applied to spherical mirrors.

For a spherical mirror, M in Fig. 41(a), the center of curvature, C, lies on an axis of symmetry through the vertex, V. Any ray incident on M which passes through C is reflected back through C, while any ray which is incident parallel to the axis is reflected through a point, F, on the axis. To first order, the relation holds that:

$$\overline{FV} = \frac{\overline{CV}}{2} \quad (114)$$

For a roof reflector, R in Fig. 41(b), there is no "center of curvature." But through any point, C', on the axis, a unique ray making an angle  $\alpha$  with the axis will be reflected back through C'. If a point, P', is then located on a line perpendicular to the axis through C' (the line  $\overline{P'V'}$  makes an angle  $\alpha$  with the axis), an incident ray through P' parallel to the axis will be reflected back through P'. This latter ray crosses the axis at a point, F', where the exact relationship is

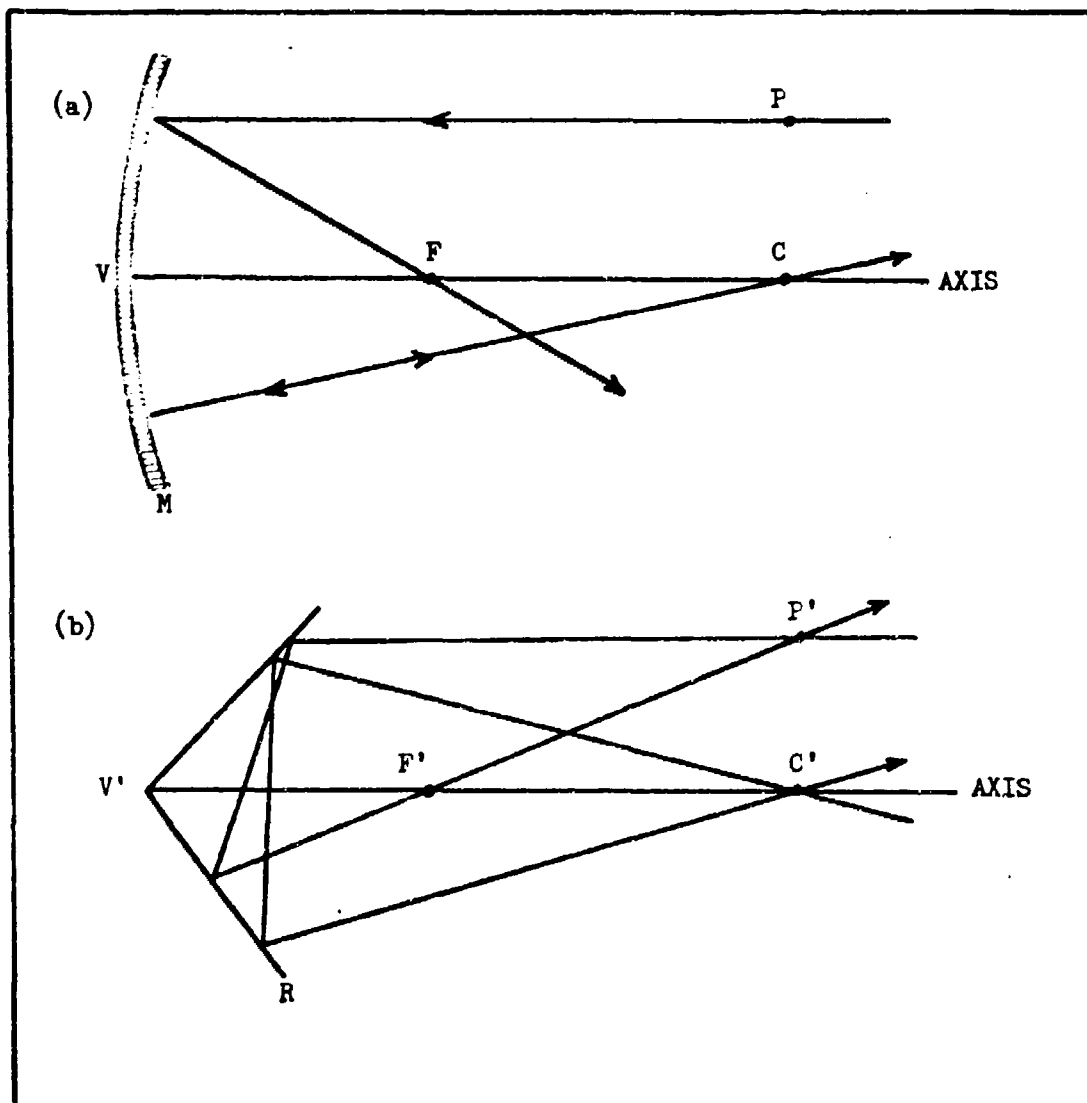


Fig. 41. Similarities Between Roof Reflectors and Spherical Mirrors

$$\overline{F'V'} = \frac{\overline{C'V'}}{2} \frac{1}{\cos^2 \alpha} \quad (115)$$

If  $\alpha$  is small, then the first-order statement of this expression is

$$\overline{F'V'} = \frac{\overline{C'V'}}{2} \quad (116)$$

which is analogous to spherical mirrors.

The rays traced through  $C'$  and  $P'$  of  $R$  are reminiscent of the imaging of an object placed at  $C$  in front of  $M$ . The analogy can be forced by finding a "focal length" for a roof reflector that can be used in a homogeneous ray transformation. (Call it " $f^*$ " to distinguish it from an ordinary focal length.) That is, let the transformation:

$$\begin{bmatrix} x_2 \\ \theta_2 \end{bmatrix} = \begin{bmatrix} -1 & 0 \\ \frac{1}{f^*} & -1 \end{bmatrix} \begin{bmatrix} x_1 \\ \theta_1 \end{bmatrix} \quad (117)$$

carry the ray  $(x_1, \theta_1)$  through a roof reflector just the same as the inhomogeneous transformation of Chapter III:

$$\begin{bmatrix} x_2 \\ \theta_2 \end{bmatrix} = \begin{bmatrix} -1 & 0 \\ 0 & -1 \end{bmatrix} \begin{bmatrix} x_1 \\ \theta_1 \end{bmatrix} + \begin{bmatrix} 0 \\ 2\alpha \end{bmatrix} \quad (23)$$

(The 2x2 matrix of Eq. (117) takes into account the inverting, and Eq. (23) assumes the ray is incident on the roof reflector above the axis.) Equating these last two expressions, the quantity  $f^*$  is found to be:

$$f^* = \frac{x_1}{2\alpha} \quad (118)$$

In terms of the dimension  $d$ , which measures the distance from the vertex to where the ray strikes the roof reflector surface, this is

$$f^* = \frac{d}{2} \frac{2 + 2\theta_1 - \alpha}{\sqrt{8} \alpha} \quad (119)$$

The concept of focal length for roof reflectors (and consequently radius of curvature) is not a particularly useful one since this quantity turns out to depend on the components of the incident ray. If, however, only rays crossing the axis at the angle  $\alpha$  are considered, then putting  $\theta_1 = \alpha$  in Eq. (119) results in:

$$f^* = \frac{d}{2} \frac{2 + \alpha}{\sqrt{8} \alpha} \quad (120)$$

Or, if  $\alpha$  is also considered to be a small angle:

$$f^* = \frac{\sqrt{2} d}{4 \alpha} \quad (121)$$

Comparing this last formula with Eq. (15) of Chapter III, it is then seen that:

$$f^* = \frac{D}{2} \quad (122)$$

where  $D = \overline{C'V'}$  in Fig. 41(b).

While  $f^*$  is seen to be variable, there is an easily recognized constant parameter associated with roof reflectors. This has to do with the discrete roof angle, and is contrasted with spherical mirrors in Fig. 42. Here two resonators are drawn which have concentric properties:

(1) The spherical mirror resonator has a unique point,  $C$ , through which all stable rays pass. Within the limits of the apertures, the rays make a continuum of angles with the resonator axis.

(2) The roof reflector resonator has a unique angle,  $\alpha$ , with which all stable rays cross the axis. Within the limits of the apertures, the rays cross the axis at a continuum of points between  $C_1'$  and  $C_2'$ .

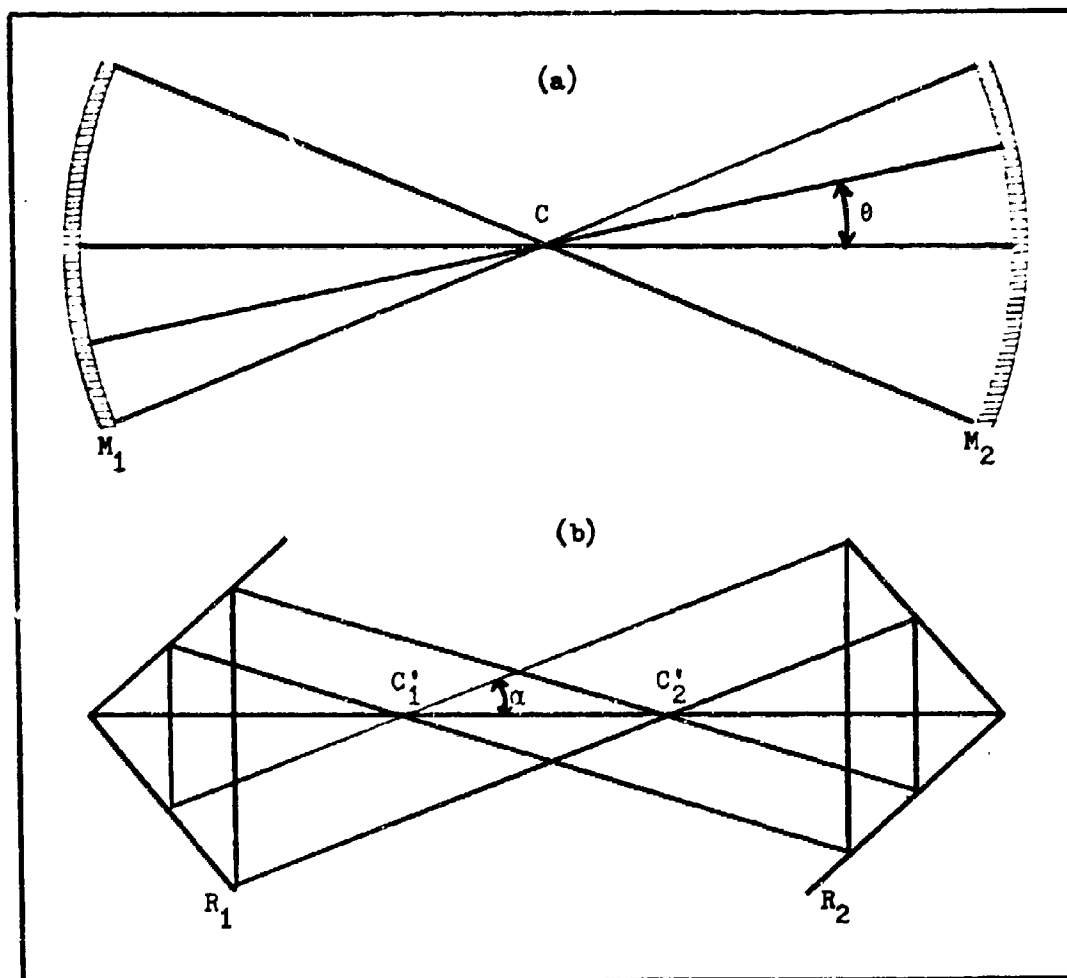


Fig. 42. Dissimilarities Between Roof Reflectors and Spherical Mirrors

## Appendix B

### Roof Reflectors and the g-Parameter

For spherical mirrors, a frequently used parameter in laser resonator design is

$$g_1 = 1 - \frac{L}{R_1} \quad (i = 1, 2) \quad (123)$$

where  $L$  is the resonator axis length and  $R_1$  is the radius of curvature of the  $i^{\text{th}}$  mirror. The condition for stability is often expressed in terms of these  $g$ -parameters as:

$$0 \leq g_1 g_2 \leq 1 \quad (124)$$

That is, the resonator operates in a low-loss regime when this relation is satisfied.

For roof reflectors, there is no radius of curvature. But if the ray crossing distance,  $D$ , is taken to be a characteristic (on-axis) radius, then the dimensionless parameter:

$$g^* = 1 - \frac{L}{D} \quad (125)$$

can be considered by definition. In terms of the roof variant angle,  $\alpha$ , and the dimension  $d$ , this is

$$g^* = 1 - \frac{\sqrt{2} L \alpha}{d} \quad (126)$$

from Chapter III. Although this is characteristic of a roof reflector, it is not a constant except when  $\alpha = 0$  (or  $D \rightarrow \infty$ ). In this case,

$g^* = 1$  which, by way of comparison, is what would be expected for a plane mirror ( $R \rightarrow \infty$ ).

The product,  $g_1^* g_2^*$ , is then seen to involve three dimensions ( $L$ ,  $D_1$  or  $d_1$ , and  $D_2$  or  $d_2$ ). But for a given pattern number,  $p_2$ , these lengths are not independent in the parallel-roof resonator, and it can be shown from Chapter IV that:

$$D_1 + D_2 = p_2 L \quad (127)$$

Substituting from Eq. (125), it is found that:

$$g_1^* g_2^* - \frac{p_2 - 1}{p_2} (g_1^* + g_2^*) + \frac{p_2 - 2}{p_2} = 0 \quad (128)$$

Apparently, this relation describes a curve on a  $g_1^*$  vs.  $g_2^*$  graph on which a parallel-roof resonator operates when a ray makes  $p_2$  round-trips before spatially repeating.

A particular resonator operates on only a portion of the curve. For example, consider a stable parallel-roof resonator ( $\alpha_1 = \alpha_2$ ) operating in the  $p_2 = 1$  pattern with resonator length  $L = 3D_0/2$ . Then it is seen that:

$$\frac{D_0}{2} \leq D_1 \leq D_0 \quad \text{and} \quad \frac{D_0}{2} \leq D_2 \leq D_0 \quad (129)$$

$$-2 \leq g_1^* \leq -\frac{1}{2} \quad \text{and} \quad -2 \leq g_2^* \leq -\frac{1}{2} \quad (130)$$

$$g_1^* g_2^* = 1 \quad (131)$$

from Eqs. (127), (125), and (128), respectively. This is shown in Fig. 43 together with possible resonator configurations that will operate on the curve. Note that  $\alpha_1 = \alpha_2$  does not imply  $g_1^* = g_2^*$ .

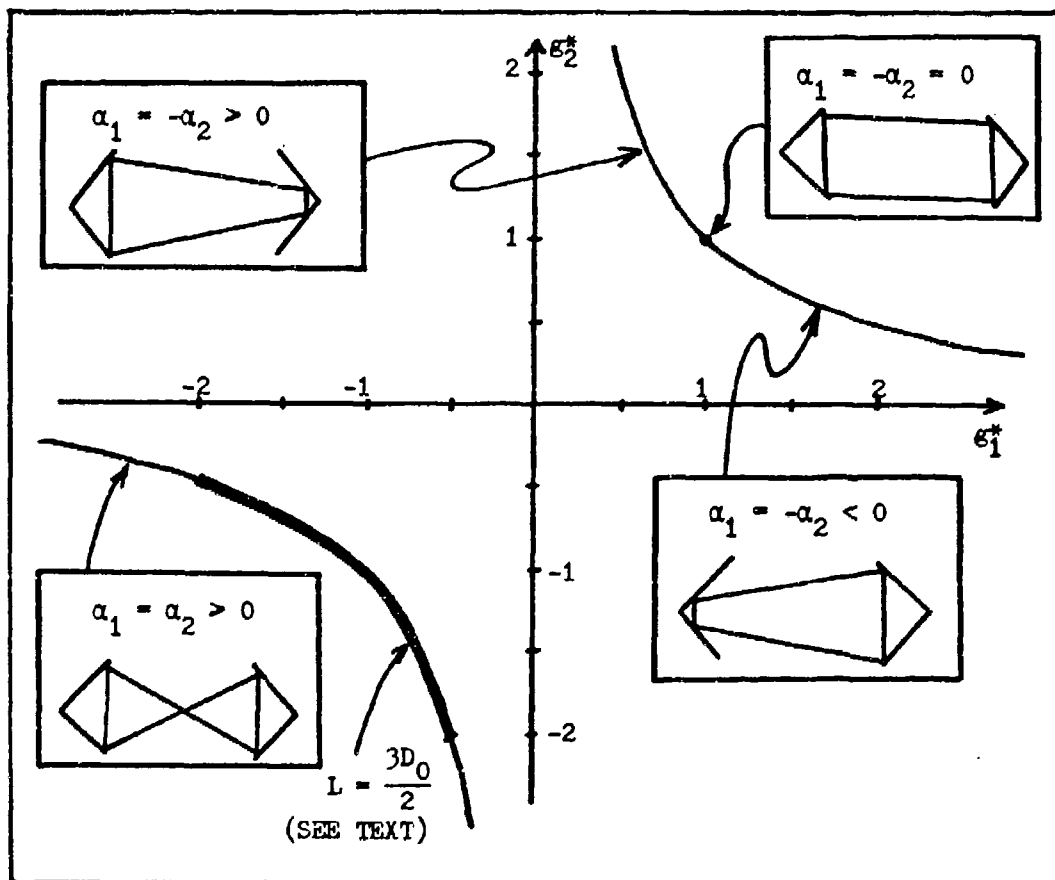


Fig. 43. Operating curve for  $p_2 = 1$

In general, Eq. (128) is a rectangular hyperbola, sketched in Fig. 44, having horizontal and vertical asymptotes:

$$\epsilon_1^* = \epsilon_2^* = \frac{p_2 - 1}{p_2} \quad (132)$$

and transverse axis:

$$t = \frac{2\sqrt{2}}{p_2} \quad (133)$$

The curve has two branches: resonator configuration for the lower branch is  $\alpha_1$  and  $\alpha_2$  both positive, while the variant angles are of opposite sign on the upper branch.

In the limit of  $p_2 \rightarrow \infty$  (a large number of round-trips), it is seen that the hyperbola degenerates into the crossed straight lines:

$$\epsilon_1^* = \epsilon_2^* = 1 \quad (134)$$

Thus, the point (1, 1) satisfies Eq. (128) for all values of  $p_2$ . Therefore, a parallel-roof resonator with two  $90^\circ$  reflectors is infinitely degenerate.

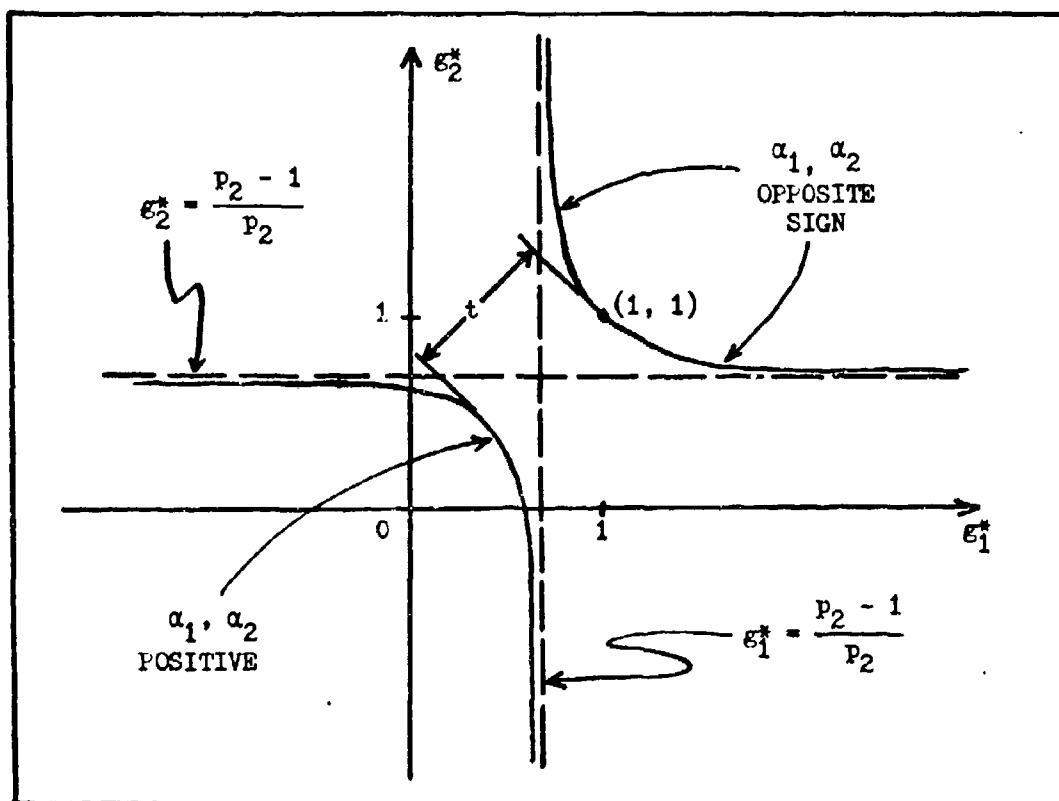


Fig. 44. Operating Curve for Parallel-Roof Resonator in Pattern  $p_2$

## VITA

Howard Elmus Evans II was born on 6 October 1945 in Yakima, Washington. He graduated from high school in Fort Collins, Colorado in 1963 and attended Colorado State University. In 1965 he transferred to the Massachusetts Institute of Technology in Cambridge, Massachusetts, where he received the degree of Bachelor of Science in Physics in June 1968 and was commissioned in the USAF as a Distinguished Military Graduate of ROTC. While attending M.I.T., he worked as a student engineer with Applied Lasers of Stonham, Massachusetts, and the M.I.T. Instrumentation Laboratory. Following graduation, he entered active duty with the Air Force and completed navigator and advanced training at Mather AFB, California. In subsequent assignments, he served as a Weapon Systems Officer in tactical aircraft at MacDill AFB, Florida, Korat Royal Thai AFB, Thailand, and Torrejon AB, Spain, until entering the School of Engineering, Air Force Institute of Technology, in June 1975.

Permanent address: 805 Colorado Street

Fort Collins, Colorado 80521

This thesis was typed by the author.

Unclassified

SECURITY CLASSIFICATION OF THIS PAGE (When Data Entered)

REPORT DOCUMENTATION PAGE		READ INSTRUCTIONS BEFORE COMPLETING FORM
1. REPORT NUMBER GEF/PH/76-3	2. GOVT ACCESSION NO.	3. RECIPIENT'S CATALOG NUMBER
4. TITLE (and Subtitle) THE GEOMETRIC THEORY OF ROOF REFLECTOR RESONATORS		5. TYPE OF REPORT & PERIOD COVERED MS Thesis
7. AUTHOR(s) HOWARD E. EVANS II Captain, USAF		6. PERFORMING ORG. REPORT NUMBER
9. PERFORMING ORGANIZATION NAME AND ADDRESS Air Force Institute of Technology (AFIT-EN) Wright-Patterson AFB, Ohio 45433		8. CONTRACT OR GRANT NUMBER(s)
11. CONTROLLING OFFICE NAME AND ADDRESS		10. PROGRAM ELEMENT, PROJECT, TASK AND A WORK UNIT NUMBERS
14. MONITORING AGENCY NAME & ADDRESS (if different from Controlling Office)		12. REPORT DATE December 1976
		13. NUMBER OF PAGES 132
		15. SECURITY CLASS. (of this report) Unclassified
		15a. DECLASSIFICATION/DOWNGRADING SCHEDULE
16. DISTRIBUTION STATEMENT (of this Report)  Approved for public release; distribution unlimited.		
17. DISTRIBUTION STATEMENT (of the abstract entered in Block 20, if different from Report)		
18. SUPPLEMENTARY NOTES  Approved for public release; IAW AFR 190-17 <i>Jerrald F. Guess</i> JERRALD F. GUESS, Captain, USAF Director of Information		
19. KEY WORDS (Continue on reverse side if necessary and identify by block number) LASERS RING LASERS LASER CAVITIES PRISMS CAVITY RESONATORS MIRRORS OPTICAL RESONATORS WAVEGUIDES LASER BEAMS RESONANT MODES		
ABSTRACT (Continue on reverse side if necessary and identify by block number) Laser resonators using roof reflectors with $90^\circ$ - $\alpha$ roof angles ( $\alpha$ small and positive) are analyzed geometrically when the roof edges at opposite ends of the resonator are aligned either parallel or perpendicular (crossed). Stability conditions, involving reflector dimensions, are found which specify a maximum axis length for the existence of stable rays. In the parallel-roof case, stable rays are shown to be ring-type, making any given number of round-trips before spatially repeating. Stable rays in the crossed-roof case are superpositions of two parallel-roof ray patterns		

Unclassified

Unclassified

SECURITY CLASSIFICATION OF THIS PAGE(When Data Entered)

Block 20. (Continued)

in orthogonal planes. For any pattern, the reflector roof edges are shown to be geometrically excluded when the axis length is greater than one-half the maximum length for that pattern. It is then predicted that when the roof edges are excluded, the resonant modes are pure Gaussian.